Final Report

Joint Industry Project

DESIGN OF CATHODIC PROTECTION RETROFITS FOR OFFSHORE STRUCTURES – Part I: Experimentation and Data Analyses

submitted by

William H. Hartt (Principal Investigator) and Edward Lemieux
Center for Marine Materials
Florida Atlantic University – Sea Tech Campus
101 North Beach Road
Dania Beach, Florida 33004

February 28, 2000

Executive Summary

This report describes the findings of a three year joint industry project that had as its objectives to 1) establish a protocol for determining if and when the cathodic protection (cp) system on a particular structure should be retrofitted and 2) specify a design practice for cathodic protection retrofits in cases where retrofitting has been determined as necessary. These objectives were, in turn, accomplished in terms of three project tasks as:

I. Identification and qualification of protocol(s) for determination of maintenance current density; that is, of the current density that is required to maintain adequate cathodic protection,

II. Development of a retrofit cathodic protection design method(s) for structures that have depolarized or partially depolarized, and

III. Identification of a cathodic protection retrofit timetable for aged structures that are still polarized.

This final report consists of two parts, of which this is Part I and which provides the results of experiments and analyses that were performed in conjunction with the above three tasks. In Part II, the results from Part I are synthesized and developed into a recommended practice for design of retrofit cp systems.

The first task was intended to address the realization that a fundamental requirement for retrofit cp design is knowing the current density required for protection. This effort included experiments that were performed at the Naval Research Corrosion Laboratory in Key West upon one-half scale (approximate) stand-off galvanic aluminum anodes. Based upon these experiments, appropriate current density determination methods were identified and investigated; and the protocol that was ultimately developed, which utilized either 1) a calculation procedure based upon anode and cathode potentials and anode dimensions as inputs (the $\Delta\phi$-*MDE* method) or 2) a Gauss (Swain) meter, were qualified based upon their being applied to three Gulf of Mexico structures. It was demonstrated that the average current density demand of older Gulf of Mexico structures is approximately 25 percent of the mean current density that is specified in existing recommended practices.

The second task focused upon the current density required to repolarize a partially or fully depolarized structure and relationships between 1) current density demand prior to depolarization, 2) current density demand upon partial depolarization, 3) current density required to repolarize, and 4) steady-state current density upon repolarization were developed. An understanding of the latter two parameters is particularly important with regard to specification of anode requirements for cp retrofits. The third task, on the other hand, considered that the timetable for cp retrofit of structures that are protected by galvanic systems and that are still polarized is governed by anode properties. It was projected that present anode performance assessment methods are non-conservative; that is, they overestimate current capacity in the long-term due, first, to maintenance current density being lower than anticipated and, second, because of acidification of the electrolyte beneath corrosion products on the anode. Recognition of the second of these two factors is projected to be a key factor in developing a short-term anode test that projects long-term performance.

Table of Contents

Table of Contents (Continued)

Table of Contents (Continued)

I. INTRODUCTION

Principles of Cathodic Protection

General. Cathodic protection (cp), utilized either alone or in conjunction with coatings, is generally recognized as the most cost effective and technically appropriate methodology for controlling corrosion of offshore petroleum production platforms. Basically, the technique involves cathodic polarization or rendering of the structure potential, ϕ, sufficiently negative relative to its native value (the corrosion potential or ϕ_{corr}) that corrosion rate is nil. For steel in sea water, such protection is generally recognized as being achieved upon polarization to a potential of –0.80 $V_{Ag/AgCl}$ or more negative (1,2), in which case there is no net anodic activity. Such polarization occurs in conjunction with the oxygen reduction reaction,

$$\frac{1}{2}O_2 + H_2O + 2e^- \rightarrow 2OH^-. \qquad (1\text{-}1$$

Also, while both theory and practice have indicated that corrosion is mitigated at excessively negative potentials (ϕ < -1.05 $V_{Ag/AgCl}$), such over-protection causes a second cathodic reaction, water dissociation, or

$$H_2O + 2e^- \rightarrow H + OH^- \qquad (1\text{-}2$$

that results in higher than necessary current and anode consumption rate, the possibility of hydrogen embrittlement, and possible damage to any protective coatings than might be present. On this basis, the optimum polarized potential range is $-1.05\ V_{Ag/AgCl} < \phi \leq -0.80\ V_{Ag/AgCl}$.

Cathodic Protection Design of Offshore Structures. The earlier approach to cathodic protection design of offshore petroleum production structures was based upon application of sufficient current via either an impressed current or galvanic system that polarization to –0.80 $V_{Ag/AgCl}$ plus perhaps a factor of safety resulted in from several months to a year (3). The fact that such polarization requires time to occur is a consequence of the gradual formation of calcareous deposits which serve as a coating upon the steel, as discussed subsequently, and which cause oxygen concentration polarization and a reduced limiting current density (reduced current demand of the structure). Design of these systems based upon galvanic anodes involves

determination of the current output per anode, I_a, as calculated from Ohm's law according to the expression

$$I_a = \frac{\phi_c - \phi_a}{R_a}, \qquad (1\text{-}3$$

where

ϕ_c = closed circuit cathode potential,

ϕ_a = closed circuit anode potential, and

R_a = resistance of an individual anode.

Application of this expression assumes that R_a is the dominant component of the total circuit resistance, as is normally the case for space-frame type structures; and so it alone is considered. Figure 1-1 graphically illustrates the principle behind Equation 1-3 as a schematic polarization curve for both anode and structure.

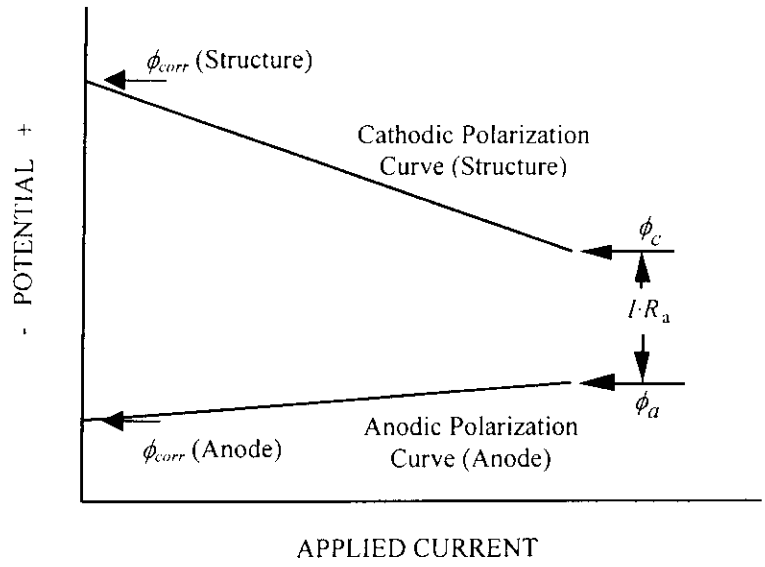

Figure 1-1: Schematic illustration of the potential, current, and resistance terms for cathodically polarized steel in sea water.

From the net anode current output (Equation 1-3), the number of anodes required for protection, N, is determined from the relationship

$$N = \frac{i_c \cdot A_c}{I_a}, \qquad (1\text{-}4$$

where

i_c = cathode current density for polarization and
A_c = cathode surface area.

However, surveys of structures that were designed according to this practice have often revealed potentials that are 100 to 250 mV more negative than -0.80 $V_{Ag/AgCl}$; and the life of the cathodic protection system for these has often exceeded what was projected in the initial design. For example, Evans (4) reported that potential for several platforms in the Arabian Gulf was on the order of -0.94 $V_{Ag/AgCl}$ after 15 years, although the original design was for only ten. Most of the anodes on these structures had become depleted, but apparently the small current that continued to flow provided protection. Similarly, Cochran (5) indicated that 77 of 100 platforms protected by galvanic anodes exhibited potentials of -0.92 $V_{Ag/AgCl}$ or more negative. A 33 year cp system life was estimated for one platform that exhibited potentials of from -0.91 to -0.99 $V_{Ag/AgCl}$ after 4.5 years, whereas the original design was for 20 years.

The above observations can be explained by the experiments of Cox (6) who, some fifty-plus years ago, demonstrated that application initially of a relatively high current density resulted in rapid formation of calcareous deposits that were particularly protective and yielded a lower maintenance or long-term current density, i_{maint}, than if the initial value for this parameter was low. Based either upon laboratory data or service experience, several investigations (7-12) reconfirmed more recently the high initial current density concept; and this approach is now being employed routinely for cp system design of offshore petroleum production platforms. Accordingly, the present recommended practices for marine cp design (1,2) incorporate what has become known as "rapid polarization" which involves application of a relatively high initial current density (i_o), such that a structure potential in the range -0.90 to -1.00 $V_{Ag/AgCl}$ results "...within a reasonably short period of time" (1). The design also includes two other criteria, one based upon a mean current density (i_m) and the other upon a final current density (i_f). Values for N to satisfy the requirement imposed by i_o and i_f, N_o and N_f, respectively, are determined using Equations 1-3 and 1-4, where each of these current densities replaces i_c. The criterion upon which i_f is based intends to ensure that adequate anode mass remains at the end of the design life

to affect repolarization should this become necessary. The mean current density, on the other hand, is the time-averaged value over the design life and, as such, is equivalent to the single current density employed in the earlier protocol (3). The number of anodes required to provide this latter current density, N_m, is calculated from the relationship

$$N_m = \frac{i_m \cdot A_c \cdot T_d}{C \cdot w}, \qquad (1\text{-}5$$

where

T_d = design life,
C = anode current capacity, and
w = weight of a single anode,

which is a modified form of Faraday's law. The purpose of this calculation is to ensure that adequate anode mass is present for the cp system to achieve its design life. Typical values for these three design current densities are listed in Table 1-1 (2). Ideally, the N that is calculated from each of the three current densities should be the same; however, this is normally not the case; and so the highest of the three is specified. For uncoated structures, this is invariably N_o. Accordingly, the cp system may be over-designed in terms of i_m and i_f. This failure of the design procedure to yield a common number of anodes for each of the three current density criterion

Table 1-1: Design Criteria for Cathodic Protection Systems.

Production Area	Typical Design Current Density, mA/m^2 (mA/ft^2)		
	Initial	Mean	Final
Gulf of Mexico	110 (10)	55 (5)	75 (7)
U.S. West Coast	150 (14)	90 (8)	100 (9)
Cook Inlet	430 (40)	380 (35)	380 (35)
Northern North Sea	180 (17)	90 (8)	120 (11)
Southern North Sea	150 (14)	90 (8)	100 (9)
Arabian Gulf	130 (12)	65 (6)	90 (8)
Australia	130 (12)	90 (8)	90 (8)
Brazil	180 (17)	65 (6)	90 (8)
West Africa	130 (12)	65 (6)	90 (8)
Indonesia	110 (10)	55 (5)	75 (7)

arises because the procedure is an algorithm rather than being first principles based.

Basis for Rapid Polarization. The nature of rapid polarization is illustrated by the experimental data of Wang et al. (12) who polarized a series of API 2H-Grade 42 steel specimens using a galvanic Al-Zn-Hg anode according to the experimental arrangement in Figure 1-2, where the two electrodes were connected through an appropriately sized resistor. From a modified form of Ohm's law (9),

$$\phi_c = \left(R_t \cdot A_c\right) \cdot i_c + \phi_a , \qquad (1\text{-}6$$

where R_t is the net circuit resistance ($R_t \approx R_x$, in this case, where R_x is the magnitude of the external resistance), a linear relationship between ϕ_c and i_c is projected to occur as the cathode polarizes in conjunction with calcareous deposit formation provided R_t, A_c, and ϕ_a are constant. This latter condition is normally met for such galvanic systems in sea water. Accordingly, Figure 1-3 shows the results of a series of experiments that employed the arrangement in Figure 1-2 where each test involved a different value for R_x. Here, the individual specimens polarized with

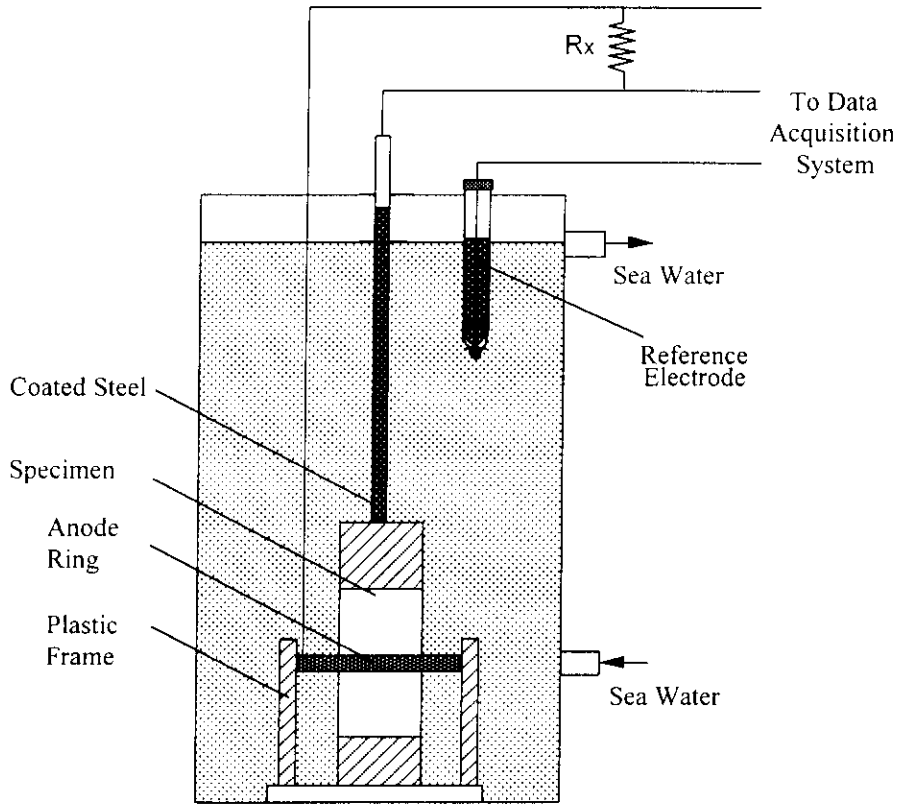

Figure 1-2: Schematic illustration of the expeimental arrangement of Wang et al. (12).

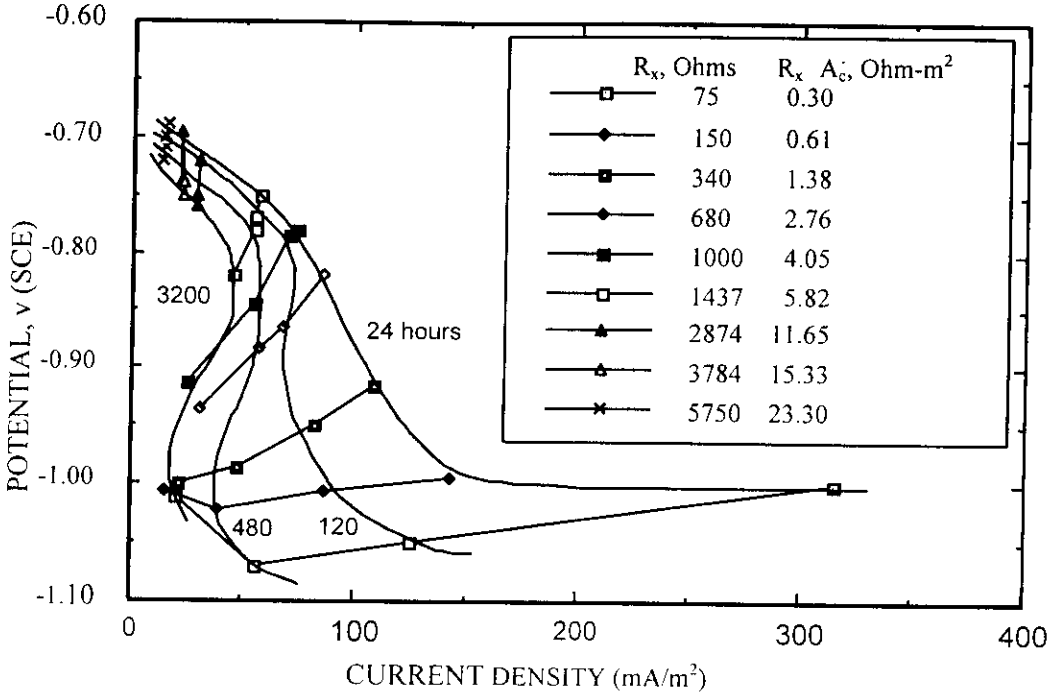

Figure 1-3: Cathode Potential versus current density for representative laboratory experiments at different exposure times.

time from a relatively high initial current density and positive potential to the long-term, steady-state value along an approximately straight line in conformity with Equation 1-6. In effect, the curves that interconnect the data points at 24, 120, 480, and 3,200 hours define the cathodic polarization curve at these times. The long-term data (3,200 hours and greater) are shown on a more expanded scale in Figure 1-4 which reveals in greater detail the sigmoidal potential-current density trend that results from this type of experiment.[1] These results and the data representation that has been employed here render apparent the basis, if not the mechanism, for rapid polarization in that the current density that ultimately results from modest cathodic polarization, such that the protection potential (-0.80 $V_{Ag/AgCl}$) is achieved only in the long-term, was about 2.5 times greater than if the long-term potential were near -1.00 $V_{Ag/AgCl}$. The trend in Figures 1-3 and 1-4, where current density increased with increasing cathodic polarization for potentials below about -1.00 $V_{Ag/AgCl}$, was attributed to the hydrogen reaction (Reaction 1-2). Thus, the optimum situation is one where the steady-state potential of protected structures is in the range from -0.90 to -1.05 $V_{Ag/AgCl}$.

[1] The potential axis in Figures 1-3 and 1-4 and for some of the data representations to follow are referenced to the saturated calomel electrode (SCE). Because only a few millivolts separate this from the Ag/AgCl electrode, no distinction has made between the two.

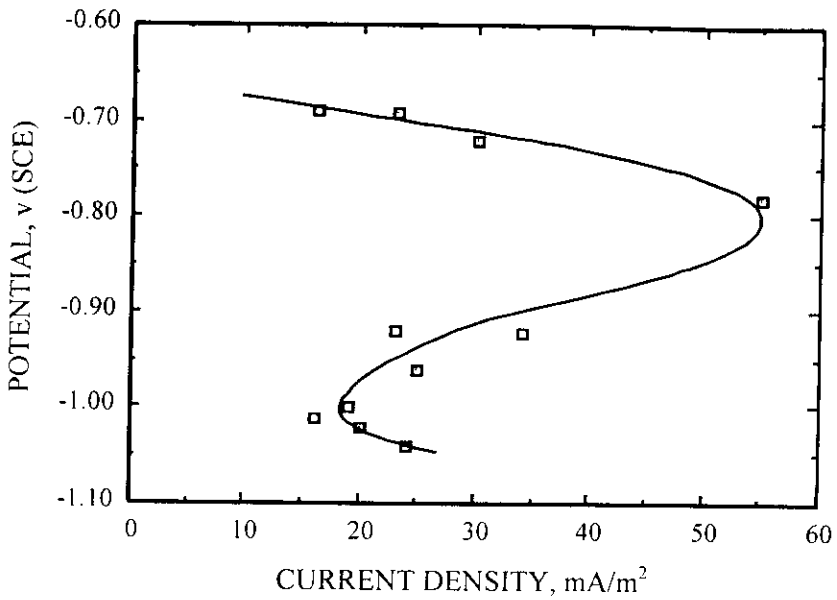

Figure 1-4: Long-term potential versus current density relationship for steel in sea water as determined from laboratory experiments.

Calcareous Deposits. Any comprehensive effort to advance marine cathodic protection practice should incorporate an understanding of the long-term ϕ_c-i_c relationship (Figure 1-4), the variables upon which it depends, and how and why this trend evolves. To this end, it is generally recognized that the relatively low maintenance current density that results in the potential range from -0.90 to -1.05 $V_{Ag/AgCl}$ is a consequence of formation of a particularly protective calcareous deposit (13-19). Such deposits occur as a consequence of Reactions 1 and 2 displacing the inorganic carbon equilibria, as expressed by

$$CO_2 + H_2O \rightarrow H_2CO_3, \quad (1\text{-}7$$

$$H_2CO_3 \rightarrow HCO_3^- + H^+, \text{ and} \quad (1\text{-}8$$

$$HCO_3^- \rightarrow CO_3^{2-} + H^+, \quad (1\text{-}9$$

to the right such that pH in the vicinity of the cathode is increased and calcium and magnesium rich compounds precipitate according to

$$Ca^{2+} + CO_3^{2-} \rightarrow CaCO_3 \downarrow \text{ and} \quad (1\text{-}10$$

$$Mg^{2+} + 2OH^- \rightarrow Mg(OH)_2 \downarrow. \quad (1\text{-}11$$

Presumably, the observation that potentials in the range from -0.90 to -1.05 $V_{Ag/AgCl}$ result in the most protective deposits (that is, in ones that are most impermeable to oxygen ingress such that current density is minimum) is caused, on the one hand, by those that form at more positive potentials being relatively thin and ones at more negative potentials becoming dislodged by hydrogen gas generation. It is also possible that deposits which form outside the above potential range have a different composition or microstructure, or both, and less protective properties.

Slope Parameter Approach to Cathodic Protection Design

Equation 1-5 projects a linear relationship between ϕ_c and i_c with slope $R_t \cdot A_c$ and vertical intercept ϕ_a subject to R_t, A_c and ϕ_a remaining constant, as noted above; and the appropriateness of this expression has now been substantiated by several investigators (12,20-22). From this, the slope parameter, S, is defined as

$$S = R_t \cdot A_c \qquad (1\text{-}12$$

or for the case of space-frame structures protected by multiple, identical galvanic anodes,

$$S = \frac{R_a \cdot A_c}{N}, \qquad (1\text{-}13$$

such that Equation 1-6 becomes

$$\phi_c = \frac{R_a \cdot A_c}{N} \cdot i_c + \phi_a. \qquad (1\text{-}14$$

Figure 1-5 combines a schematic representation of the long-term ϕ_c-i_c curve from Figure 1-2 with Equation 1-14 to illustrate several design alternatives (choices for S) from which the implication of the different choices becomes apparent. Thus, a design according to S_1 results in inadequate protection, since the polarized potential does not achieve the minimum value for arrestment of corrosion (-0.80 $V_{Ag/AgCl}$). Slope parameter S_2 provides marginal protection but at a potential for which current density is relatively high. Slopes from S_3 to S_4, however, result in polarization to the potential range where i_m is minimum. The choice of S requires either that results from prior experience for cp installations at or near the site of interest be available or that instrumented test

panels be deployed and current and potential decay monitored with time. This approach can be interfaced with the existing standardized design method (1,2) by recognizing an alternative expression for the slope parameter as

$$S = \frac{\phi_c - \phi_a}{i_o}, \qquad (1\text{-}15$$

where ϕ_c in this case is the cathode potential at which the initial current density is defined (-0.80 $V_{Ag/AgCl}$ according to the present method (1,2)).

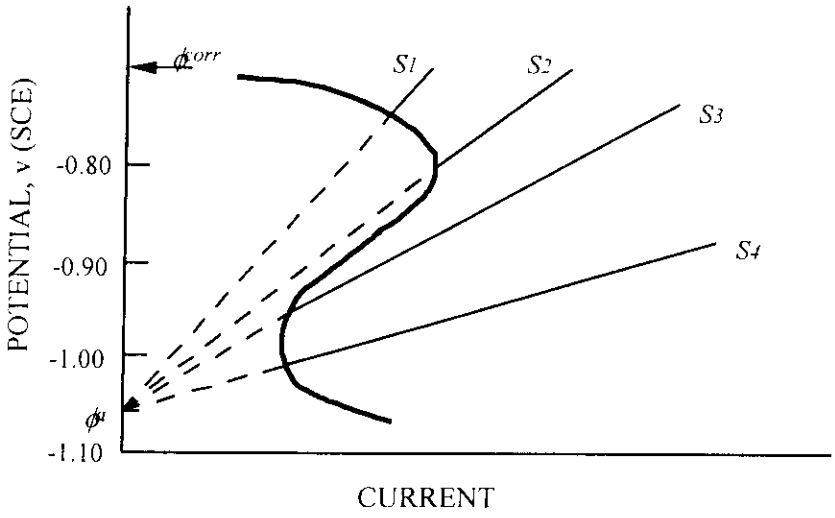

Figure 1-5: Schematic illustration of alternative design slopes in perspective to the long-term ϕ_c-i_c curve.

Further, several authors (20-22) have shown that by combining Equations 1-5 and 1-13 a unified design equation of the form

$$R_a w = i_m \cdot T \cdot K \cdot S \qquad (1\text{-}16$$

results, where T is exposure time and K is the anode consumption rate or $1/C$. Since all terms on the right side are known from the design choices; the process is reduced to determination of the optimum combination of R_a and w. This may be accomplished in terms of anodes of standard dimensions or, alternatively, by elongated anodes or by dualnodes (23). As an example (21), if anode resistance is represented in terms of Dwight's modified equation,

$$R_a = \frac{\rho}{2\pi L} \cdot \left[\ln\left(\frac{4L}{r}\right) - 1 \right], \qquad (1\text{-}17$$

where

ρ = electrolyte resistivity,
L = anode length, and
r = anode radius,

then the left side of Equation 1-16 becomes

$$R_a \cdot w = \frac{\rho \cdot \rho' \cdot r^2 \cdot v}{2} \left[\ln \frac{4L}{r} - 1 \right], \qquad (1\text{-}18$$

where

ρ' = anode density and
v = volume fraction of the anode that is galvanic metal as opposed to core.

The required number of anodes can then be calculated from Equation 1-13. The advantage of this method over the current approach (1,2) is that Equation 1-16 is first principles based and includes both i_a and i_m, the former implicitly within S (see Equation 1-15) and the latter explicitly. As such, design can be optimized in terms of both parameters instead of just one. An alternative view is that, of the two terms on the left side of Equation 1-16, R_a determines i_a, while w is governed by i_m.

Mean Current Density

The design choice for mean current density, i_m, (see Table 1-1) is based largely upon historical experience. However, results from several investigations are now available indicating that the Table 1-1 values may be unnecessarily conservative. For example, Mateer and Kennelley (24) reported the maintenance current density or current density demand, i_{maint}, for two Gulf of Mexico structures that were retrofit candidates as 3.4 and 8.8 mA/m^2 (ages 19 and 22 years, respectively). Also, Kiefer et al. (25) determined i_{maint} values of 5.4 to 34.4 mA/m^2 for 15 Arabian Gulf structures (ages 13-24 years); and Jelinek et al. reported a value of 20 mA/m^2 for a

North Sea structure (26). In a recent study, values for i_{maint} from both offshore structures and long-term laboratory test specimen exposures were compiled and analyzed for the purpose of developing an improved technique for projecting both this parameter and i_m (27). Figures 1-6 and 1-7 show these data for warm and cold water exposures, respectively (data from 19 structures are represented in Figure 1-6 and for six structures in Figure 1-7). It was concluded from this that, subsequent to an initial exposure period during which i_{maint} was constant, this parameter decayed with time according to a power law expression of the form

$$i_{maint} = 10^{(a+k_i \cdot \sigma_i)} \cdot T^b, \qquad (1\text{-}19$$

where

T is exposure time,
σ_i is the standard deviation for i_{maint} (actually, for the constant a),
k_i is a multiple upon σ_i (for the mean curve, $k_i = 0$), and
a and b are constants.

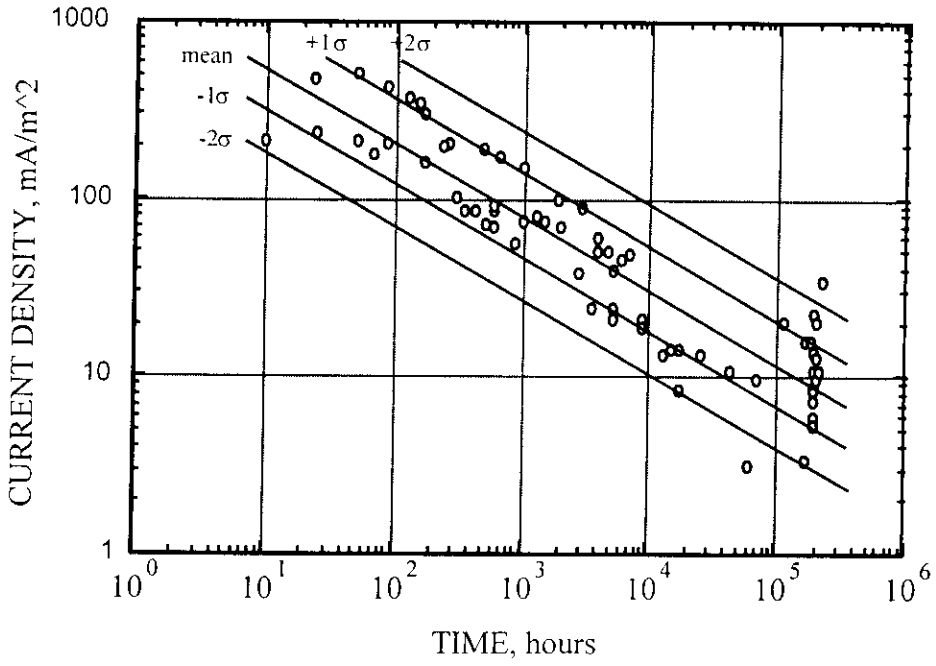

Figure 1-6: Plot of (i_{maint}) versus time for various structures at warm sea water exposure locations. The different symbols pertain to different structures.

Table 1-2 lists values of a, b, and σ for both the warm and cold sea water cases. From this, an expression for i_m was developed as

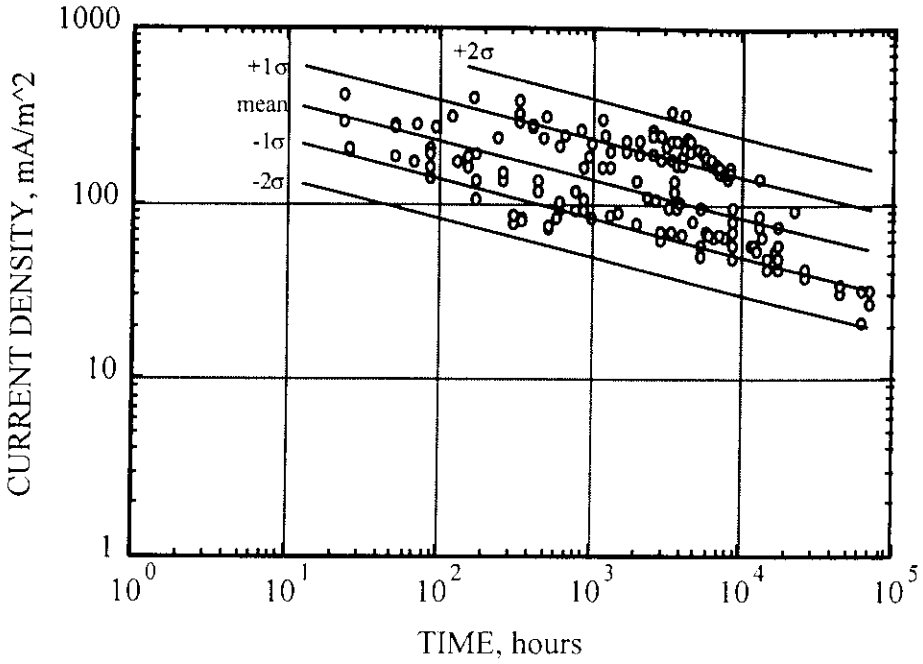

Figure 1-9: Plot of (i_{maint}) versus time for various structures at cold sea water exposure locations. The different symbols pertain to different structures.

Table 1-2: Curve-fitting parameters for Equation 1-20.

	Warm/Shallow Parameters	Cold/Deep Water Parameters
σ_i	0.233	0.229
a	3.130	2.820
b	-0.410	-0.226

$$i_m = \frac{10^{(a+k_i \sigma_i)} \cdot T_d^b}{b+1}. \qquad (1\text{-}20$$

It was proposed that this serve as the basis whereby values for i_m are specified in design. The choice of k_i can vary depending upon the degree of conservatism that is considered appropriate or the extent to which data exist for the specific site in question (k_i need not be a whole number). By this procedure, i_m is projected to be a function of the design life. Table 1-3 tabulates i_m values for different design lives, and Table 1-4 lists i_m for the specific case of T_d = 20 years according to three levels of conservatism along with the percent difference between these and presently recommended values (2). Thus, the proposed mean+2σ value for i_m (high level of

Table 1-3: List of i_m values as a function of T_d and for different degrees of design conservatism.

Time, years	Mean Current Density, mA/m^2					
	k_i= 0		k_i= 1		k_i= 2	
	Cold	Warm	Cold	Warm	Cold	Warm
1	109	55	185	95	314	162
5	76	29	129	49	218	84
10	65	22	110	37	186	63
15	59	18	100	31	170	53
20	56	16	94	28	159	47
25	53	15	89	25	151	43
30	51	14	86	23	145	40

Table 1-4: Listing of the proposed i_m and the percent difference compared to current practice for a design life of 20 years at three levels of conservatism.

DEGREE OF CONSERVATISM	WARM WATER		COLD WATER	
	i_m (prop.), mA/m^2	% Diff. Compared to Reference 2*	i_m (prop.), mA/m^2	% Diff. Compared To Reference 2*
None, k_i = 0	16	-71	56	-38
Intermediate, k_i = 1	28	-49	94	4
High, k_i = 2	47	-15	159	77

* A positive % difference indicates that i_m for the present method exceeds that from the current recommended practice.

conservatism, k_i = 2) is about 15 percent less than the recommended Gulf of Mexico value (2) (47 compared to 55 mA/m^2), while the mean+1σ value (intermediate conservatism, k_i = 1) is about one-half of this. The mean itself, on the other hand, is 71 percent less than the presently recommended value. In the cold water case, these same values range from 77 percent greater to about the same to 38 percent below the present North Sea design i_m (2) (90 mA/m^2) for the same three degrees of conservatism (mean+2σ, mean+1σ, and mean, respectively). It was considered based upon this that the presently recommended North Sea design i_m reflects an appropriate level

of conservatism for a 20 years life, while the Gulf of Mexico one constitutes over-design by about a factor of two. These projections are important to design of cp retrofits since determination of i_{maint} is the single most important point of information that is required, as explained subsequently.

Retrofit Cathodic Protection for Offshore Structures

Offshore petroleum production structures have now been deployed in the Gulf of Mexico for over 50 years with more than 1,400 major platforms having been set between 1973 and 1981 (28). Because cp design is normally based upon a 20 year life, retrofitting has been required in some cases; however, information pertaining to these has typically been limited to a description of anode configuration and attachment methods (29-33). Computer modeling has been promoted as having utility (26,34), but this is likely to be employed only in specialized circumstances. In the absence of a retrofit design specification, the general approach has been to employ the same current density criterion as for new structures (1,2); However, Hartt and Chen (35) described the theoretical basis whereby the slope parameter approach can be applied to retrofit cp design and detailed the advantages that can be realized; and several investigators have reported using this method to affect actual designs (24,25,36) based upon a reduced current density compared to what is employed for new structures (1,2). Since the cost of a particular retrofit can range from multi-thousands to millions of dollars depending upon structure size and water depth, the incentive for design optimization can be significant. The need for a retrofit design protocol is indicated further by activities wherein a state-of-the-art report on this topic is being developed (37).

II. PROJECT OBJECTIVES

The present project was conceived, developed, and accomplished in response to the perceived need for criteria and a protocol whereby cathodic protection systems of offshore petroleum production platforms can be retrofitted according to the most technically viable and economically justifiable method. Specifically, the project had the following two overall objectives:

1. Establishment of a protocol for determining if and when the cathodic protection system on a particular structure should be retrofitted.

2. Specification of a design practice for cathodic protection retrofits in cases where retrofitting has been determined to be necessary.

These objectives were, in turn, accomplished in terms of three project tasks as:

I. Identification and Qualification of Protocol(s) for Determination of Maintenance Current Density.

II. Retrofit Cathodic Protection Design for Structures That Have Depolarized or Partially Depolarized.

III. Cathodic Protection Retrofit Timetable for Aging Structures That Are Still Polarized.

The project did not address hardware type topics such as anode configurations and distributions and electrical connection details. Also, while specific consideration was given to performance of galvanic anodes, since these are much more widely employed compared to the impressed current counterpart, the question as to what type system should be selected (galvanic anode versus impressed current or possibly hybrid) was not considered because such a decision should be structure and circumstance specific.

III. TASK I: IDENTIFICATION AND QUALIFICATION OF PROTOCOLS FOR DETERMINATION OF MAINTENANCE CURRENT DENSITY

Background

As noted above, a fundamental step in any retrofit decision or design is definition of the current demand of the structure in question. Consequently, an initial undertaking was to review the literature and identify methods whereby current demand for a particular structure might best be determined. This revealed five possibilities, as listed and discussed below.

Protocol Alternatives

1. Polarization of the Structure

Thomason et al. (38) reported the results of a field test where an eight year old Gulf of Mexico platform was polarized by up to about 10 mV using a direct current 30 A galvanostat in conjunction with an impressed current anode and the resultant potential and current (I) data were recorded. The structure was an eight leg jacket in 30 m water and was protected by 68 190 kg (416 lb) Al-Zn-In anodes. The submerged surface area was 5,800 m^2 and was coated with a primer and epoxy topcoat. In addition, there were 13 well casings and eight piles (bare); but these were neglected in the analysis. Potential of the structure had always been found during routine surveys to be in the protected range and at the time of the polarization was –0.947 $V_{Ag/AgCl}$. The experimentally determined ϕ-I curve was approximately linear with a slope of 2.68 A per mV. From the equation

$$I_{a(Al)} = \frac{I_{IC}}{1 - \exp\left(\frac{-2.303 \cdot \Delta E}{\beta_a}\right)}, \qquad (3\text{-}1$$

where

$I_{a(Al)}$ is the total current output of the aluminum anodes,

I_{IC} is the impressed current to achieve a potential change of ΔE and

β_a is the Tafel constant for the anodic (aluminum) reaction,

a current output per anode of 0.53 A was calculated. From this, the total current output was calculated and, in turn, the value for i_{maint} was determined as 3.7 mA/m^2.

Shortcomings of this approach are, first, the procedure becomes impractical for larger surface area, uncoated structures because of the high impressed current that must be provided. Second, Equation 3-1 assumes that potential and current density are uniform throughout the structure. This is likely not to be the case for larger structures, in which case multiple, distributed impressed current anodes may be required. Third, the derivation of Equation 3-1 assumes that oxygen reduction is the only cathodic reaction. However, at a pH of 9.5, which is the approximate value at the surface of cathodically polarized steel in sea water, the reversible hydrogen potential is about –0.840 $V_{Ag/AgCl}$. Consequently, an over-potential for this electrode (hydrogen) of 100 mV or more may result, in which case the assumption of a single cathodic process may lead to error.

It was concluded that the structure polarization approach to determination of cp current demand can be advantageous in certain specific cases, but it is not generally applicable and, as such, was not pursued in the present study.

2. Potential Difference-Modified Dwight Equation ($\Delta\phi$-*MDE*) Method

Mateer (39) and Mateer and Kennelley (24) proposed a method for i_{maint} assessment, and the latter authors applied this to two Gulf of Mexico structures that were retrofit candidates. This involves the following steps:

A. The potential of individual anodes (ϕ_a) was measured at three positions along their length using a reference electrode with a 51 mm (2.0 inch) standoff. A procedure was developed whereby the measured potential was corrected for the IR drop between the reference electrode and the anode surface.

B. The structure potential, ϕ_c, was measured near the anode and the potential difference between the anode and structure was calculated as

$$\Delta\phi = \phi_c - \phi_c. \qquad (3\text{-}2$$

C. From the anode dimensions and water resistivity, as determined by survey measurements, the anode resistance was calculated using the modified Dwight equation (Equation 1-17).

D. The anode current output, I_a, was then calculated using Ohm's law.

E. The procedure was repeated for a number of anodes, and the net current output of the cp system, I_t, was determined from the expression

$$I_t = I_a \cdot N . \qquad (3\text{-}3$$

F. Maintenance current density was then determined as

$$i_{ma\,int} = \frac{I_t}{A_c} . \qquad (3\text{-}4$$

Figure 3-1 schematically illustrates the basis for this approach as a sketch of a tubular member with a stand-off galvanic anode and the corresponding potential profile. Thus, from Ohm's law and knowledge of $\Delta\phi$ and R_a, the anode current output can be calculated.

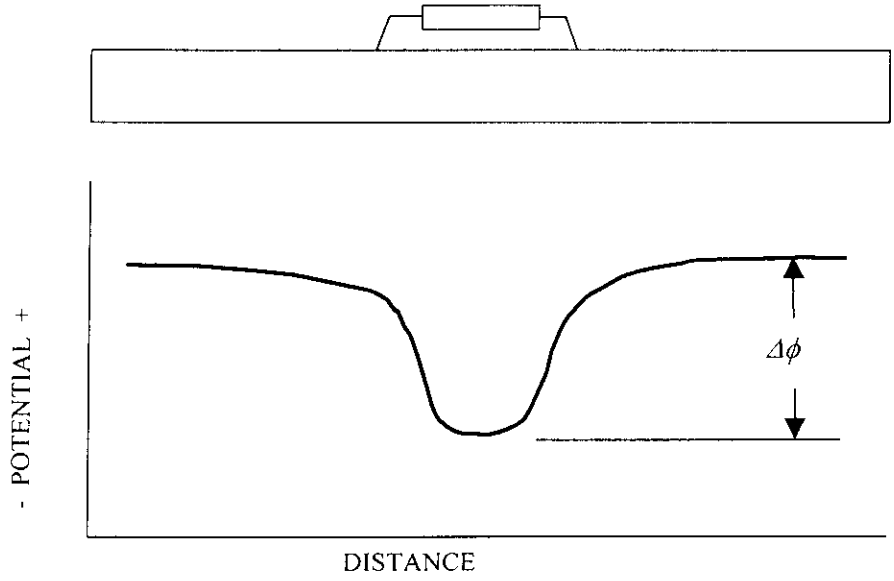

Figure 3-1: Schematic illustration of an anode on an offshore structure member and the resultant potential profile.

Figure 3-2 (39) compares anode current output determinations using the $\Delta\phi$-*MDE* method with those from a gauss (Swain) meter[2] for 57 anodes on 13 different structures. This shows the scatter between the two methods to be relatively large, a finding that Mateer attributed to the reference electrode not being sufficiently close to the anode when the structure potential measurements were made. However, one structure was identified for which the ϕ_c values were spatially invariant; and in this case a linear relationship with little scatter existed between the gauss meter current measurements and the $\Delta\phi$-*MDE* results, as shown by Figure 3-3.

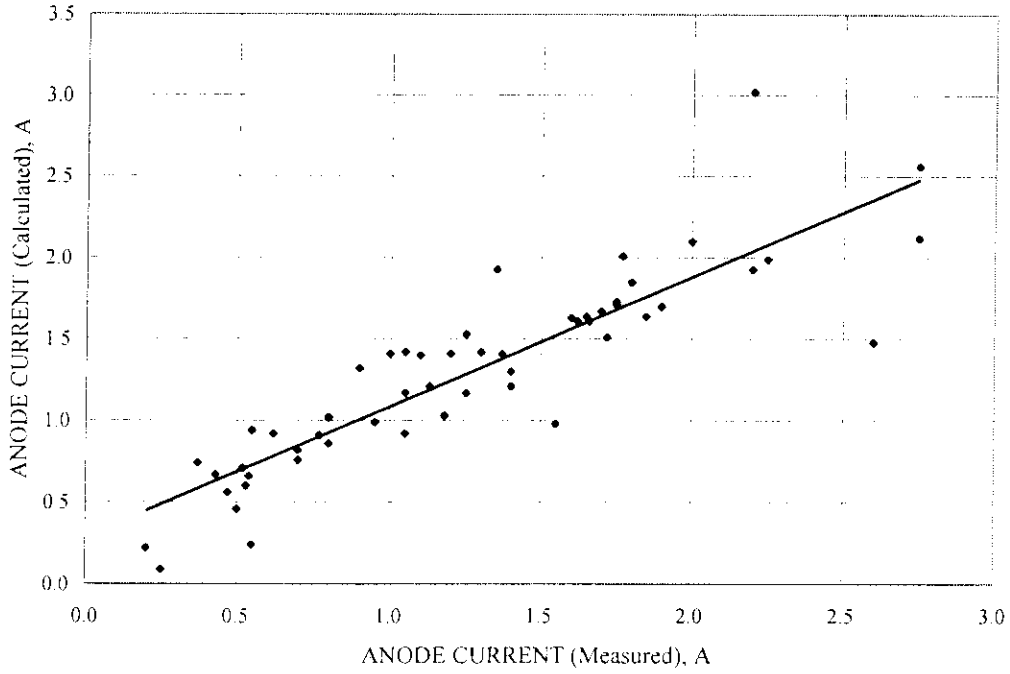

Figure 3-2: Comparison of current output from 57 anodes on 13 different structures according to 1) Swain meter (measured) and 2) $\Delta\phi$-*MDE* (calculated). The R^2 value for the best fit line is 0.80.

Deepwater Corrosion Services, Inc. employs a modified/refined version of the procedure described above (24,39)[3]. Items in this that appear to differ from or are more specific compared to those of Mateer (39) are as follows:

A. Potential of individual anodes is taken as the most negative of three measurements. This should yield a higher calculated $\Delta\phi$ than the Mateer procedure and, hence, a higher value

[2]The possible utility of current measurements using this instrumentation for projecting i_{maint} is addressed subsequently.

[3]Actually, the Mateer procedure (39) was developed in consultation with Deepwater Corrosion Services, in which case the latter procedure is probably an evolution of the former.

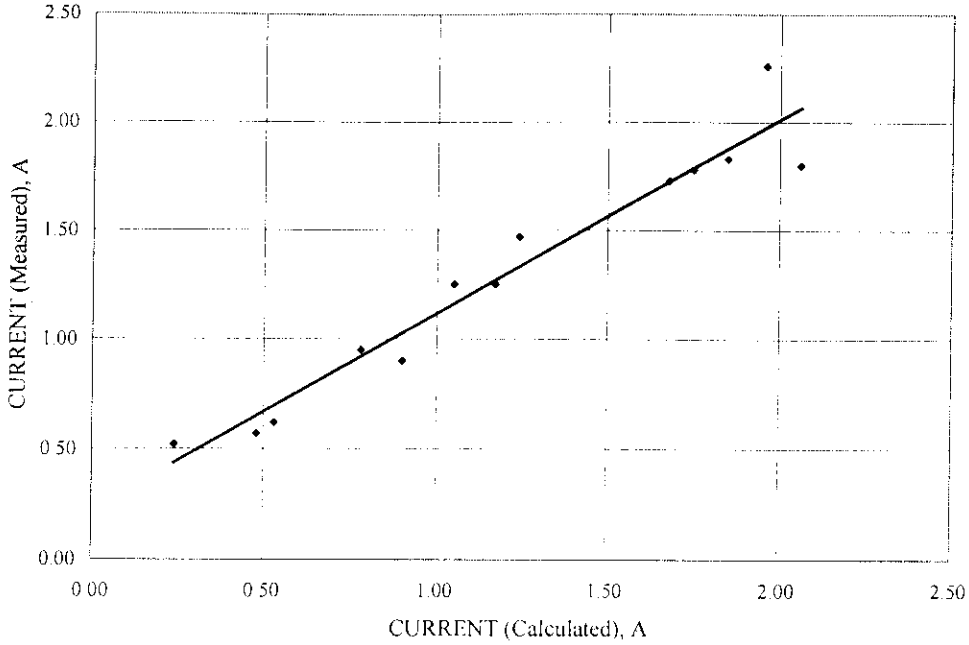

Figure 3-3: Comparison of current output from anodes on a single structure that exhibited a spatially uniform ϕ_c according to 1) Swain meter (measured) and 2) $\Delta\phi$-*MDE* (calculated). The R^2 value for the best fit line is 0.94. (Data estimated from author's graph)

for i_{mant}. These potentials are measured with the reference electrode flush against the anode (actually, against the fouled surface of the anode such that a voltage drop may still be present).

B. The cathode is scanned either between anodes or from an anode to a node (whichever applies), and ϕ_c is taken as the average value.

C. Anode circumference is measured at three locations along with the length. The effective radius that is calculated from the average of these and sea water resistivity are used to calculate anode resistance (Equation 1-17).

D. Remaining anode life is estimated from 1) A-hr delivered and 2) remaining anode weight. The more conservative of the two results is used to estimate remaining life of the cp system.

Deepwater Corrosion Services indicated that they have performed 30-40 surveys upon structures according to the above protocol (40).

Limitations and problems with either approach (Mateer or Deepwater Corrosion Services) are 1) anodes must be cleaned in order to acquire reasonably accurate dimensions (irrespective of anode cleaning, errors/inaccuracies in the anode dimensional measurements (r and L) may occur, 2) the value for ϕ_a may include an IR drop of unknown magnitude and techniques to account for this may be relatively inaccurate, and 3) ϕ_c may vary spatially, thus leading to uncertainty as to how this parameter should be defined and, in turn, to an error in the determination of $\Delta\phi$ (Equation 3-2). Irrespective of these, it was concluded that the $\Delta\phi$-MDE method has potential as a method for projecting i_{maint} and that a commitment should be made within the project to further explore the approach. A particularly attractive feature of this method is that the necessary data is in many cases being acquired in conjunction with routine Level II surveys, and so all that may be required is adjustments in the data acquisition methods and additional data analysis. To make this a viable method, however, the above problems need to be addressed and the finalized procedure qualified by otherwise independent measurements.

3. Anode Current Output Determination Using the Swain Meter

This approach employs a non-contact meter based upon the principle that a direct current induces a magnetic field in its vicinity, the magnitude of which is proportional to the current. By clipping the sensing element about each of the two stand-offs of a given anode, the net current passing through the metallic path and, hence, the anode current output is determined. However, the sensing element does not discriminate between the metallic path current and current in the sea water within the element or magnetic field effects either in the water or steel other than from the cp current. Apparently, residual magnetism in the steel has been a historical source of error; and this has prompted concerns regarding accuracy. A relatively new version of this meter, designated as the MER (magnetic error resistive) is advertised as reducing this latter error by a factor of two or three. Of particular concern, however, is the lack of data where Swain meter measurements have been compared with independent current measurements under conditions relevant to offshore applications. Also, with this instrument there is no accuracy self-check; and unlike the $\Delta\phi$-MDE method, there is no way to incorporate judgment into evaluation of the results. Of two companies that were questioned, one related that they had difficulties training divers to properly use the instrument and that the current readings were sensitive to how the

sensor was oriented. The second company, on the other hand, was an advocate. The fact that Mateer obtained a good correlation between the Swain meter current measurements and anode-structure potential differences for the one structure he evaluated for which potential was uniform (see Figure 3-3) tends to support accuracy of the former approach, at least indirectly. It was decided to develop a set of experiments for the purpose of further understanding the utility of the Swain meter for i_{maint} determinations.

4. Two Probe IR Drop Determination

Pipeline cp surveys have historically involved determination of current density from the potential drop between two reference electrodes that are positioned at different radial distances from the structure. By knowing the resistance difference for these two radial positions, which can be calculated either by computer modeling techniques of from closed form expressions, the current can be determined. While this technique has not been widely employed for platforms, it was considered potentially useful for determining anode current output. This approach was, in fact, employed by Mateer to correct the anode potentials he measured using a stand-off reference electrode, as described above. It was considered that this technique should be investigated as a method for current demand determinations.

5. Anode Potential As a Current Demand Indicator

As a part of previous research that utilized the experimental arrangement in Figure 1-2 (12,21), potential and current data were acquired as a function of time from a series of aluminum-steel galvanic couples. Figure 3-4 presents typical results for one of these couples that was exposed in ambient laboratory temperature sea water with R_x = 149 Ω as a plot of ϕ_c versus i_c. Data at the upper right (relatively positive potentials and high current densities) pertain to the initial period of the exposure, whereas with increasing exposure time the steel polarized progressively according to a linear trend to the lower left (more negative potential and reduced current density). Except for an initial transient, the anode potential was relatively constant at about -1.04 $V_{Ag/AgCl}$ during this period of polarization. As the current density demand of the steel dropped below about 30 mA/m^2, however, potential of both the anode and cathode tended to become more positive. This was attributed to passivation or partial passivation of the anode. Figure 3-5 provides a plot of ϕ_a versus i_c in this low current density regime and reveals an apparent relationship between these two parameters such that a one mV change in ϕ_a

corresponded to a 0.36 mA/m^2 variation in i_c. Since the ϕ_a variations were random during this period, the interdependence was independent of time. On this basis, i_c can be estimated from measurement of the anode potential.

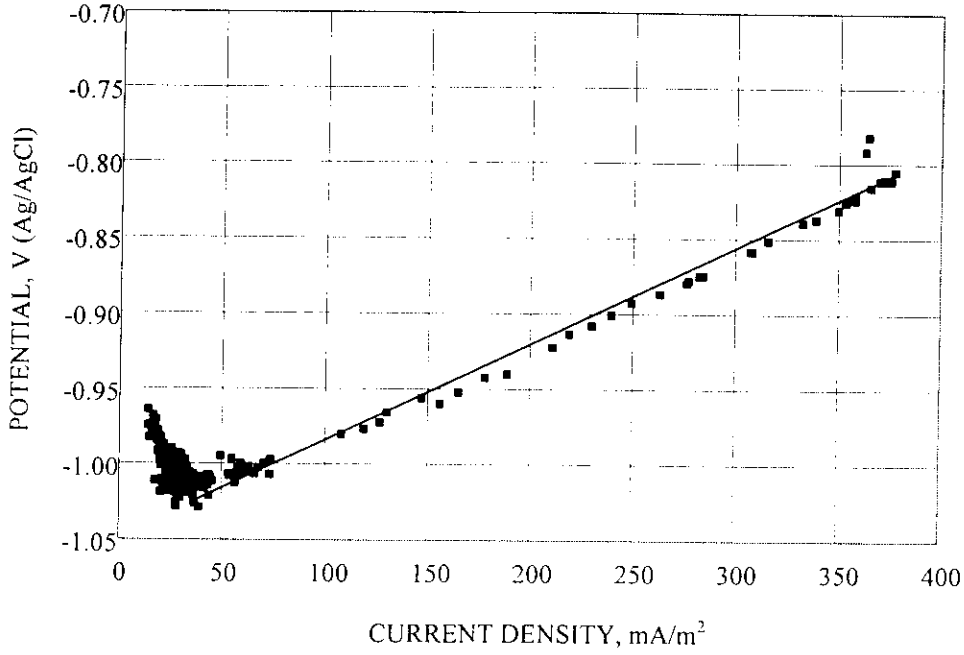

Figure 3-4: Plot of cathode potential versus cathode current density for a steel specimen that was cathodically polarized by coupling to a galvanic aluminum anode.

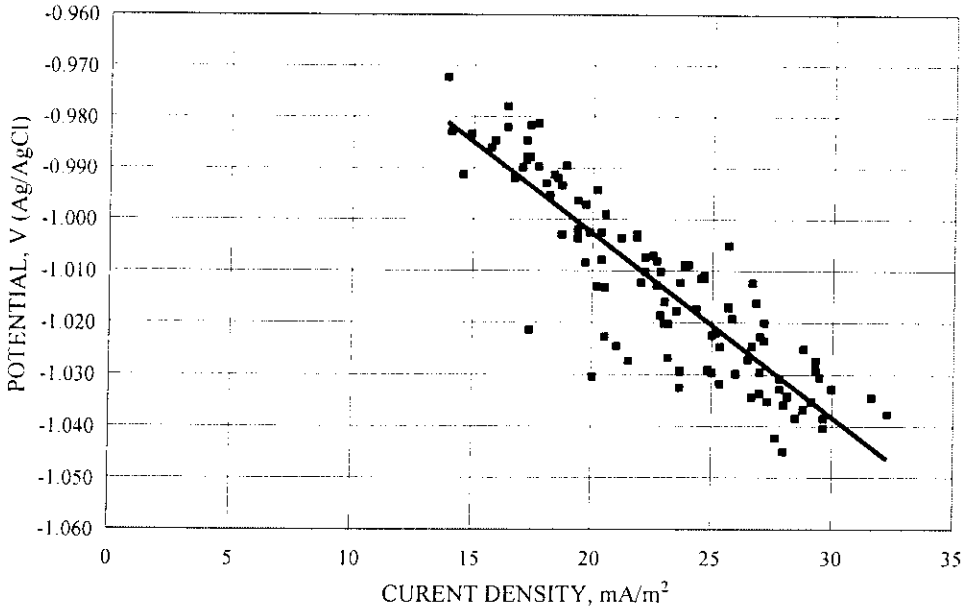

Figure 3-5: Plot of anode potential versus cathode current density in the low current density regime of Figure 3-4.

However, a review of survey data from the literature failed to confirm any ϕ_a-i_{maint} trend; and it was concluded that the relationship in Figure 3-5 may hold for individual anode-cathode pairs but that it cannot be quantitatively generalized. Consequently, this possible approach to i_{maint} determination was not pursued.

Research Approach

Experiments

Anode Configuration. Three 1.5 m (5.0 foot) long by 102 mm (4.0 inch) square cross-section indium activated aluminum anode castings with a centrally positioned 51 mm (2.0 inch) diameter steel core were acquired from Corrtherm, Inc. Chemical composition for these anodes is listed in Table 3-1. A 102 mm (4.0 inch) diameter steel pipe section was welded to each end of the anode core to simulate configurationally the stand-offs of an actual anode so that the Swain meter measurements could be performed under realistic conditions. Each of the two tubulars of an anode was welded to an approximately 0.3 m (1.0 foot) square steel plate that represented an ajoining tubular brace or cord member. The anode stand-off distance was approximately 0.3 m (1.0 foot). Figure 3-6 illustrates this configuration schematically. The anodes were exposed in 1.5-2.5 m (5-8 feet) deep natural sea water at the Naval Research Corrosion Laboratory in Key West (NRLKW) and were electrically coupled to an uncoated steel sea wall through a current controlling resistor. Figure 3-7 illustrates this arrangement schematically. Included in the electrical wiring for each stand-off was a 0.01 Ω resistor, such that net current output of each anode could be measured as a voltage drop independent of the other methods. Figure 3-8 provides a schematic illustration of this circuit, and Figure 3-9 shows a photograph of an anode assembly prior to deployment.

Table 3-1: Chemical composition for anodes.

ANALYSIS NUMBER	COMPOSITION, w/o						
	Zn	In	Hg	Si	Cu	Fe	Cd
1	5.61	0.028	-	0.033	0.001	0.046	<0.002
2	5.72	0.028	-	0.032	0.0009	0.046	<0.002

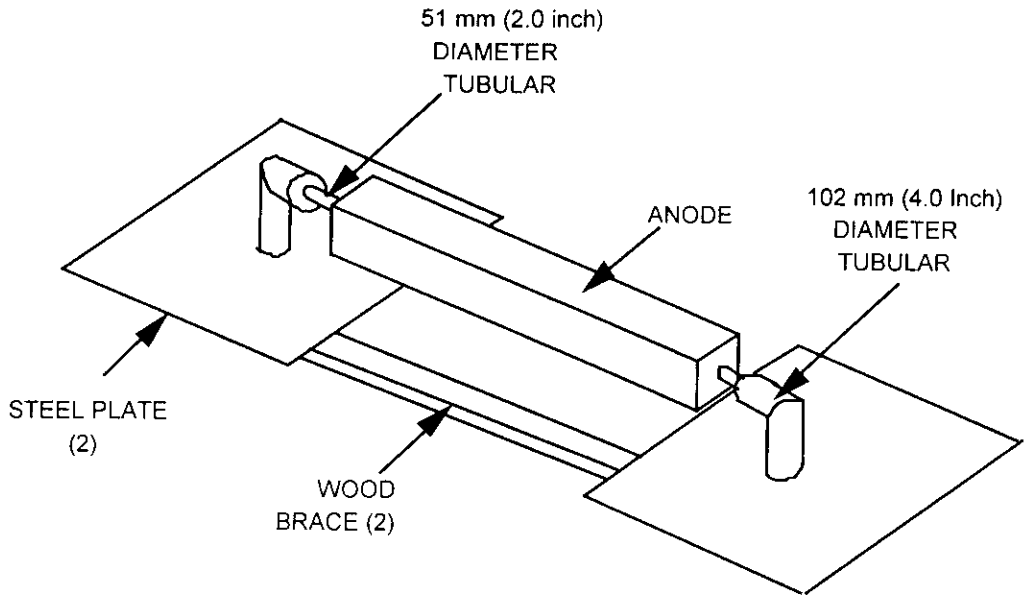

Figure 3-6: Schematic illustration of anode configuration.

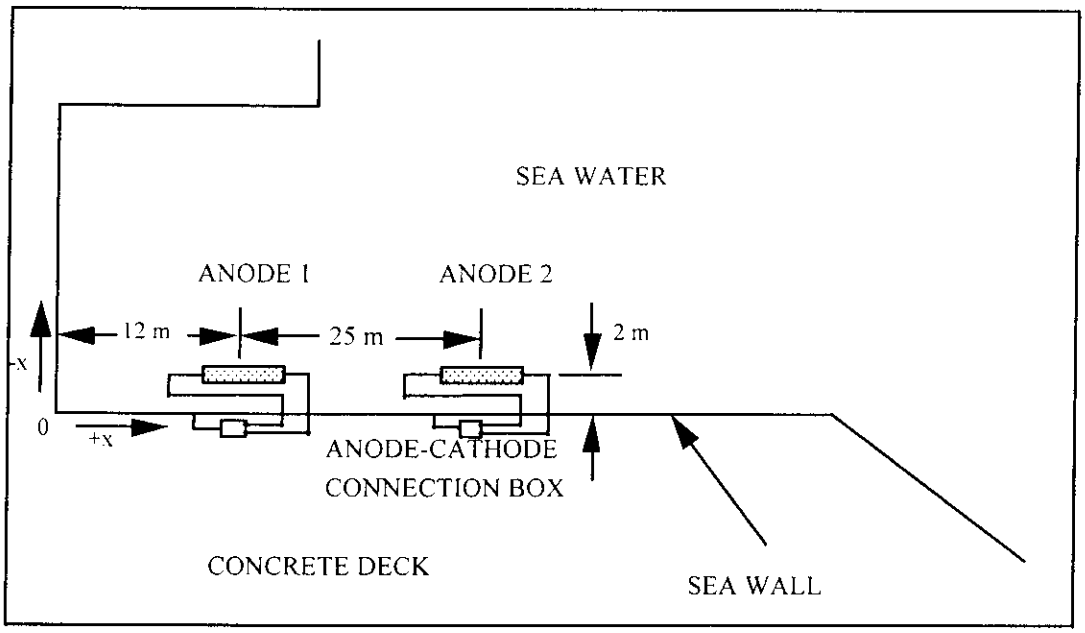

Figure 3-7: Schematic illustration of the deployment site and anode arrangement.

Measurement Procedures. Anode current outputs were measured according to each of the three techniques listed below:

1. Voltage drop across 0.01 Ω resistors,

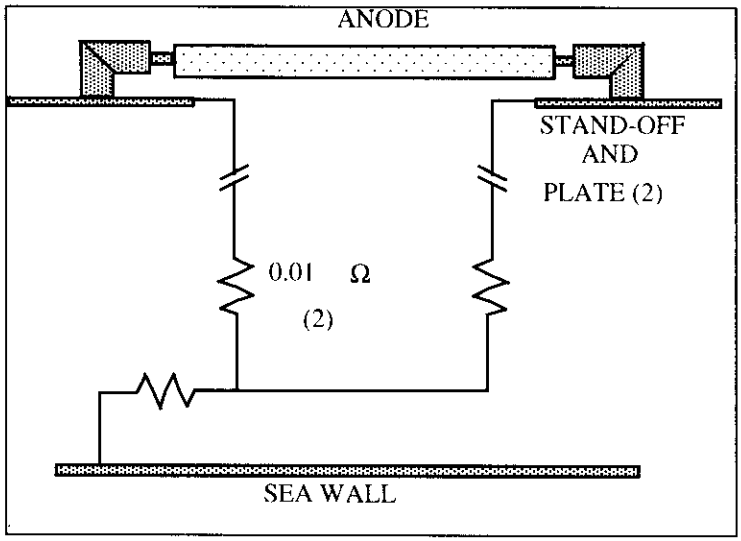

Figure 3-8: Electrical circuitry for anode test arrangement.

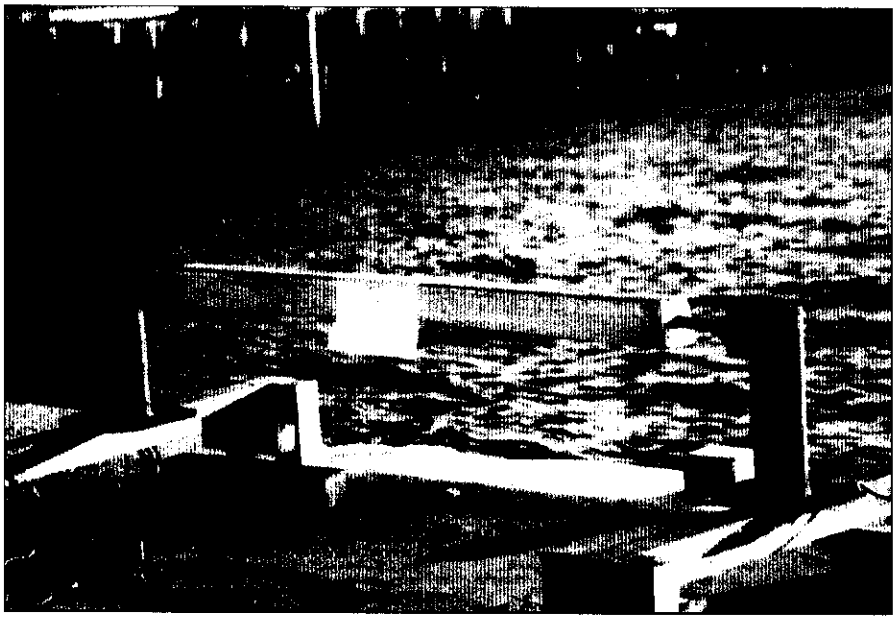

Figure 3-9: Photograph of an anode assembly beside the sea wall prior to deployment.

2. Swain meter, and

3. Two electrode potential drop.

The first of these, voltage drop across 0.01 Ω resistors, is first principles based and reflects generally accepted corrosion current measurement practice.

The procedure employed for the Swain meter measurements involved taking reading pairs (one reading with the sensor about the current conducting element in one orientation and a second with the sensor reversed (in the 180° orientation)) and then averaging the absolute value of these (one reading is negative and the other positive) to yield a single datum. This was repeated at each of the following five locations:

1. About the lead wire where this connects to the plate upon which the anode is attached,
2. About the stand-off where this is welded to the plate,
3. At the mid-height of the stand-off,
4. At the stand-off 90° weld, and
5. About the core adjacent to the anode.

Each of these locations is identified in Figure 3-10. Factors considered in making measurements at multiple locations were, first, the need to develop information regarding how component geometry or geometry differences might affect readings and, second, the fact that the plate and standoff pair, in addition to the sea wall, are receiving current, the magnitude of which is not indicated by the voltage drop across the 0.01 Ω shunt.

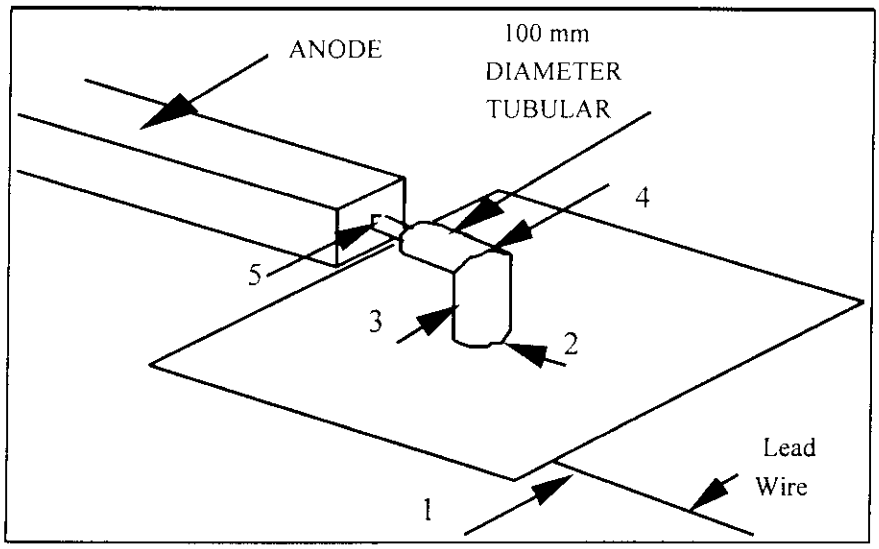

Figure 3-10: Swain meter measurement location.

Field gradient measurements, on the other hand, were based upon the experimental arrangement shown in Figure 3-11, where a Ag/AgCl reference electrode was positioned above

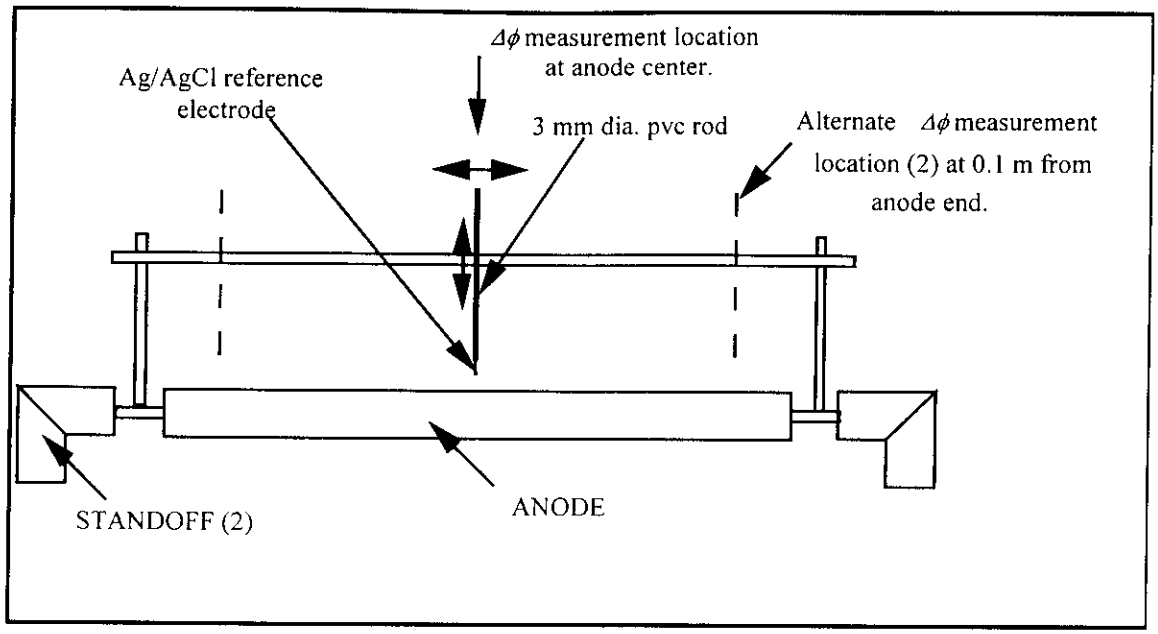

Figure 3-11: Schematic illustration of the experimental arrangement and locations for field gradient measurements.

the anode and potential readings were recorded at different distances. As indicated, these measurements were performed at three different locations along the anode length.

Structure Surveys

Project personnel participated in potential surveys on three Gulf of Mexico platforms during the summer of 1998. The purpose of this was to apply the *Δφ-MDE* and Swain meter methods for I_a determination to actual structures and to define the utility and limitations of each. Table 3-2 provides a listing of these structures and basic information regarding each.

The age of EI354D (three years) should disqualify it as a retrofit candidate. However, from the standpoint of evaluating the I_a determination methods (Swain meter and *Δφ–MDE*), this was not of principal concern. As indicated in Table 3-2, EI 176-JT has an unusual anode configuration. In all cases, the surveys were performed by divers as opposed to ROV (FAU participation was limited for GB 236A to a maximum depth of –61 m (-200 ft) but below this an ROV was used). Diver mounted video was employed in the case of GB 236A and EI 176 JT but not EI 354D.

Table 3-2: Listing of surveyed structures.

STRUCTURE	AGE, years	WATER DEPTH, m(ft)	ORIG. ANODE DIMENSIONS	ANODE TYPE	SURVEY COMPANY
Eugene Island (EI) 354D (Texaco)	3	91 (300)	7.75"x10.75"x8"*	Al, End Exiting Core	AOD & Deepwater. Corr. Services
Garden Banks (GB) 236A (Chevron)	18	209 (685)	-	Al, End Exiting Core	Global and OPS
Eugene Island (EI) 176-JT (Shell)	30	24 (80)	-	Al, Goalpost, Paired at 90o on Legs	AOD & Deepwater. Corr. Services

*Not verified by survey (present dimensions greater than indicated on drawings).

For each structure, the potential measurements involved a diver held reference electrode that was moved along the surface of the members and anodes. The resultant data were electronically entered into a spreadsheet at intervals triggered by a topside technician. As such, there was no specific distance between successive data acquisitions. The diver verbally indicated when the electrode was being traversed from a structural member to an anode and visa versa. Swain meter measurements were made using a 12.7 cm (5.0 inch) diameter clip. Prior to the measurements the standoffs but not the anodes were cleaned of fouling.

Results and Discussion

Experiments

Δϕ-MDE Method. Figure 3-12 plots cathode potential, as acquired approximately three months after anode deployment at NRLKW, as a function of position along the seawall for two of the anodes (the third was disconnected at this time) and shows that protection had been achieved for the portion of the seawall directly opposite or closest to each anode. As, indicated, the measured potential varied slightly depending upon which of two stud welded connections to the seawall was employed. The reason for this is unclear, but it may have been due to contact resistance between the heavily corroded, various seawall sheet pile sections. Table 3-3 provides the results of calculations based upon two ϕ_c choices according to the equation

$$I_a = (\phi_c - \phi_a) \cdot R_a . \qquad (3\text{-}5$$

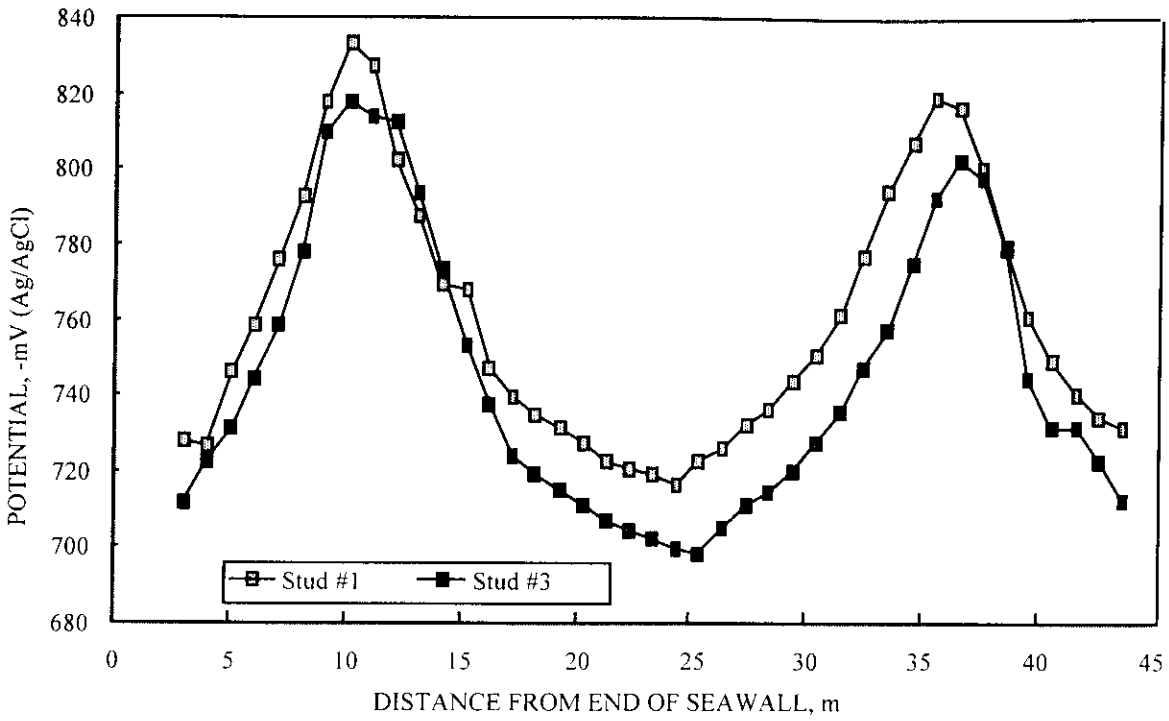

Figure 3-12: Potential as a function of position along the seawall after approximately three months exposure.

A critical aspect of this is determination of the values of ϕ_a and ϕ_c that are employed in the calculation. In the present case, these were the average ϕ_a and the average ϕ_c over a certain distance to either side of the anode (either 3 or 5 m (10 or 16.5 feet, respectively)). These distances were selected based upon hindsight that resulted from independent current calculations from the measured voltage drop across the shunts. Also listed is the value for ϕ_c that gave the same result as for current calculated from the shunt voltage drop. Complicating features of this experiment were that, first, the measured ϕ_a for Anode 1 was abnormally negative, the reason for this being unclear, and, second, the relatively steep potential gradient along the sea wall. Either or both of these factors complicated specification of the respective ϕ_a and ϕ_c values or resulted in error for these. As such, no method was defined for establishing the most appropriate value for ϕ_a and ϕ_c that should be used in conjunction with the $\Delta\phi$-*MDE* method. It was considered, however, that this approach would be pursued further in the field surveys.

Swain Meter. Table 3-4 presents typical results of shunt and Swain meter measurements that were recorded approximately two month after the anodes were deployed (the current limiting resistance values were different here compared to the time when the data in Figure 3-12 and

Table 3-3: Seawall potential survey data and anode current output calculations.

	ϕ_c (3 m avg.), $V_{Ag/AgCl}$	ϕ_c (5 m avg.), $V_{Ag/AgCl}$	AVG. ϕ_a, $V_{Ag/AgCl}$	Ia (3 m ϕ_c avg.), A	Ia (5 m ϕ_c avg.), A	I_a (shunt), A	I_a RATIO (actual to 3 m avg), A	I_a RATIO (actual to 5 m avg), A	ϕ_c TO YIELD ACTUAL I_a, $V_{Ag/AgCl}$
Stud 1									
Anode 1	-0.826	-0.815	-1.139	4.156	4.303	3.502	0.843	0.814	-0.875
Anode 2	0.-812	-0.795	-1.080	3.559	3.785	3.641	0.978	1.036	-0.810
Stud 2									
Anode 1	-0.806	-0.747	-1.139	4.422	5.206	3.502	0.792	0.673	-0.875
Anode 2	-0.797	-0.789	-1.080	3.758	3.865	3.641	0.969	0.942	-0.806

Table 3-3 were acquired). These data indicate that, first, the scatter between the different measurements sites (Figure 3-10) was small and within the anticipated experimental error and, second, the currents measured with the Swain meter were in excellent agreement with those calculated from the voltage drop across the shunts.

Table 3-4: Anode current output data from shunts and Swain meter.

ANODE NUMBER	V (SHUNT), mV		I, A (Shunt)			CURRENT, A (Swain Meter)							
	L	R	L	R	Total		Left			Right			Total
							Pos.	Neg.	Avg.	Pos.	Neg.	Avg.	
1	22.57	23.49	2.26	2.35	4.61	Site 1	2.39	2.37	2.38	2.29	2.25	2.27	4.65
						Site 2	2.40	2.41	2.41	2.20	2.30	2.25	4.66
						Site 3	2.29	2.40	2.36	2.26	2.21	2.24	4.60
						Site 4	-	-	-	-	-	-	-
						Site 5	2.40	2.31	2.36	2.26	2.21	2.34	4.70
						Avg.							4.65
2	4.6	4.77	0.46	0.48	0.94	Site 1	0.44	0.45	0.45	0.46	0.45	0.46	0.91
						Site 2	0.36	0.51	0.46	0.36	0.40	0.38	0.84
						Site 3	0.43	0.43	0.43	0.36	0.40	0.38	0.81
						Site 4	-	-	-	-	-	-	-
						Site 5	0.40	0.39	0.40	0.43	0.42	0.43	0.83
						Avg.							0.85

An additional experiment was performed where the Swain meter was used with both a 13 and 30 cm (5.0 and 12 inch, respectively) clip to measure current through stand-offs. Doing this considered that the larger clip should be advantageous for situations where stand-offs are heavily fouled. For this experiment, all three anodes were connected to the sea wall with the external

resistors sized to provide target current outputs of 4, 2, and 1 A. Table 3-5 presents the data from these measurements and shows that current readings for each of the two clips are in excellent mutual agreement and correspond closely with results from the shunt measurements. It was concluded based upon the above results that the Swain meter provided an accurate determination of anode current output for the present experimental arrangement.

Table 3-5: Comparison of shunt and Swain meter current determinations using two different clip sizes.

ANODE NUMBER	STANOFF	*I* (Swain, 13 cm clip), A	*I* (Swain, 30 cm clip), A	*I* (Shunt), A
1	Left	2.23	2.22	2.12
	Right	2.09	2.09	2.20
	Both	4.32	4.31	4.32
2	Left	1.02	1.09	1.01
	Right	1.13	1.13	1.09
	Both	2.15	2.22	2.1
3	Left	0.43	0.49	0.43
	Right	0.40	0.43	0.42
	Both	0.83	0.92	0.85

Field Gradient Results. Table 3-6 lists typical results from the field gradient measurements upon two anodes. Comparison of these with the Swain meter results from Table 3-4 reveals that currents calculated from the field gradient measurements were less than the Swain meter ones by approximately a factor of two. The fact that projection of anode current output by field gradient determinations is first principles based indicates that there must have been a systematic problem or error in the data collection; however, the cause of this was not determined. A difficulty with applying this procedure on actual offshore structures may arise from complexities of the electric field in the vicinity of any one anode from presence of the others. It was concluded that this technique was not practical for this application, and it was not pursued further.

Structure Surveys

General. A critical aspect of evaluating and qualifying the *Δϕ-MDE* method involved

Table 3-6: Typical field gradient measurement results.

ANODE NO.	READING NUMBER	REF. ELECT.	r_{eff}, cm	ϕ, $V_{Ag/AgCl}$	$\Delta\phi$ (1-2), Ohm's	R (Eqn 1-17), Ohms	ΔR, Ohms	I, A
1	1	1	10.16	-1.009	0.024	0.0641	0.0084	2.82
		2	15.24	-0.985		0.0557		
	2	1	10.16	-1.013	0.024	0.0641	0.0084	2.93
		2	15.24	-0.989		0.0557		
	3	1	10.16	-1.000	0.014	0.0641	0.0084	1.64
		2	15.24	-0.986		0.0557		
							Avg.	2.46
2	1	1	10.16	-1.056	0.009	0.0641	0.0084	1.14
		2	15.24	-1.047		0.0557		
	2	1	10.16	-1.062	0.03	0.0641	0.0084	1.37
		2	15.24	-1.020		0.0557		
	3	1	10.16	-1.066	0.022	0.0641	0.0084	1.12
		2	15.24	-1.034		0.0557		
							Avg.	1.21

addressment of the following factors:

1. Accuracy with which ϕ_c and ϕ_a are measured,
2. Appropriateness of the criterion that is established for defining values for the ϕ_c and ϕ_a terms in Equation 3-5, and
3. Accuracy with which anode radius and length are measured.

With regard to Item 1 and, specifically, to the technique for measuring ϕ_a, a method was developed that was considered an improvement over the procedures of both Mateer (39) and Deepwater Corrosion Services (40). By this, the reference electrode is traversed along the fouled anodes (prior to cleaning). The fact that the resultant potential readings differ from the true ϕ_a (measured with the reference electrode positioned directly upon the anode surface or with the voltage drop eliminated) by the magnitude of the voltage drop through the fouling layer was compensated for by using the fouled anode radius and length in the Dwight equation calculation (Equation 1-17).

In the case of Item 2, a criterion was adapted whereby ϕ_a is taken as the most negative value recorded during the potential scan of each anode and ϕ_c as either the most positive value for the

structural member in question or the far field value if this is available. An explanation for these choices is presented subsequently. With regard to the third of these concerns (error/inaccuracy in anode dimension determinations), Figure 3-13 plots R_a, as calculated using Dwight's modified equation (Equation 1-17), versus r for a 244 cm long anode in 20 $\Omega \cdot$cm water. Radii corresponding to the r_{eff} value of an uncorroded conventional 330 kg anode, with and without 7.6 cm (3.0 inches) of fouling buildup (the reason for this determination is presented subsequently), and for this same anode at 50 and 80 percent depletion are identified. Also shown are the corresponding I_a versus r trends for $\Delta\phi$ values of 0.005 and 0.200 V. These latter values are likely to encompass the range of driving voltages that exist on older structures. Correspondingly, the error that occurs in the calculated value for R_a as a consequence of measurement error in r is shown in Figure 3-14 for examples where the actual r is 13.7 cm (r_{eff} for a 330 kg anode based upon its original dimensions), 10.5 cm (r_{eff} for a 50 percent depleted 330 kg anode), and 8.0 cm (r_{eff} for an 80 percent depleted 330 kg anode). Relatedly, Figure 3-15 shows how the error in the calculated anode current output varies as a function of measurement error for anode radius and reveals the former term to be relatively insensitive to variations in the latter. Thus, while accurate measurement of anode radius is difficult, the fact that this is included in Dwight's modified

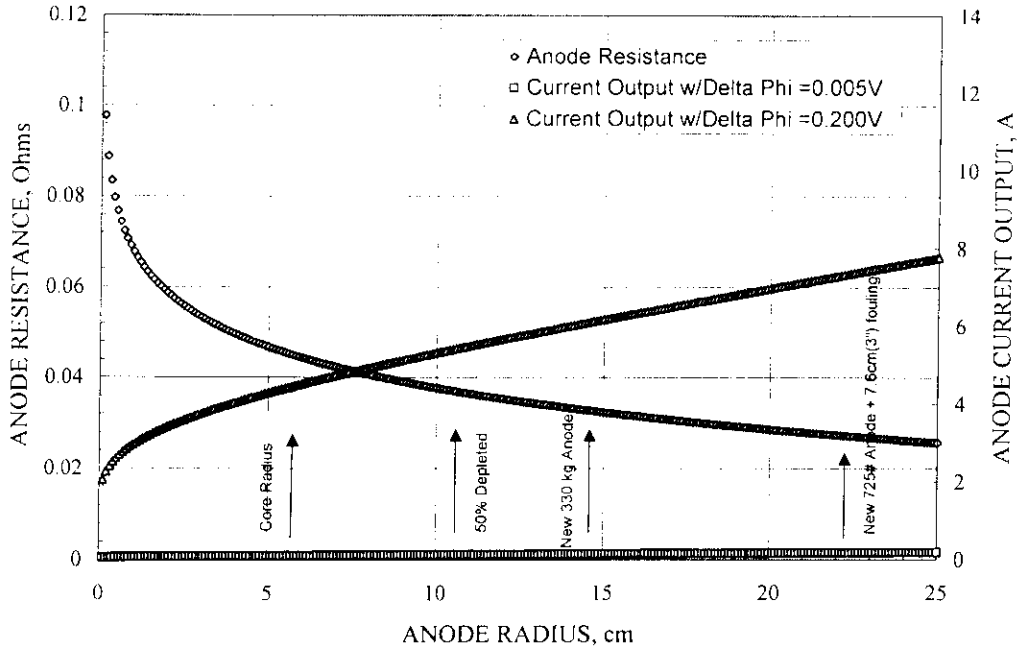

Figure 3-13: Plot of anode resistance as a function of anode radius for a 244 cm long anode. Values for the current output at two driving voltages are also illustrated.

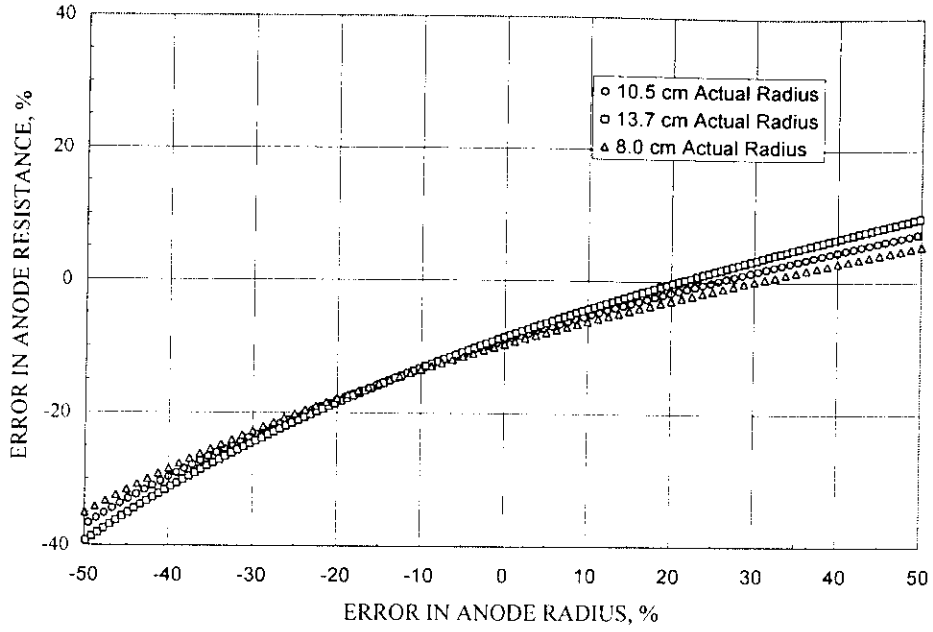

Figure 3-14: Plot of the error in calculated anode resistance as a function of measurement error of anode radius.

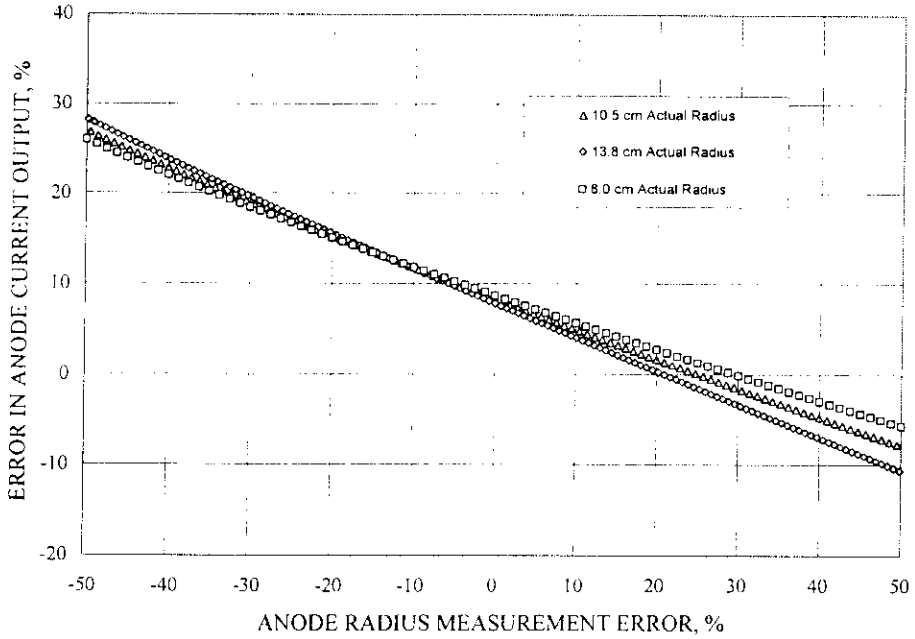

Figure 3-15: Plot of error in the calculated anode current output as a function of measurement error for anode radius.

equation as a logarithmic term renders R_a and I_a relatively insensitive to errors in its measurement.

Inspection Survey Protocol. Based upon the above considerations, a protocol for acquiring data for application of Equation 3-5 and for making other projections relevant to retrofitting was developed. This is included here as Appendix III-A.

Survey Data and Analyses. Figures 3-16 and 3-17 show examples of the resultant data as plots of potential versus reference electrode position along the respective members, as recorded for platform EI354D. These indicate that the structure potential became progressively more positive with increasing distance from the anode and that anode potentials tended to be relatively positive near the ends. This latter point may have been an artifact of transitioning the reference electrode from the structural member to the anode and visa versa, and occurrence of these relatively positive ϕ_a values was the reason for adapting the most negative potential as the value for ϕ_a. On the other hand, the ϕ_c employed was the most positive value recorded for the particular structural member in question. In some cases the diver swam into the central area of the structure some distance from any anode and steel and recorded a "semi-remote" potential; and this was used as ϕ_c. The rational behind this considered that since Dwight's modified equation (Equation 1-17) determines R_a with respect to "remote earth," the corresponding ϕ_c should be that of the "far field." For EI354D, anode dimensions were determined from diver measurements upon cleaned anodes (no video for the survey of this structure was available), whereas for GB236A and EI176-JT they were estimated from video images such that the r value that was employed in Equation 3-5 included thickness of the fouled layer. This is appropriate since the reference electrode was invariably positioned upon the fouled surface and not directly on the anode, as explained above. In the case of structure EI354D, the Equation 3-5 calculation was also made using r values that were increased by 25 and 50 mm (1.0 and 2.0 in., respectively) compared to the actual measured ones to address the probability that a fouling layer of some unknown thickness was present. This, however, made little difference in the results because of the relative insensitivity of R_a upon r.

The Swain meter measurements were acquired using the same procedure that was developed in conjunction with the anode exposures at NRLKW, as detailed above. These employed a 127 mm (5.0 in.) diameter clip, which was sufficiently large for the stand-offs in question once the fouling was removed, and making current measurements at each of three locations on each stand-off (adjacent to the anode, adjacent to the member, and at the mid-position) with the clip oriented both positively and negatively. A net current per stand-off was determined as the average of the three readings, where each reading was the average of the two clip orientation readings. The net anode current output was determined as the sum of the two stand-off currents.

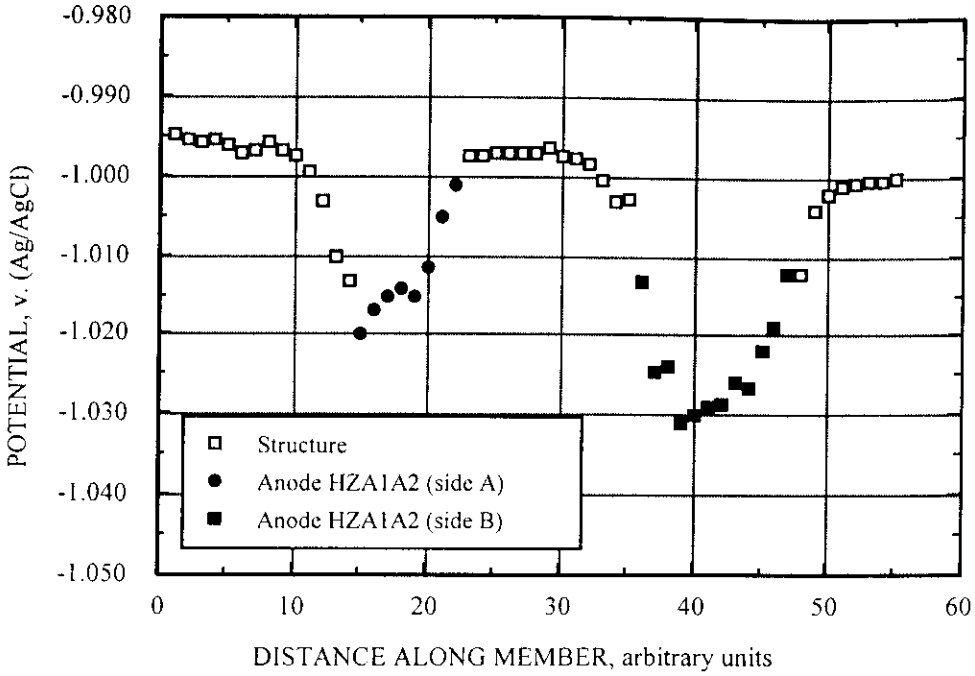

Figure 3-16: Potential as a function of distance for member with anodes HZA1A2(side A) and HZA1A2(sideB).

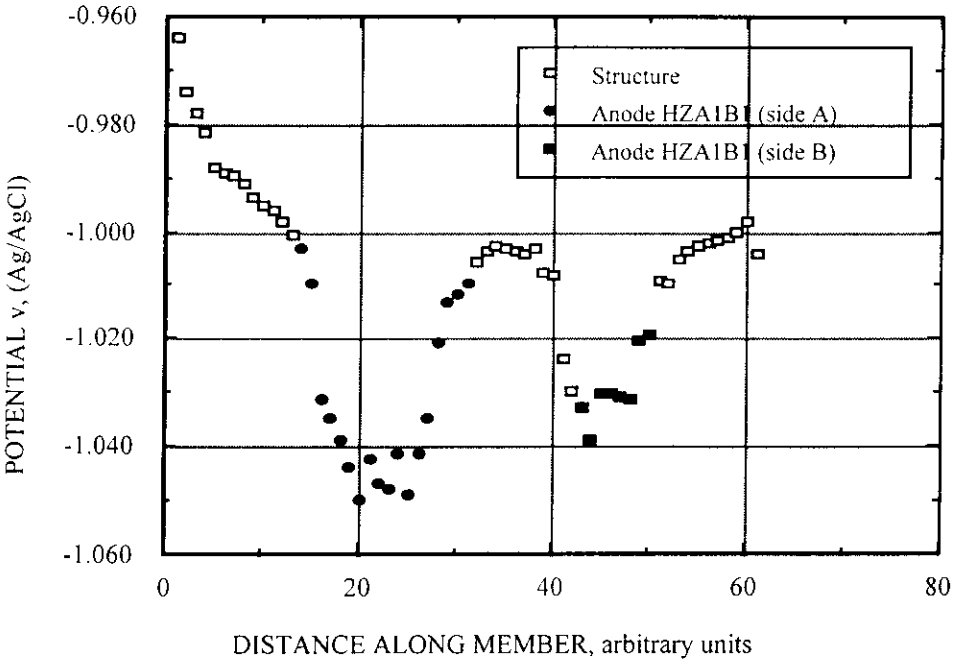

Figure 3-17: Potential as a function of distance for member with anodes HZA1B1(side A) and HZA1B1(sideB).

Structure maintenance current density, i_{maint}, was, in turn, determined from the expression

$$i_{maint} = \frac{\bar{I}_a \cdot N}{A_c}, \qquad (3\text{-}6$$

where $\bar{I}_a$ is the average current output per anode as determined from the Swain meter measurements. It was assumed that one-seventh of the total current extended into the mud zone.

EI354D. Tables 3-7, 3-8, and 3-9 present the results of calculations and measurements that were made in conjunction with the three surveyed anodes on this structure. These data indicate that I_a values determined by the *Δϕ-MDE* method ranged from about 75 to over 200 percent of those projected by the Swain meter. For the three anodes overall, the net current indicated by the Swain meter was 4.50 A and via the *Δϕ-MDE* method 5.97-6.81 A depending upon the assumed reference electrode location relative to the actual anode surface. This amounts to a difference between the two methods of 25-34 percent. Table 3-10 lists information relevant to projection of i_{maint} and shows this to be 21 mA/m^2.

Table 3-7: Current output determinations for anode HZA1A2 according to the *Δϕ-MDE* method and comparison of this with Swain meter measurements.

ANODE NO. HZA1A2	ASSUMED DISTANCE OF REF. ELECT. FROM FOULED ANODE SURFACE, mm(in.)		
	0 (0)	25 (1.0)	50 (2.0)
R_a, Ohms	0.0293	0.0275	0.0260
ϕ_c(max), $V_{Ag/AgCl}$	-0.995		
ϕ_a (min), $V_{Ag/AgCl}$	-1.020		
I_a (*Δϕ-MDE*), A	0.851	0.906	0.961
I_a (Swain), A	1.159		
I_a(*Δϕ-MDE*)/I_a Swain	0.73	0.78	0.83

GB236A (Chevron): In the case of this structure, measurements to evaluate the *Δϕ-MDE* method were made on six anodes, with the data being given in Table 3-11. Calculated I_a values and Swain meter measurements are shown in Table 3-12. These indicate that the ratio I_a(*Δϕ-MDE*)/I_a(*Swain*) varies from 0.69 to 1.69 with an average on 1.11. Thus, while relatively large distinctions in I_a are apparent between the two methods, as for structure EI354D, these tended to balance out such that the overall average difference was only by 11 percent. The i_{maint} for this

Table 3-8: Current output determinations for anode HZA1B1-A according to the $\Delta\phi$-*MDE* method and comparison of this with Swain meter measurements.

ANODE NO. HZA1B1-A	ASSUMED DISTANCE OF REF. ELECT. FROM FOULED ANODE SURFACE, mm(in.)		
	0 (0)	25 (1.0)	50 (2.0)
R_a, Ohms	0.033	0.0306	0.0286
ϕ_c(max), $V_{Ag/AgCl}$	-0.964		
ϕ_a (min), $V_{Ag/AgCl}$	-1.050		
I_a ($\Delta\phi$-*MDE*), A	2.607	2.809	3.004
I_a (Swain), A	1.319		
I_a($\Delta\phi$-*MDE*)/I_a Swain	1.98	2.13	2.28

Table 3-9: Current output determinations for anode HZA1B1-B according to the $\Delta\phi$-*MDE* method and comparison of this with Swain meter measurements.

ANODE NO. HZA1B1-B	ASSUMED DISTANCE OF REF. ELECT. FROM FOULED ANODE SURFACE, mm(in.)		
	0 (0)	25 (1.0)	50 (2.0)
R_a, Ohms	0.0299	0.0280	0.0264
ϕ_c(max), $V_{Ag/AgCl}$	-0.964		
ϕ_a (min), $V_{Ag/AgCl}$	-1.039		
I_a ($\Delta\phi$-*MDE*), A	2.508	2.679	2.841
I_a (Swain), A	2.018		
I_a($\Delta\phi$-*MDE*)/I_a Swain	1.24	1.33	1.41

Table 3-10: Maintenance current density (calculated from the Swain meter anode current output) and parameters relevant to its determination for structure EI354D.

	EI354D
Submerged Surface Area, m^2	8,606
Mud Area, m^2	3,522
Number of Anodes	141
Average Current Output per Anode, A	1.5
Total Anode Current, A	211
Maintenance Current Density, mA/m^2	21.1

structure was determined to be 15 mA/m^2, as indicated by Table 3-13. Also listed are parameters relevant to this calculation.

EI176-JT (Shell): Table 3-14 presents the anode dimensions and ϕ_c and ϕ_a data for this structure; and Table 3-15 shows the computed I_a values, as determined by the $\Delta\phi$-*MDE* method, and the

Table 3-11:Anode dimensions and ϕ_a and ϕ_c values, as measured for structure GB236A.

ANODE NO.	ANODE LOC., m	AVG. ANODE CIRCUM., m	AVG. ANODE LENGTH, m	PRE-CLEAN EST. DEPL., %	REMOTE ϕc, VAg/AgCl	MIN. ϕa, VAg/AgCl
1	-30	0.861	2.45	40	-0.976	-0.976
2	-11	0.851	2.46	30	-0.975	-0.999
3	-11	0.856	2.45	35	-0.975	-0.997
4	-11	0.853	2.15	35	-0.976	-0.997
5	-17	0.831	2.32	25	-0.971	-0.997
6	-11	0.889	2.52	50	-0.947	-0.994

Table 3-12: Current output determinations for anodes on structure GB236A according to the *Δϕ-MDE* method and comparison of these with Swain meter measurements.

ANODE NO.	I_a, A (Remote ϕ_c and Minimum ϕ_a w/ R_a=*r(eff)*+10mm)	I_a, A (Swain Meter)	I_a(*Δϕ-MDE*)/ I_a (Swain)
1	0.731	0.433	1.69
2	0.812	0.968	0.84
3	0.729	1.055	0.69
4	0.644	0.447	1.44
5	0.825	0.688	1.20
6	0.786	1.016	0.77
		Average I_a Ratio	1.11

Table 3-13: Maintenance current density (calculated from the Swain meter anode current output) and parameters relevant to its determination for structure GB236A.

	GB236A
Submerged Surface Area, m^2	627,274
Mud Area, m^2	109,900
Number of Anodes	1,362
Average Current Output per Anode, A	0.77
Total Anode Current, A	1046
Maintenance Current Density, mA/m^2	15

Swain meter I_a measurements and a comparison of the two. As noted in conjunction with Table 3-2, the anodes in this case were mounted upon legs in pairs at a common elevation. As such, the anodes in each pair were sufficiently close to one another that overlap (interaction) of the respective potential/current fields was anticipated. Consequently, anode resistance for each pair, R_{II}, was computed using the expression (41)

$$R_{II} = \frac{1}{2}[R(r) + R(D)], \qquad (3\text{-}7$$

Table 3-14:Anode dimensions and ϕ_a and ϕ_c values, as measured for structure EI176-JT.

ANODE DESIGNATION		DEPTH, m	AVG. ANODE CIRCUM., m	AVG. ANODE LENGTH, m	EST. DEPL., % Pre/Post Clean)	REMOTE ϕ_c, $V_{Ag/AgCl}$	MIN. ϕ_a, $V_{Ag/AgCl}$
	B Face	-6.1	0.884	2.29	30/30	-0.881	-0.927
Along	Row 1 Side	-6.1	0.828	2.44	30/40		
B leg	Row 1 Side	-16.2	0.726	2.18	30/35	-0.881	-0.945
	B Face	-16.2	0.889	2.13	30/35		

Table 3-15: Current output determinations for anodes on structure EI176-JT according to the *Δϕ-MDE* method and comparison of these with Swain meter measurements.

ANODE DESIGNATION		I_a, A (Remote ϕ_c and Minimum ϕ_a w/ R_a=*r(eff)*+64mm)	I_a, A (Swain Meter)		I_a(*Δϕ-MDE*)/ I_a (Swain)
			Individual	Anode Pairs	
	B Face	2.265	1.563	2.802	0.81
Along	Row 1 Side		1.239		
B leg	Row 1 Side	2.963	1.249	2.673	1.11
	B Face		1.424		
			Average I_a Ratio		0.96

where *R(r)* is the resistance of a single anode of effective radius *r* and *R(D)* is the resistance of a cylindrical anode of diameter *D*, where *D* is the distance between the two anodes in question. Thus, the anode current outputs in Table 3-15, as determined by the *Δϕ-MDE* method, are for each anode pair. Also, average fouling thickness on these anodes was 64 mm (2.5 in.), as estimated from the video; and the effective radius employed in conjunction with determination of R_a (Equation 1-17) included this.

Table 3-16 presents information used to calculate i_{maint} for this structure and shows the value for this parameter as 25 mA/m^2. However, no mud, conductor, conductor guide, or other non-structural member surface areas were available; and so this i_{maint} is probably an overestimation.

Summary

General. Table 3-17 summarizes current output data for the 13 anodes that were surveyed on the three structures according to each of the two methods (*Δϕ-MDE* and Swain meter). This

Table 3-16: Maintenance current density (calculated from the Swain meter anode current output) and parameters relevant to its determination for structure EI176-JT.

	EI176JT
Submerged Surface Area, m^2	9,465
Mud Area, m^2	-
Number of Anodes	19
Average Current Output per Anode, A	1.37
Total Anode Current, A	26
Maintenance Current Density, mA/m^2	25

Table 3-17: Summary of I_a data for all anodes surveyed.

ANODE NO.	AVG. CURRENT OUTPUT, A		$I_a(\Delta\phi\text{-}MDE)/I_a(Swain)$
	Δφ-MDE	Swain Meter	
EI354D			
HZA1A2	0.906	1.159	0.78
HZA1B1-A	2.809	1.319	2.13
HZA1B1-B	2.679	2.018	1.32
Sub-Avg.	2.131	1.499	1.42
GB236A			
GB236A-1	0.731	0.433	0.69
GB236A-2	0.812	0.968	0.84
GB236A-3	0.729	1.055	0.69
GB236A-4	0.644	0.447	1.44
GB236A-5	0.825	0.688	1.20
GB236A-6	0.786	1.016	0.77
Sub-Avg.	0.755	0.768	0.94
EI176-JT			
B Face (-6.1) Row 1 (-6.1)	2.265	2.801	0.81
B Face (-16.2) Row 1 (-6.1)	2.963	2.672	1.11
Sub-Avg.	2.614	2.737	0.96
Net Average	1.242	1.180	1.05

information shows that, although the difference was as high as a factor of 2.13 for a particular anode, overall the two sets of data differed by only five percent. Based upon the earlier evaluation of the Swain meter in conjunction with exposures at NRLKW, which showed this instrument to be accurate within several percent, the difference in the two sets of data probably reflects errors in the *Δφ-MDE* method. Also, Figure 3-18 illustrates the i_{maint} values for the three

structures in comparison to field data that are available from various literature sources (27). With the possible exception of the i_{maint} for structure EI176-JT, the two sets of current densities are mutually comparable (an explanation was given above for the relatively high i_{maint} for structure EI176-JT). Both the *Δϕ-MDE* method and the Swain meter measurements are qualified as appropriate procedures for determining I_a. Advantages and disadvantages of each of the two techniques are listed and below:

Δϕ-MDE Method. The advantages here include the following:

1. The method is first principles based.

2. The method can be applied based upon data that are invariably collected from a Level II or III survey, and so only analysis time is required.

3. Only far-field ϕ_c values are necessary, thus eliminating the need for a close interval survey of the structural members. This applies both to application of the *Δϕ-MDE*

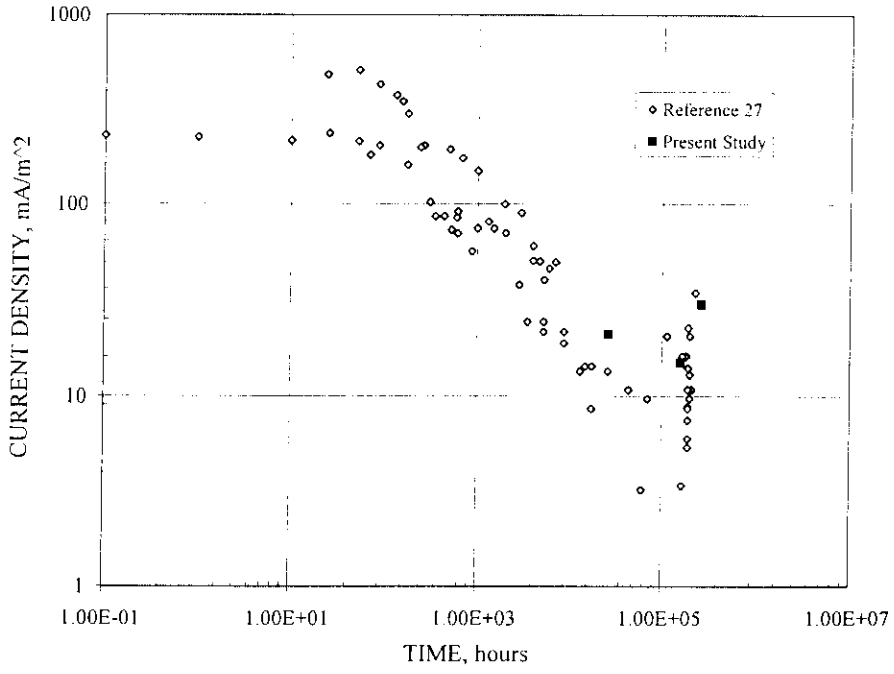

Figure 3-18: Plot of current density versus time showing a comparison of i_{maint} values for the three structures evaluated here in comparison to data from the literature (27).

method and to generalized aspects of assuring that protection is adequate since, if ϕ_c (semi-remote) is more negative than about -0.90 $V_{Ag/AgCl}$, it is unlikely that under-protection exists anywhere. This is the case because sea water cannot support a 100 mV voltage drop at the current densities present on older structures. Judgement must be exercised in acquiring ϕ_c(semi-remote) data, however, and consideration given to shielded areas such as within conductor arrays and to spatial variations (depth, for example).

4. Reference electrode error or lack of calibration is not a factor since the parameter of interest is the difference in potential ($\phi_c - \phi_a$).

The disadvantage is that relatively small absolute errors in measurement of ϕ_c or ϕ_a (or both) can translate to a large error in I_a. This is a consequence of these two potentials typically being close to one another on older structures. For example, if $\Delta\phi$ (ϕ_c - ϕ_a) is actually 20 mV and an error of 5 mV occurs in measuring each of these parameters, then the calculated I_a differs from the true value by from 50 to 200 percent depending upon the relative sense of the errors. However, this error is apparently random and not systematic.

Swain Meter. The primary advantage of the Swain meter, on the other hand, is that it is more accurate than the *Δϕ-MDE* method. Disadvantages include the following:

1. Calibration should be routinely verified, and there is no means to confirm accuracy of readings that are taken.

2. The clips and cabling, as presently manufactured, are not sufficiently rugged for offshore applications. Susceptibility of the clips to mechanical damage limits use to diver-held applications and precludes mounting on an ROV. Consequently, the method is applicable only to diver depth limits.

3. Additional effort beyond what might otherwise be employed is required.

IV. TASK II: RETROFIT CATHODIC PROTECTION DESIGN FOR DEPOLARIZED AND PARTIALLY DEPOLARIZED STRUCTURES

Background

The objective of this task was to determine the current demand to repolarize and maintain cathodic protection for depolarized and partially depolarized steel in sea water. This effort was predicated upon previous research (35) that implied that institution of adequate protection to previously under-protected steel could require an abnormally high current. Such a finding is relevant to retrofit cp where, in the worse cases, depolarization or partial depolarization has occurred. To accomplish this task, 24 108 mm internal diameter steel cathode pipe sections were exposed in a 0.03 m/s (0.1 ft/s) sea water flow loop while galvanically coupled to individual aluminum anode rings. It was originally intended that once these steel sections polarized and steady-state was achieved, three degrees of depolarization (potentials of –0.80 and –0.72 $V_{Ag/AgCl}$ and free corrosion) would be affected for three different times (6, 12, and 18 months); and then the specimens would be repolarized. The depolarization was affected by increasing the external resistance (R_x) between the anode and cathode which was intended to simulate anode expiration. This second polarization, on the other hand, represented response of the steel to a cp retrofit. The experiments involved determination of potential and current density demand history, first, during the period of depolarization and, second, upon repolarization until steady-state was achieved. Table 4-1 shows the originally proposed test matrix for this task.

Experimental System

Sections 152 mm (6.0 inches) long were saw cut from a 144 mm (4.5 inch) diameter by 3.7 m (12 foot) long UNS G10230 steel pipe, while rings of this same inside diameter were machined from a 330 kg Al-Zn-Hg anode casting. Figure 4-1 illustrates the final geometry, while Tables 4-2 and 4-3 indicate the chemical composition for each of these components. Subsequent to sectioning, the interior steel surface was sand blasted, acetone rinsed, and atmospherically exposed at the FAU Marine Laboratory (approximately 200 m inland from the Atlantic Ocean in Boca Raton) for six weeks. The machined surface of the Al anodes was acetone rinsed only.

Assembly of the test system involved compression fitting a pvc slip flange about each end of the steel sections and sealing the joint at the outer surface. The aluminum rings, on the other hand, were compression mounted between two flanges. These were then assembled in pairs as

Table 4-1: Originally proposed Task II Work Plan.

SPECIMEN NUMBER	TEST CONDITIONS*	PURPOSE OF TESTS
II-1 and 2	1. Atmospherically pre-rust. 2. Expose and protect at ~-1.00v until steady-state reached. 3. Free corrosion for 6 months (assumed potential -0.65v). 4. Repolarize to ~-1.00v and monitor potential and current.	To determine the affect of the time of complete depolarization upon the current demand upon reapplication of protection.
II-3 and 4	1. Atmospherically pre-rust. 2. Expose and protect at ~-1.00v until steady-state reached. 3. Free corrosion for 12 months (assumed potential ~-0.65 v. 4. Repolarize to ~-1.00v and monitor potential and current.	
II-5 and 6	1. Atmospherically pre-rust. 2. Expose and protect at ~-1.00v until steady-state reached. 3. Free corrosion for 18 months (assumed potential -0.65v). 4. Repolarize to ~-1.00v and monitor potential and current.	
II-7 and 8	Same as for Specimens II-1 and 2 except depolarization is to -0.72v.	To determine the affect of the time at one level of partial depolarization upon the current demand upon reapplication of protection.
II-9 and 10	Same as for Specimens II-3 and 4 except depolarization is to -0.72v.	
II-11 and 12	Same as for Specimens II-5 and 6 except depolarization is to -0.72v.	
II-13 and 14	Same as for Specimens II-1 and 2 except depolarization is to -0.80v.	To determine the affect of the time at a second level of partial depolarization upon the current demand upon reapplication of protection.
II-15 and 16	Same as for Specimens II-3 and 4 except depolarization is to -0.80v.	
II-17 and 18	Same as for Specimens II-5 and 6 except depolarization is to -0.80 v.	
II-19 and 20	Same as for Specimens II-1 and 2 except depolarization is affected gradually over 6-12 months.	To determine the affect of gradual depolarization upon potential-current density character and upon subsequent current demand once full cp is restored.
II-21 and 22	Same as for Specimens II-15 and16 except depolarization is affected gradually over 6-12 months.	To determine the affect of gradual depolarization upon potential-current density character and upon subsequent current demand once full cp is restored.

* All potentials referenced to Ag/AgCl.
Nominal velocity for all experiments 0.03m/s (0.1 ft/s).

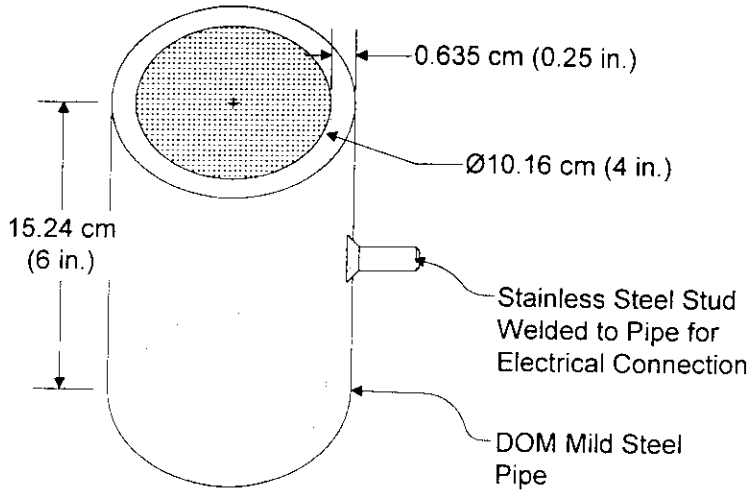

(a)

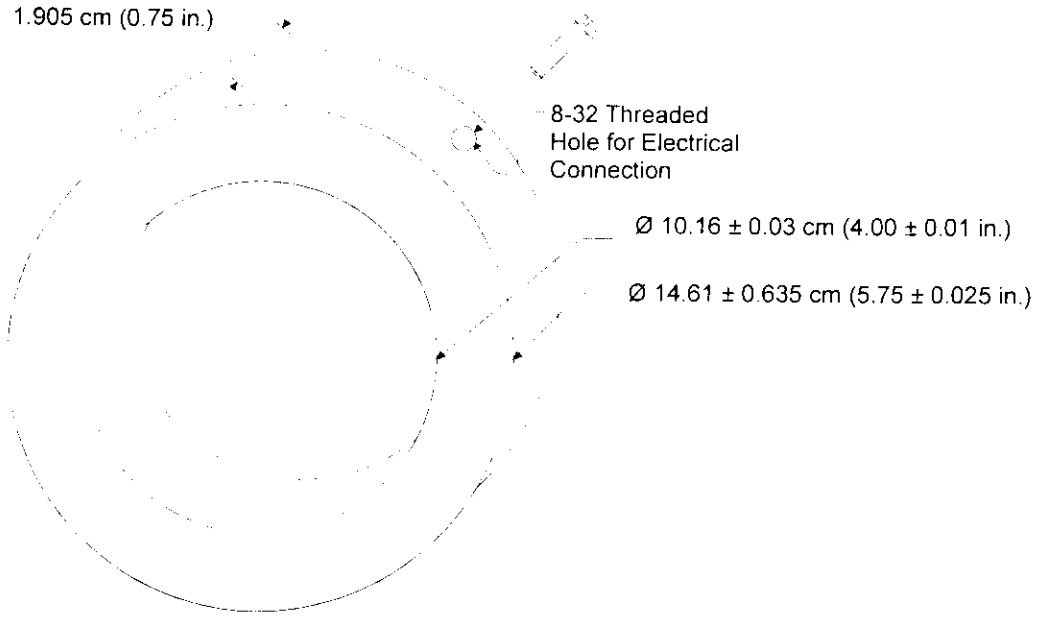

(b)

Figure 4-1: Schematic illustration of the (a) cathode and (b) anode geometries.

shown in Figure 4-2. Also included were 1) a primary Ag/AgCl reference electrode that was potted into a threaded pvc nipple such that the internal element protruded slightly from the pvc pipe interior, 2) 13 mm diameter pvc flow straighteners within the pipe section between the steel and aluminum, and 3) electrical leads from each component (steel, aluminum, and reference) to a personal computer based data acquisition system. A 6.5 Ω external resistor (R_x) in series with the

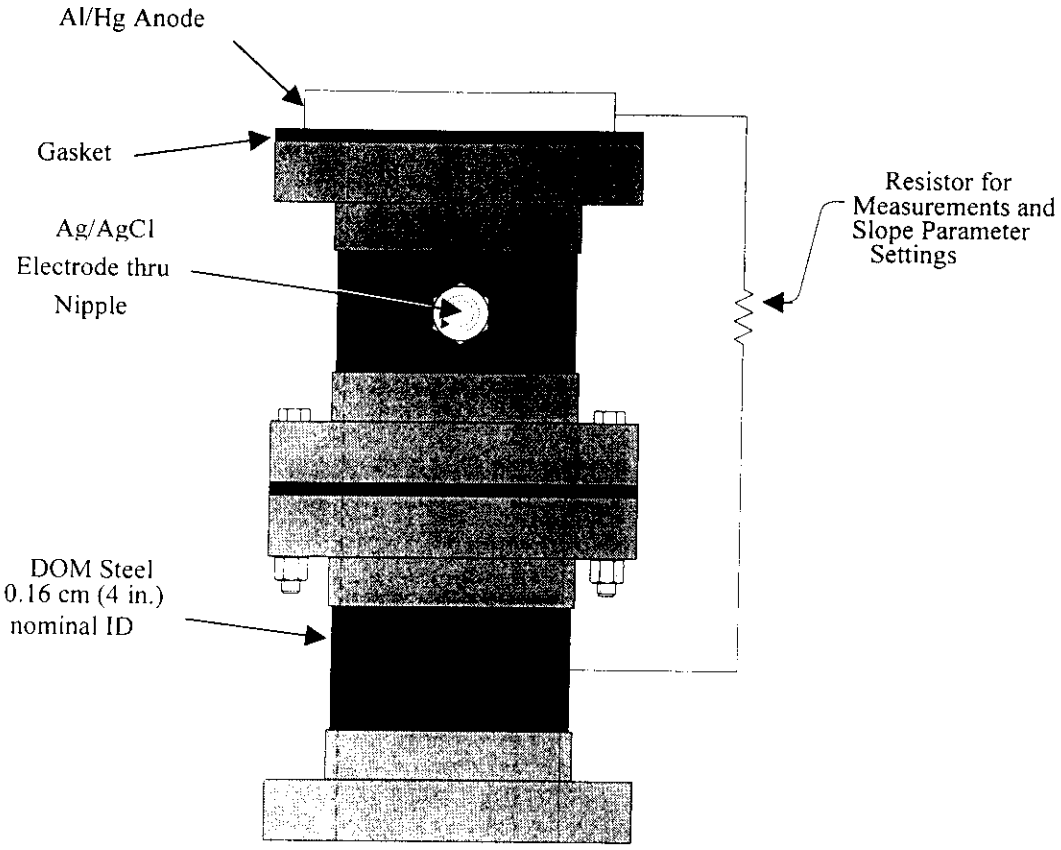

Figure 4-2:Schematic illustration of an anode-cathode assembly.

anode and cathode provided a means for current measurement and established a slope parameter (S) of 0.36 $\Omega \cdot m^2$ for each cathode. Figure 4-3 shows a photograph of an anode-cathode pair.

Four anode-cathode pairs (Figures 4-2 and 4-3) were assembled into each of six parallel legs of a sea water flow loop, as shown schematically in Figure 4-4 and by the photograph in Figure 4-5. Operation of this system involved pumping sea water to an overhead reservoir from which it flowed downward at a controlled rate through each of the six legs to a lower reservoir. The sea water was replenished at a rate of approximately 40 liters/hour. This water has been shown to be typical of near-surface semi-tropical ocean locations (42). The exposures commenced in March, 1997.

Depolarization was affected by opening the circuit between the steel and aluminum in the case of specimens that were to be fully depolarized and by increasing the value of R_x for those where depolarization was to be partial. The latter process was performed gradually in most cases because of, first, uncertainty regarding the resistor sizing and, second, a desire to replicate, to the

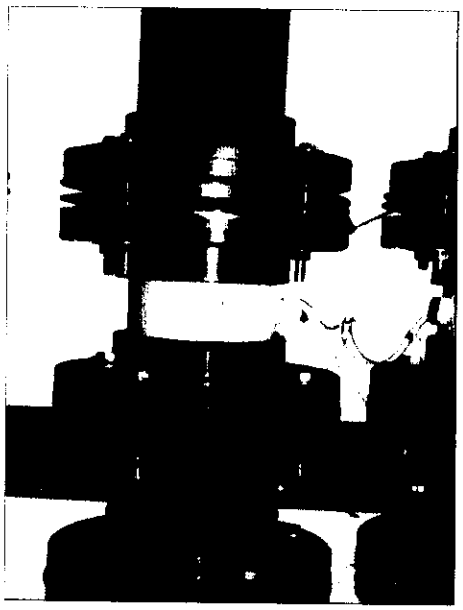

Figure 4-3: Photograph of anode-cathode pair.

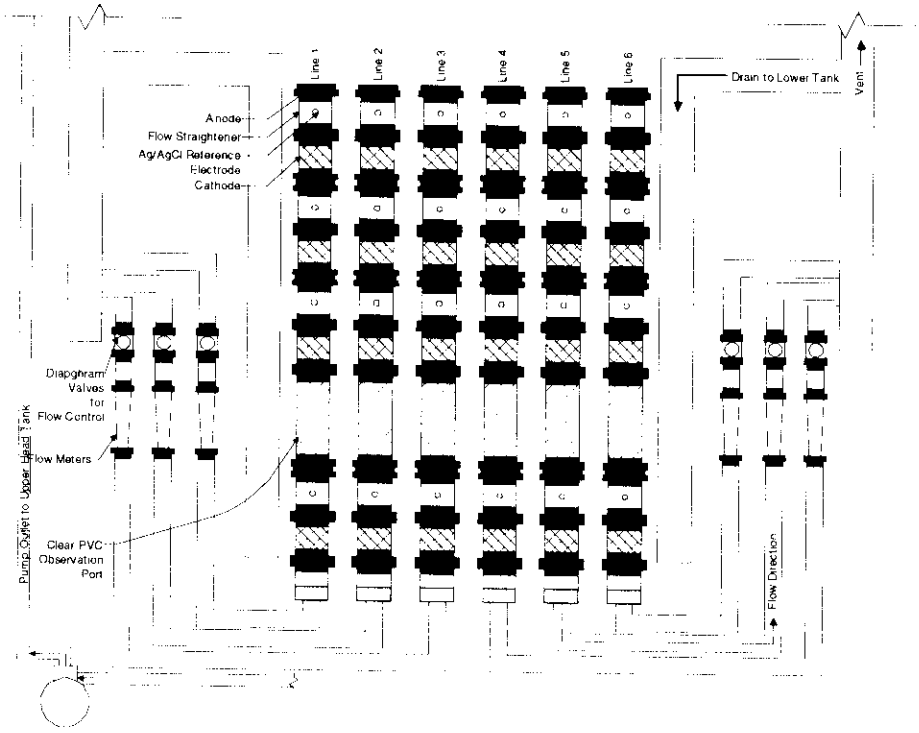

Figure 4-4:Schematic illustration of flow loop system.

extent that was feasible, the trend for actual structures where anode expiration and depolarization normally occur gradually. Repolarization in all cases was affected using a 10 Ω resistor in series between the steel and aluminum.

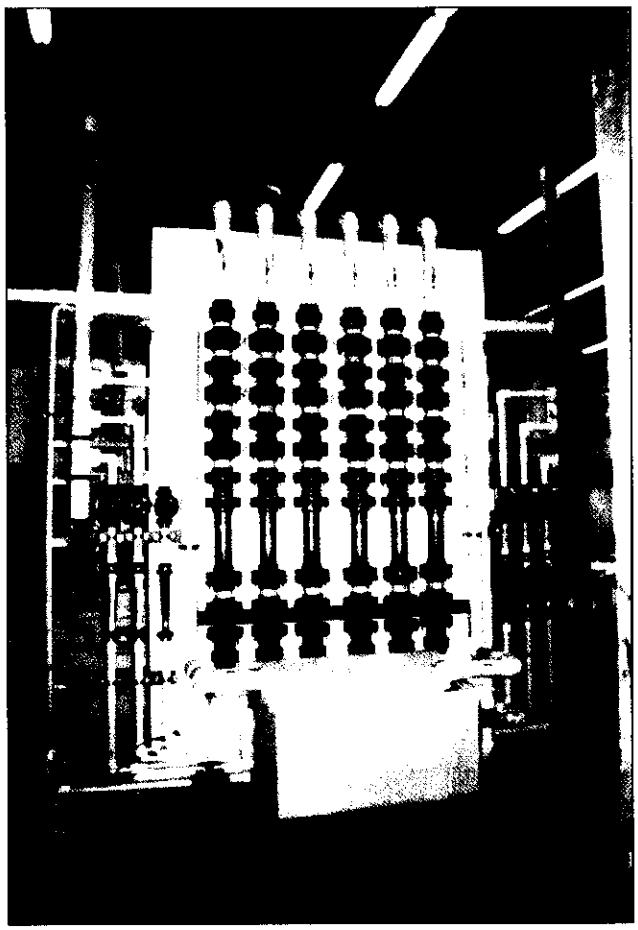

Figure 4-5: Photograph of the flow loop system.

Results and Discussion

The 24 specimens polarized rapidly upon initial exposure to a potential slightly more negative than −1.00 $V_{Ag/AgCl}$, as intended. However, current density, i_c, decreased with time at a relatively modest rate. Attempts to further reduce the rate of i_c decay by 1) lowering velocity in the flow loop and 2) cathodically polarizing one of the steel specimens by an additional 50-100 mV for a week using a potentiostat had only a minimal affect. After ten months exposure (January, 1998), the average i_c was approximately 40 mA/m^2. In response to this, the eight specimens with the highest current densities were removed from the flow loop, sand blasted, returned to the test system (no atmospheric pre-rusting), and the experiment restarted for these in February, 1998. The remaining 16 original specimens (referred to as Set 1) continued under test during the period that the eight new specimens (Set 2) were being prepared.

During the time that the Set 2 specimens were being prepared, it was determined that the relatively high i_c for the Set 1 specimens could be reduced by increasing the resistor size (increased slope parameter or $R_t \cdot A_c$). Apparently, the specimens had been polarized prior to this change such that the hydrogen reaction occurred in addition to oxygen reduction; and this elevated i_c. Depolarization of the Set 1 specimens began in April, 1998 and of some of the Set 2 specimens in August, 1998. As a departure from the original test plan (Table 4-1), the target depolarization for all Set 2 specimens was –0.80 $V_{Ag/AgCl}$. This change resulted because of data scatter that was being encountered and the fact that platform retrofit decisions are often based upon structure potential approaching or having reached this value (–0.80 $V_{Ag/AgCl}$). Repolarization of Set 1 specimens was started in September, 1998. However, a power outage from hurricane Georges (September, 1998) caused an anomalous depolarization of all Set 1 specimens such that, with the exception of two specimens that were fully depolarized, these were irreversibly disrupted and had to be terminated. Repolarization of Set 2 specimens began in November, 1998.

Figures 4-6 and 4-7 present (a) ϕ_c versus time, (b) i_c versus time, and (c) ϕ_c versus i_c plots for specimens 11 and 22, respectively, as examples of the response to the initial polarization, depolarization, and repolarization. Thus, in the case of specimen 11, polarization to about –1.00 $V_{Ag/AgCl}$ occurred relatively fast; and at the same time i_c decreased to about 100 mA/m^2. For the next 8,000-plus hours i_c continued to decrease and reached a final value of 22 mA/m^2. Depolarization to –0.67 $V_{Ag/AgCl}$ occurred quickly upon elimination of the external 6.5 Ω resistor (open circuit condition), and potential stabilized near –0.70 $V_{Ag/AgCl}$. After 4,000-plus hours, repolarization was instituted by reconnecting the steel and aluminum through a 10 Ω resistor. The specimen then quickly attained a ϕ_c and i_c that were close to the pre-depolarization values.

The same general behavior is noted for specimen 22 (Figure 4-7) as for specimen 11 except in this case only partial depolarization was affected. The potential step from about –0.88 $V_{Ag/AgCl}$ during the initial 750 hours of partial depolarization to near –0.825 $V_{Ag/AgCl}$ thereafter reflects an adjustment in the external resistance that was needed to affect the desired depolarization. Again, repolarization resulted in ϕ_c and i_c values near what existed prior to depolarization.

Table 4-2 summarizes the results for the ten specimens (two fully depolarized from Set 1 and eight partially depolarized from Set 2) in terms of hallmark parameters. These include 1) ϕ_c and i_c during each of the three phases of the experiments, 2) the final value of R_x during the

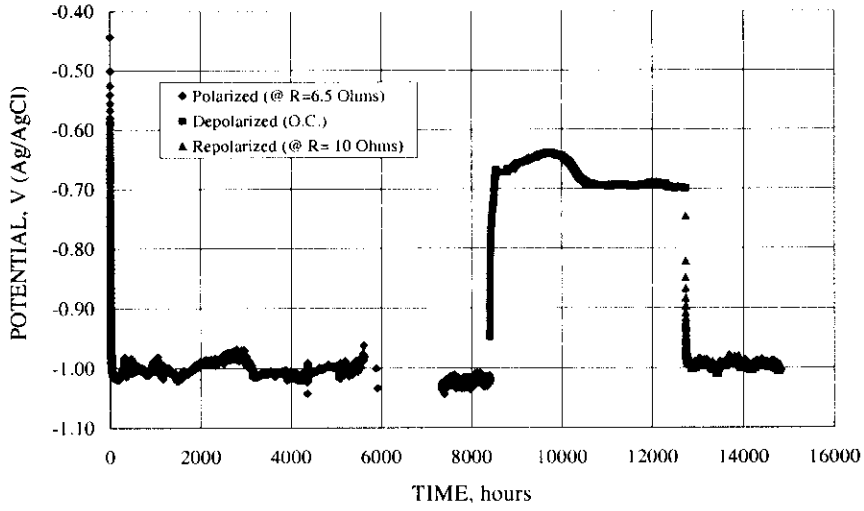

(a)

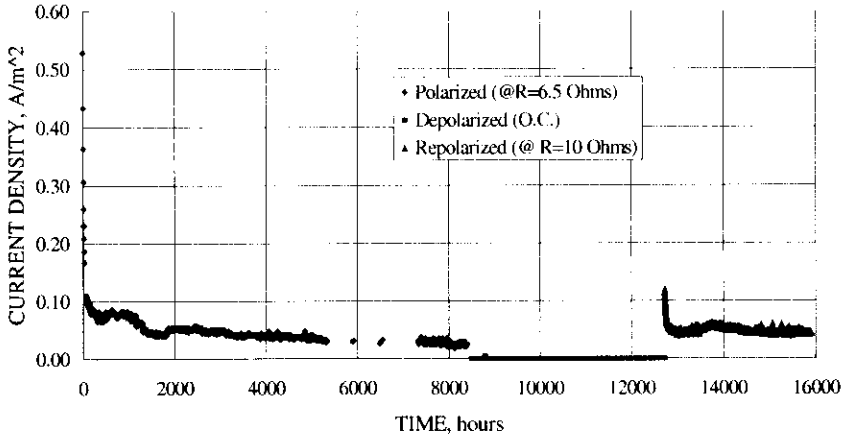

(b)

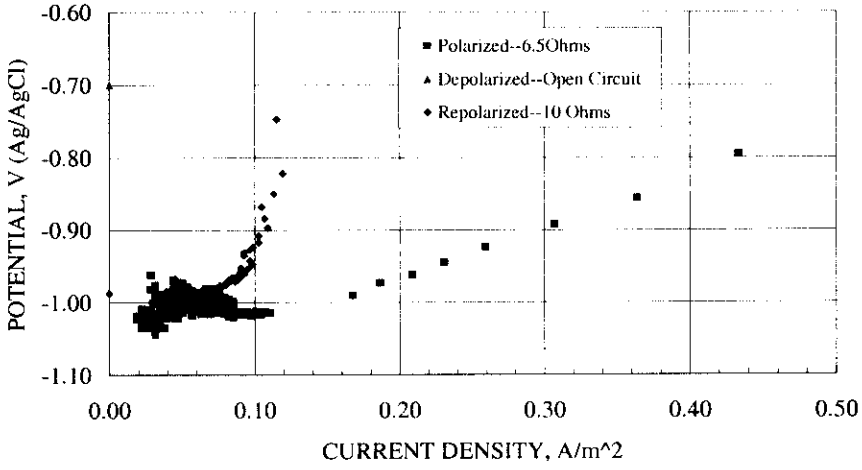

(c)

Figure 4-6: Plots of (a) potential versus time, (b) current density versus time, and (c) potential versus current density for specimen 11 during the initial polarization, depolarization, and repolarization phases. The initial current density recorded (not shown) was 0.87 A/m^2.

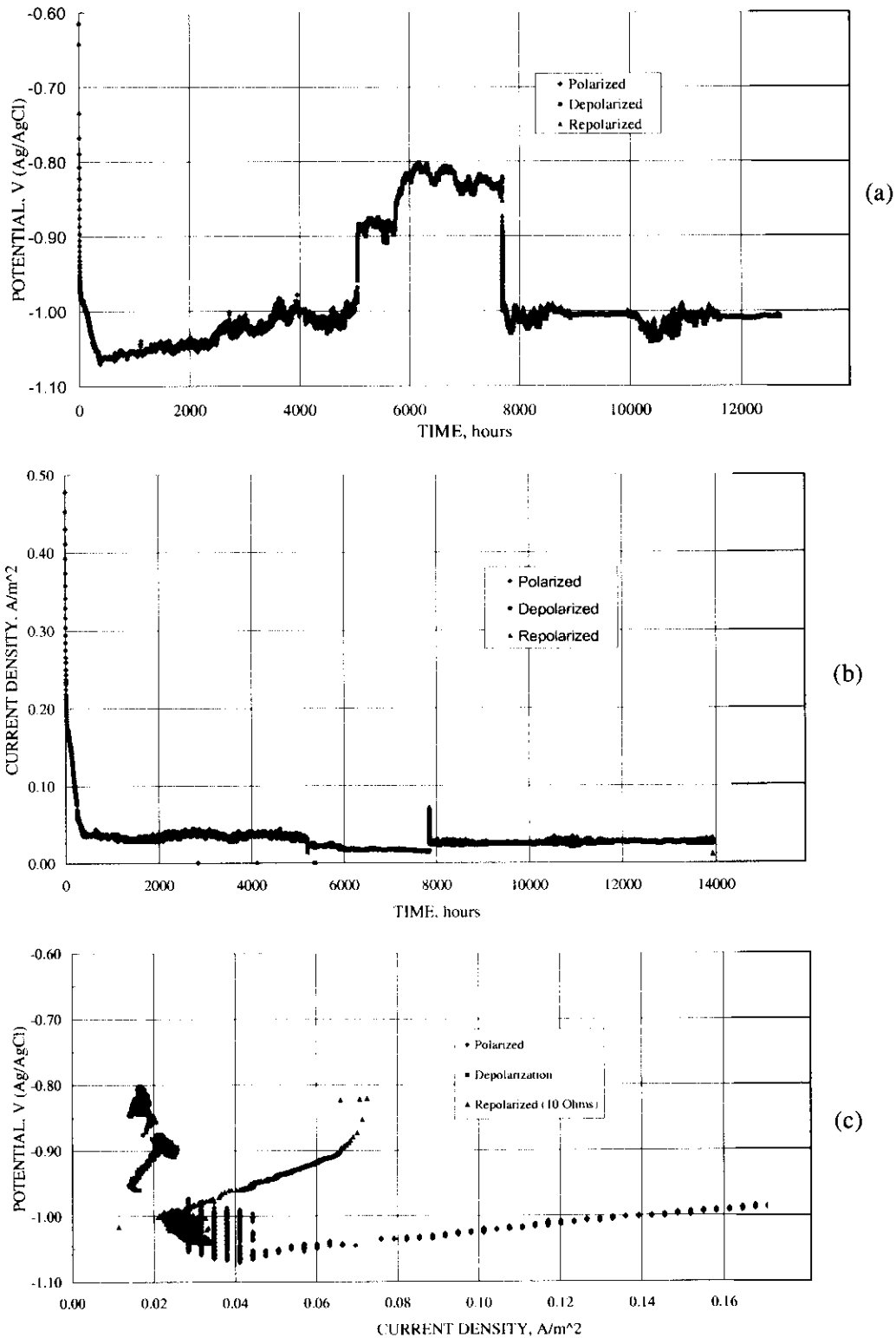

Figure 4-7: Plots of (a) potential versus time, (b) current density versus time, and (c) potential versus current density for specimen 22 during the initial polarization, depolarization, and repolarization phases. The initial current density recorded (not shown) was 0.67 A/m^2.

Table 4-2: Hallmark potential and current density results for Task II specimens.

SPEC. NO.	END OF INIT. POL.		END OF DEPOL.				INIT. REPOL.	END OF REPOL.	
	ϕ_c, V	i_c, mA/m^2	ϕ_c, V	i_c, mA/m^2	ϕ_c, V (most +ive)	R_x, Ohms	i_{or}, mA/m^2	ϕ_c, V	i_c, mA/m^2
3	-1.035	25	-0.712	0	-0.630	∞	100	-0.992	28
5	-0.952	25	-0.833	19	-0.786	172.5	100	-1.001	32
6	-1.012	11	-0.852	3	-0.835	1098	42	-1.020	11
7	-1.016	11	-0.830	1	-0.815	1720	40	-1.000	5
8	-1.015	30	-0.900	27	-0.790	230	65	-0.982	32
11	-1.028	22	-0.700	0	-0.640	∞	120	-1.000	37
21	-1.032	29	-0.781	20	-0.780	400	92	-1.010	40
22	-0.980	31	-0.837	15	-0.803	250	75	-0.996	27
23	-1.002	13	-0.899	2	-0.887	1377	18	-1.006	7
24	-1.008	10	-0.880	1	-0.868	1324	31	-1.006	4

depolarization phase, and 3) the initial current density, ϕ_{or}, at the beginning of repolarization.

Both Figure 4-6 and 4-7 show that a steeper ϕ_c–i_c path (greater apparent S) occurred upon repolarization than during the initial polarization with the difference being larger than can be accounted for by the different resistor sizes (10 versus 6.5 Ω). Thus, for specimen 11 i_o for the initial polarization (defined as the current density at a potential of –0.80 $V_{Ag/AgCl}$), was approximately 430 mA/m^2, whereas upon repolarization this was only about 120 mA/m^2. In the case of specimen 22, these values were 490 and 75 mA/m^2, respectively. The steeper ϕ_c-i_c slope upon repolarization was probably a consequence of anode polarization and not increased circuit resistance compared to the initial polarization (that the latter was not a factor was confirmed by circuit interruption and voltage drop determinations). Anode polarization was necessitated by the fact that ϕ_a and ϕ_c must differ by the voltage drop in the circuit. Thus, assuming that the external resistance, R_x, dominated R_t, then at the beginning of repolarization of specimen 22,

$$\phi_a = \phi_c - i_c A_c R_x = -0.803 - 0.075 \cdot 0.0486 \cdot 10 = -0.839\ V_{Ag/AgCl}.$$

The steeper slope for the ϕ_c-i_c data during the initial phase of repolarization resulted then from a progressive shift in ϕ_a to more negative values upon reconnecting the anode and cathode (open circuit or complete depolarization experiments) or reducing the resistance between the two (partial depolarization experiments). The fact that the net charge transferred during repolarization of depolarized and partially depolarized specimens was relatively low seems to contradict

previous results (35), as discussed above. However, as was pointed out, the test conditions for these two sets of experiments were not the same.

The data in Table 4-2 indicate that the apparent steady-state i_c at the end of the initial polarization varied from one specimen to the next by more that a factor of three. The reason for this is unclear. Also, as illustrated in Figure 4-8, there was a relationship between this same i_c and the R_x needed to affect the requisite depolarization (low i_c resulted in a high R_x). This can be explained in terms of current density in the low i_c case having greater sensitivity to potential than for the high current density situation, as illustrated schematically in Figure 4-9. Thus, assuming the cathodic polarization curves were linear, a higher slope parameter (higher R_x) was needed in the lower i_c case to affect a given level of depolarization compared to a situation where i_c was high. However, it remains unclear why i_c differences occurred to begin with for supposedly identical specimens. Probably for similar reasons, a relationship exists between the steady-state i_c upon initial polarization and i_c after partial depolarization, as shown by Figure 4-10. Also, Figure 4-11 illustrates that the steady-state current densities upon depolarization and repolarization are interdependent. On the other hand, the i_c upon repolarization was not affected by depolarization period, which ranged from 1104 to 4300 hours (46 to 179 days). A relationship was apparent, however, between the initial current density for repolarization and the partially depolarized

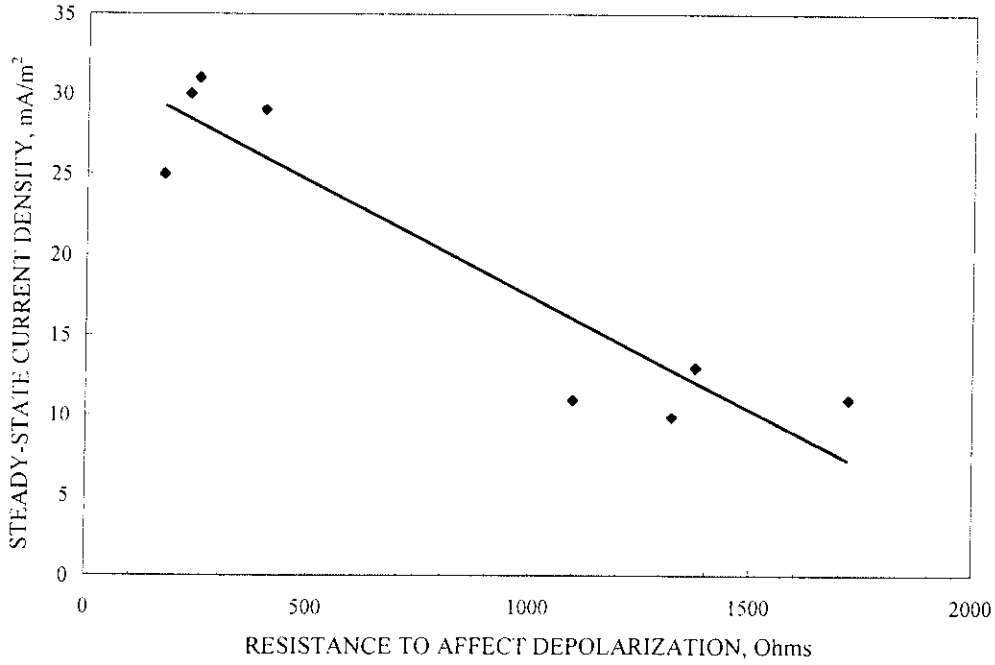

Figure 4-8: Relationship between i_c at the end of the initial polarization phase of the experiments and the R_x needed to affect depolarization.

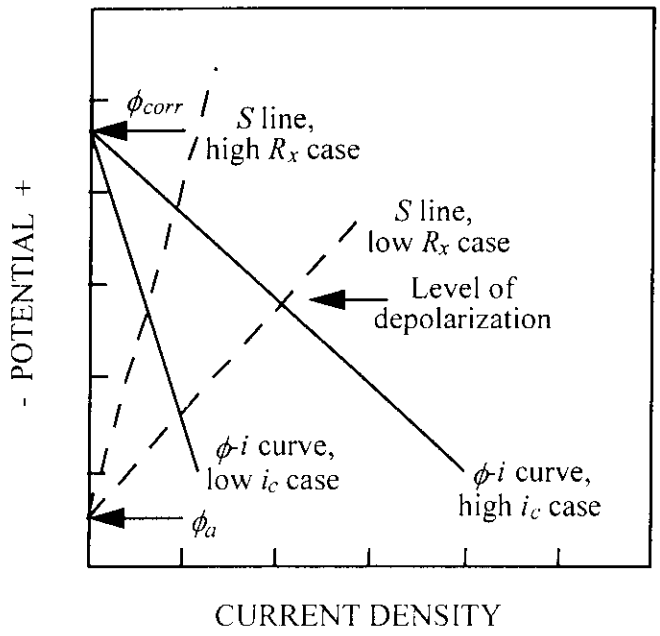

Figure 4-9: Schematic comparison the cathodic polarization curves for two specimens and how the i_c-R_x interrelationship can be explained from this.

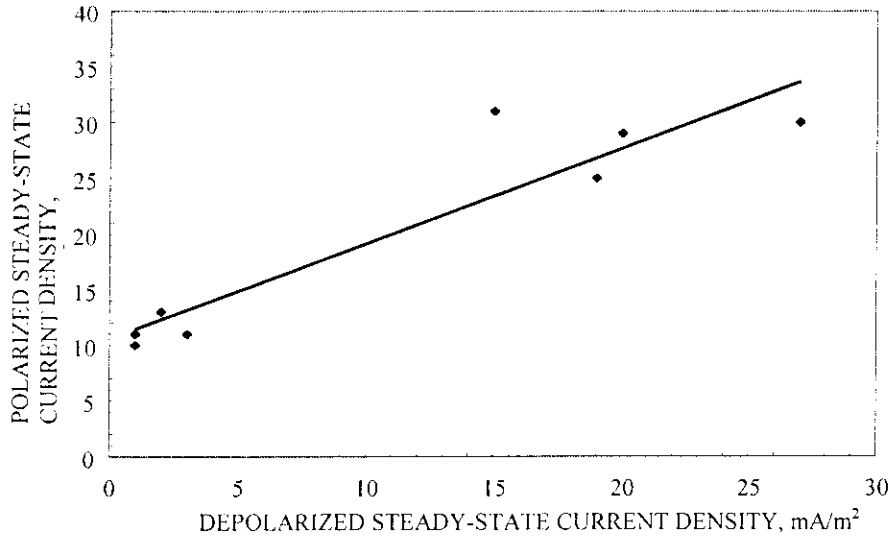

Figure 4-10: Plot of steady-state current density upon initial polarization versus depolarized steady-state current density.

steady-state current density, as shown by Figure 4-12. Thus, the three steady-state current densities and the initial current density to repolarize are interrelated such that knowledge of one permits any of the others to be projected. This has specific implications with regard to retrofit cp since, if the current density for a partially depolarized structure is known, then both the initial and maintenance current densities for repolarization can be projected. In this regard, both the mean and mean-plus-one standard deviation lines are shown in Figure 4-11. An equation for this trend

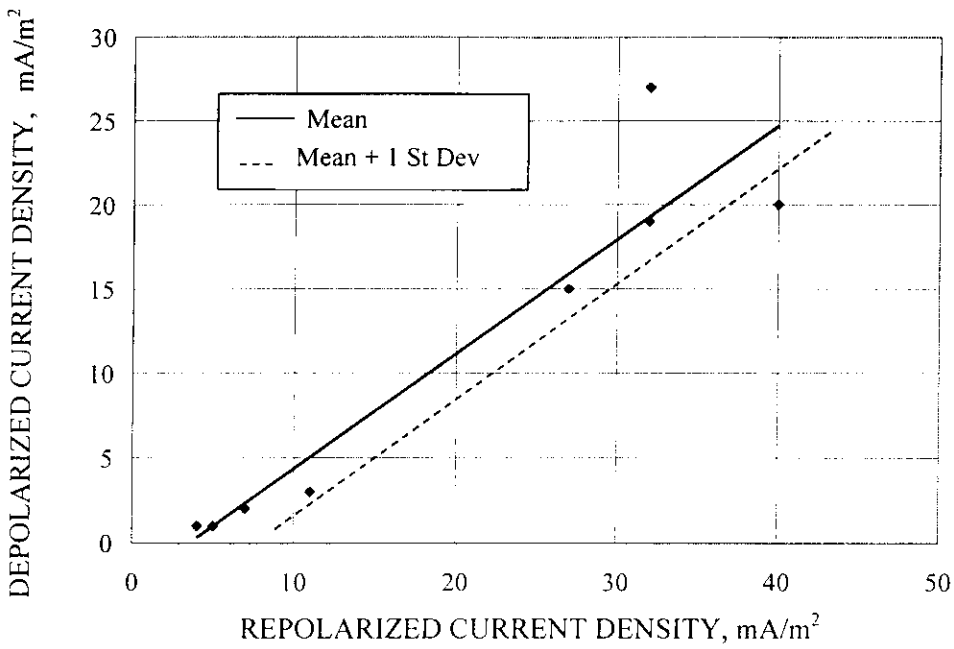

Figure 4-11: Plot of depolarized steady-state current density versus repolarized steady-state current density.

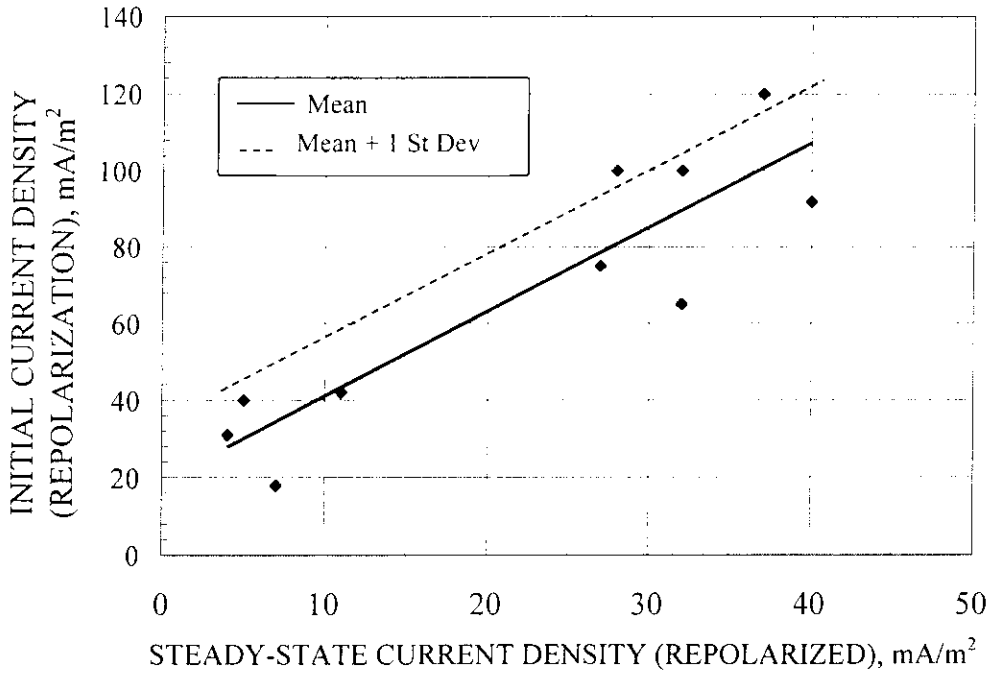

Figure 4-12: Plot of steady-state current density for repolarization versus initial current density for repolarization of partially depolarized specimens.

can be represented as

$$i_{ss}(repol) = 1.47 \cdot i_{ss}(depol) + 3.53 + k\sigma\,, \qquad (4\text{-}1$$

where $i_{ss}(repol)$ and $i_{ss}(depol)$ are the repolarized and depolarized steady-state current densities respectively, σ is the standard deviation for $i_{ss}(repol)$ (5.19 mA/m^2) and k is a constant that reflects the degree of conservatism in selecting a design value for $i_{ss}(repol)$. A related expression for the initial current density for repolarization, $i_o(repol)$, (Figure 4-12) is

$$i_o(repol) = 2.31 \cdot i_{ss}(repol) + 32.47 + k \cdot \sigma\,, \qquad (4\text{-}2$$

where, in this case, σ is the standard deviation for the $i_o(repol)$ data (17.33 mA/m^2).

V. TASK III: CATHODIC PROTECTION RETROFIT TIMETABLE FOR AGING STRUCTURES THAT ARE STILL POLARIZED

Background

The focus of this task was upon performance of aluminum galvanic anodes, since existing cp systems are overwhelmingly based upon these. Properties of galvanic anodes that determine performance include the following:

1. Potential,
2. Polarization characteristics and, specifically, the Tafel constant upon anodic polarization,
3. Current capacity, and
4. Efficiency.

Normally, it is desired that the first of these (potential) be as negative as possible in order that the driving voltage between the anode and structure is maximized. This, in turn, maximizes anode current output (Equation 1-3). Also, it is advantageous that the anodic polarization curve be relatively flat (item 2) such that current output per unit potential change is large. Current capacity, on the other hand, indicates the useful charge that the anode delivers per unit weight and, as such, is a function of valence, material density, and efficiency, where the last item expresses current capacity on a percentage basis relative to the theoretical value.

For a given amount of remaining galvanic anode mass, the additional cp system life should be determined by, first, i_{maint}, and, second, C, where low values for the former and high for the latter promote longevity. Background information pertaining to the first of these parameters, i_{maint}, was presented and discussed in the Introduction section of this report; and the entirety of Task I was devoted to means by which it can be measured. From a summary of previous studies (24,25), it was shown that the i_{maint} values for 17 structures that are located in warm waters (Gulf of Mexico and Arabian Gulf) were in the range 3.4-34.4 mA/m^2 with an average of 13.4 mA/m^2. The fact that this is approximately four times less than the mean design value (55 mA/m^2, see Table 1-1) suggests that the life of cp systems should, in fact, approach 80 years[1] and that retrofitting should not be an issue. This, of course, is not the case; and for the purpose of

[1]This rational assumes that the mean and maintenance current densities are the same, which is not necessarily the case because current density is initially high.

explaining this apparent inconsistency, effort within Task III was placed upon better understanding the current capacity of galvanic aluminum anodes. For example, if i_m for an offshore structure is one-half the design value (27.5 instead of 55 mA/m^2) and if cp retrofitting is required after ten years despite a design life of 20 years, then it must be concluded that the mean value for C, C_m, was only 25 percent of the design value.

Aluminum As a Galvanic Anode

Aluminum and alloys thereof were particularly attractive historically with regard to galvanic cp, at least in principle, because of their trivalent oxidation state (as opposed to divalent for other candidates (Zn and Mg)), low density, and relatively active potential in some cases. However, a major impediment to their being successfully utilized was a lack of understanding of requisite properties for acceptable performance (43,44), as listed above. As a consequence of research and development activities in the 1960's (45-47), aluminum alloy anodes have evolved to the point where they are now the predominant material of choice for most offshore petroleum production platform cp applications. At the same time, questions regarding reliability, reproducibility, and dependence of long-term performance upon a host of factors continue to be of concern.

Variables that have been reported as affecting performance of galvanic aluminum anodes in marine applications include 1) alloy composition (47,48), 2) microstructure (49-56), 3) electrolyte composition (including pH), temperature, and velocity (49,57-61), 4) current density (56,59,61,62), and 5) exposure time (52-54,58,60,63). With regard to the former, existing aluminum anodes invariably are comprised of about five percent Zn with a small concentration of an "activator" (Sn, Hg, or In) and Si. The first of these (Sn) was employed in early vintage alloys but has the disadvantage that heat treatment is required. Also, performance is inferior to anodes with either Hg or In as the activator. Mercury activated anodes have been largely phased out of cp systems for new structures because of environmental concerns, leaving the In activated ones as the predominant present choice. Both Sn and Hg activated anodes remain in service, however, on many structures. Proper activator functionality is critical to performance; but the mechanism(s) by which these components operate is(are) not well understood. Possibilities include 1) weakening to the otherwise protective film at locations where activator(s) is(are) segregated and 2) their incorporation into and weakening of the film by redeposition of previously dissolved activator (52,53). Special attention is given to control of impurities; Cu, Fe, and Cd in particular. Microstructural effects, including spatial variations of alloying and impurity elements

(segregation) and second phase particles, become defined in conjunction with either casting variables or subsequent thermal treatment. Both composition and microstructure affect anode potential, polarization characteristics, current capacity, and efficiency.

Emphasis in galvanic anode research has focused largely upon the interrelationship between current capacity and current density with most investigations reporting a decrease in the former parameter (C) once the latter (i_c) drops below 0.1-1.0 A/m^2 (46,59,62-64). Figure 5-1 presents a summary plot of current capacity versus current density (anode surface area) based upon short-term laboratory test data that were available at the beginning of this project and which illustrate the above trend (decreasing C with decreasing i_c)[1]. This shows that C begins to decrease as i drops below about 1 A/m^2. If an anode-to-cathode area ratio of 1:50 is assumed, this corresponds to an i_c value of 20 mA/m^2. However, limited test results have indicated either an opposite trend (decreasing capacity with increasing current density) or no interdependence between the two parameters (49,60). These differences may reflect an influence of other factors, exposure time and accumulation of solid corrosion products in particular. For example, several authors have indicated that current capacity decreased with time in tests that lasted one year and longer (52-54,58,60). Also, while the pH of bulk, near surface sea water is typically in the range 8.0-8.4,

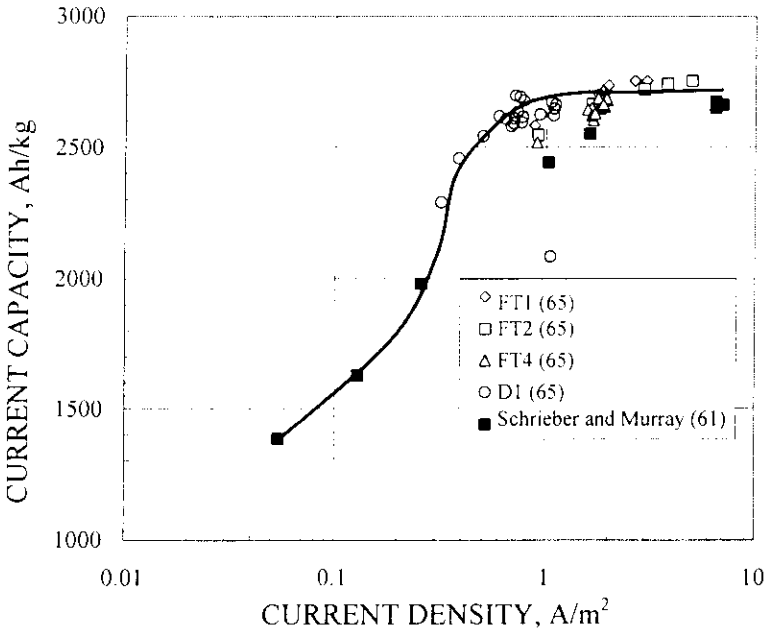

Figure 5-1: Summary of current capacity versus current density data from the literature.

[1] The data in Figure 5-1 represent typical results. Much of the literature data is difficult to read from the graphs and for that reason was not included.

values of 3.8-4.5 have been reported from measurements upon sea water samples that were extracted with a syringe from near the metal-corrosion product interface of actual anodes on offshore structures (58). Presumably, corrosion products promote a crevice situation and hydrolysis and acidification of the local electrolyte. This effect (lowered pH) may become even more pronounced for situations where anode corrosion is non-uniform such that pits develop. Consequently, the combination of reduced pH and presence of low over-voltage sites that occur in conjunction with locations where the activator concentrates result in local action cell activity and reduced current capacity and efficiency.

Testing of Galvanic Aluminum Anodes

The NACE International Standard Test Method TM0190 for galvanic aluminum anodes (66) specifies a current capacity determination procedure that uses a 2.54 cm cube specimen and a two week exposure in ASTM D-11441 artificial sea water at an impressed anodic current density of 6.2 A/m^2. The method is based upon a multi-laboratory preliminary evaluation (67) that determined C for Hg- and In-activated aluminum anodes to be in the range 2,354 to 2,949 A-h/kg (1,068 to 1,338 A-h/lb). The Test Method description indicates that it is to be used "...for screening various heats and lots of anodes to determine performance consistency ..." and "... (results) should not be used for design purposes ...." Experimental findings from several investigations (68,69) have shown that this test can result in both false positives and false negatives[2] compared to one year sea water exposures. Consequently, the approach should not be used to project long-term performance (70), although this is often done.

Relatedly, Appendix A of DnV RP B401 (1) describes a four day test method using a 10 mm diameter by 50 mm long specimen exposed to either natural sea water, ASTM D-11441 artificial sea water, or a 3 percent NaCl solution at current densities of 15, 4, 40, and 15 A/m^2 for successive 24 ± 1 hour periods. Smith and Goolsby (71) have summarized and critically compared the NACE International and DnV methods. Particularly needed at present is a short-term accelerated test that can predict long-term service performance.

---

[2] False positives are where the accelerated test indicates high C but the long-term field tests indicate low C. False negatives are the opposite of this.

Task Objective

The objective of this task was to develop a methodology for projecting the remaining life of cathodic protection systems (alternatively, of galvanic anodes) in instances where the structure is still fully polarized. This was addressed by development of a protocol whereby i_{maint} and C_{maint} (the maintenance current capacity value) can be projected and was accomplished in terms of the sub-tasks listed in Table 5-1.

Table 5-1: Listing of sub-tasks.

TASK NO.	ACTIVITY
IIIA	Survey of literature data.
IIIB	Short-term laboratory tests using small specimens.
IIIC	Data available from other tasks or related long-term exposures.
IVD	Long-term galvanic exposure of anode castings in natural sea water.

Experimental Approach

Current Capacity Determinations. Experiments pertaining to anode performance consisted of 1) field exposures and 2) laboratory exposures patterned after the NACE International TM0190 procedure (66). The former involved ASS-10 In- and Hg-activated aluminum anodes that were acquired from Galvotec Alloys, Inc. Figure 5-2 illustrates the geometry for these, and Table 5-2 lists the chemical composition. These were deployed at the NRLKW anode test pier in January, 1998. Figure 5-3 illustrates the configuration of this testing arrangement.

The laboratory experiments, on the other hand, were of two basic types. The first involved both In- and Hg-activated aluminum obtained from Corrtherm, Inc., the composition of which is as reported in Table 5-3. The test procedure conformed to the NACE International TM0190 method with regard to specimen geometry and exposure time but utilized a range of current densities. The second involved galvanic coupling of a 2.54 cm diameter by 2.54 cm high aluminum anode to a coated steel cathode with a single 6 mm diameter coating defect through

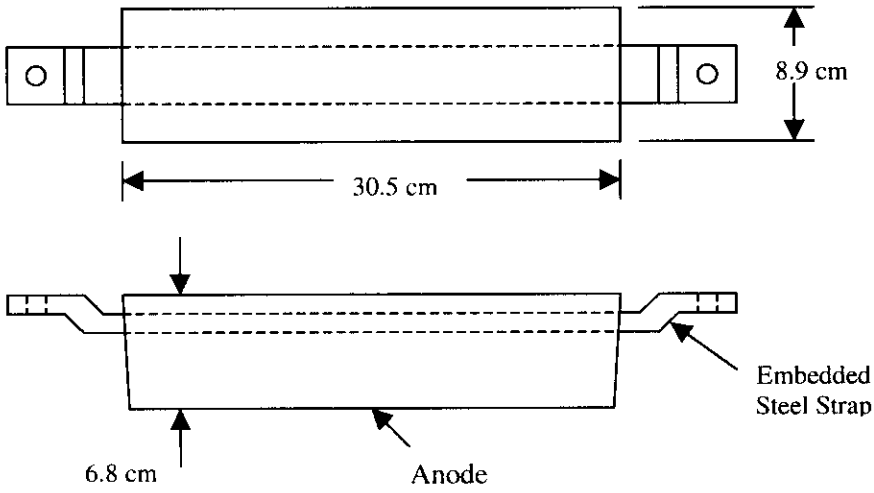

Figure 5-2: Geometry of the ASS-10 anode.

Table 5-2:Chemical composition of anodes deployed at the NRLKW pier.

Zn	In	Hg	Si	Cu	Fe	Cd	Al
5.61	0.017	-	0.11	<0.0020	0.071	<0.0010	Bal.
1.4	-	0.037	0.08	<0.0020	0.029	<0.0010	Bal.

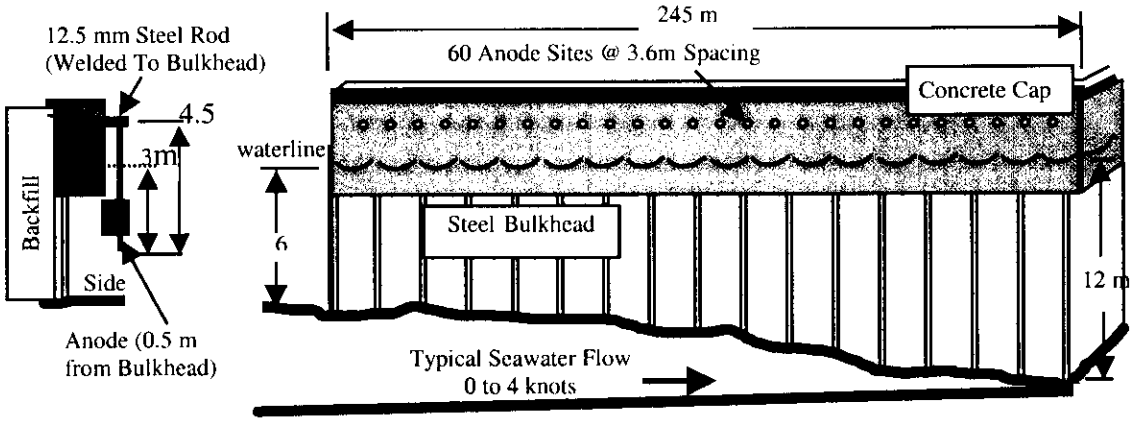

Figure 5-3:Schematic illustration of anode test pier at NRLKW.

various size resistors[3]. These tests lasted from 29 to 36 months. Table 5-4 shows the chemical composition for these anodes. Both sets of experiments involved 30.5 cm diameter by 20 cm high plexiglass containers, and the electrolyte was quiescent sea water that was exchanged periodically in the former case and continuously replenished in the latter.

(3) These experiments were part of a separate program that was funded by Chevron who agreed to made results from the anodes available to the present project.

Table 5-3: Composition of aluminum anodes employed in conjunction with NACE International TM0190 tests.

ANODE DESIGNATION	ANALYSIS NUMBER	COMPOSITION, w/o						
		Zn	In	Hg	Si	Cu	Fe	Cd
CT-1	1	5.61	0.028	-	0.033	0.001	0.046	<0.002
	2	5.72	0.028	-	0.032	9E-04	0.046	<0.002
CT-3	1	1.46	-	0.038	0.05	2E-04	0.058	0.001
	2	1.56	-	0.044	0.052	6E-04	0.059	0.001
	3	0.39	-	0.043	0.04	0.002	0.047	0.001

Table 5-4: Composition of aluminum anodes employed in conjunction with the long-term galvanic exposures.

Si	Fe	Cu	Zn	Cd	In	Hg	Al
0.09	0.037	0.0013	4.18	<0.0010	0.017	-	Bal

A limited number of impressed current experiments were performed using recirculated sea water the pH of which was adjusted to 3.5 ± 0.1 by addition of HCl and maintained using a LMI Milton Roy pH control system. The purpose of these was to measure C under conditions that are thought to develop over time beneath corrosion products once such products form. Figure 5-4 shows a photograph of this laboratory anode testing arrangement which included 1) a series of table-top test cells, 2) a reservoir of acidified sea water for recirculation, and 3) galvanostats, coulometers, and pH control system.

pH Measurements. Experiments were performed to measure pH of the sea water beneath the corrosion products of the Task II flow loop anodes and of the anodes from the long-term galvanic exposures described above. This involved removal of an anode from the test system at the time the experiment was terminated and immersing it in a bench top polypropylene container that contained sea water. For the first series of pH determinations, a syringe tip was inserted through the corrosion products to the anode surface; and about one ml of solution was extracted. The pH of this was then measured using pH paper. Subsequently, a micro-pH electrode was employed according to the following steps:

1. A 1.3 mm diameter hollow glass probe was inserted through a guide system that permitted only one-dimensional motion such that it penetrated the corrosion products and contacted the metal surface.

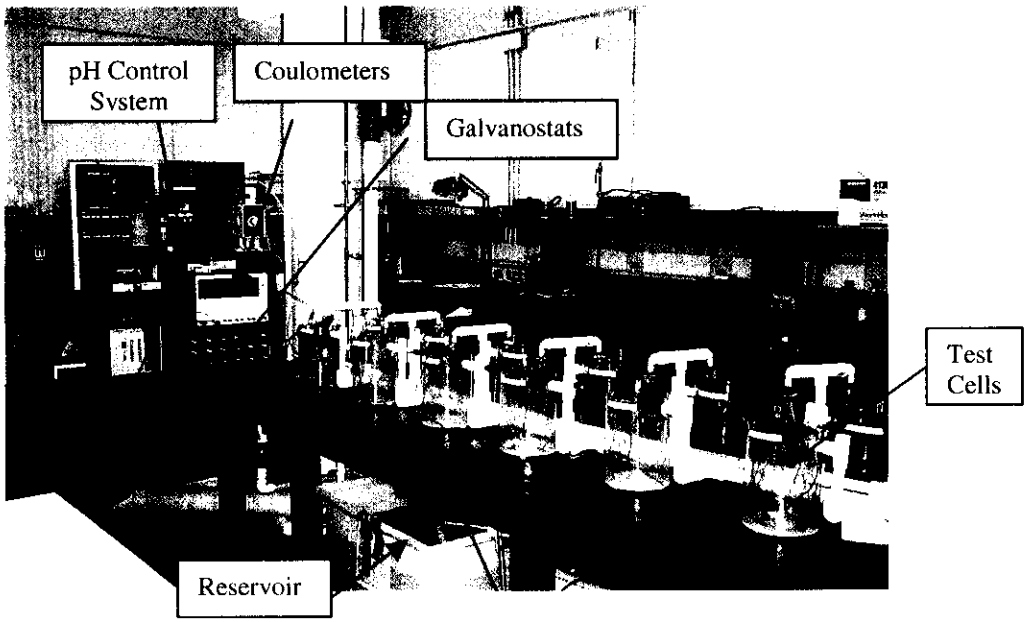

Figure 5-4:Photograph of the anode test system.

2. Next, a 0.9 mm diameter metal incased Microelectrodes, Inc. MI-407 micro-pH electrode with a 21 gauge needle was inserted into the hollow glass probe until the anode surface was contacted. The Ag/AgCl reference electrode was also inserted in the glass tube behind the pH electrode.

3. pH was then measured using a Accumet Research AR50 meter.

Figure 5-5 shows a photograph of the micro-pH electrode, and Figure 5-6 illustrates the test arrangement whereby the electrode was inserted into corrosion products on an anode.

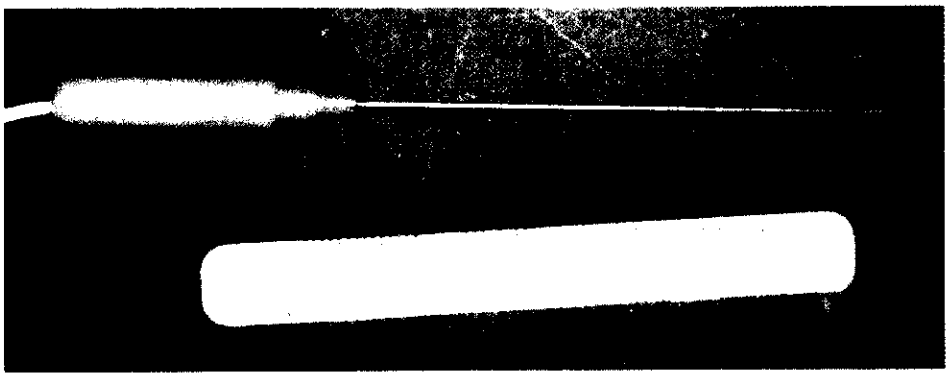

Figure 5-5: Photograph of the micro-pH electrode.

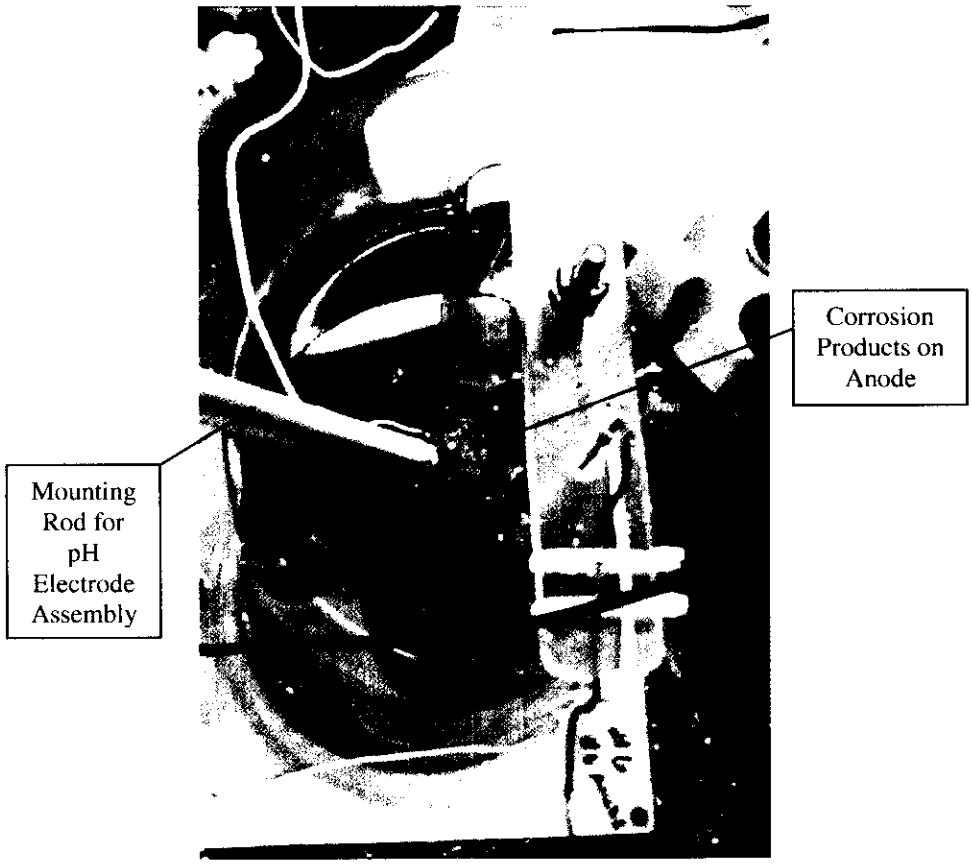

Figure 5-6: Photograph of the test cell for galvanic anode testing and rod upon which the micro-pH insertion assembly is mounted.

Results and Discussion

Effect of Current Density upon Current Capacity. Figure 5-7 plots current capacity versus current density results from the present experiments and from other recent investigations along with data from Figure 5-1. The data are represented in terms of two trend curves, the first of which is linear and applies for $i > 0.1$ A/m^2 and the second logarithmic and pertains to $i < 0.1$ A/m^2 (anode surface area basis). Data in the former category were fitted by ignoring the results from reference 61 that extended below 0.1 A/m^2 and all results from references 25 and 58, as justified subsequently. Accordingly, the best fit curve for the $i > 0.1$ A/m^2 regime is

$$C = 49.9i + 2{,}562\,. \qquad (5\text{-}1$$

Similarly, the Hg Act. (73), long-term galvanic, and low current data from reference 58 were employed to develop the fit below 0.1 A/m^2; and these conformed to the expression

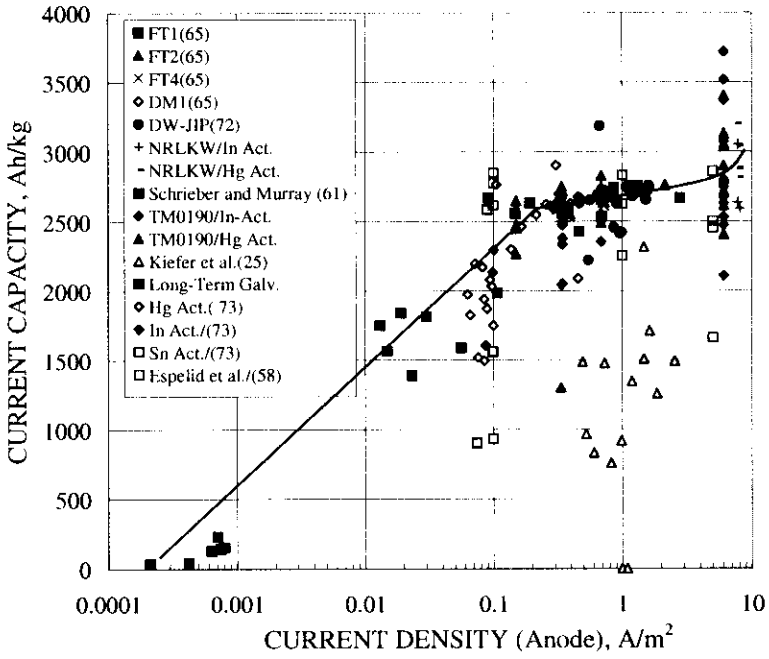

Figure 5-7: Summary plot of current capacity versus current density.

$$C = 402 Logi + 3{,}187 . \qquad (5\text{-}2$$

The Sn-activated anode data (73) were omitted from this evaluation. Clearly, the scatter that results from this *C-i* representation is large indicating that other factors as well are influential.

Effect of Time upon Current Capacity. Figure 5-8 shows the data from Figure 5-7 plotted as current capacity versus exposure time using linear coordinates for those cases where time was known[4]. Here the representation indicates that C apparently decreased linearly with time for the initial five years of exposure, the best-fit expression being

$$C = 2724 - 211 i \qquad (5\text{-}3$$

($R^2 = 0.24$) and was constant thereafter (C = 1,646 Ah/kg). If this latter value is considered as the mean C (C_m), then the design values specified by the current recommended practices (1,2) are non-conservative.

[4] The long-term galvanic data from Figure 5-7 were excluded from Figure 5-8 because of the very low current densities that were employ for these.

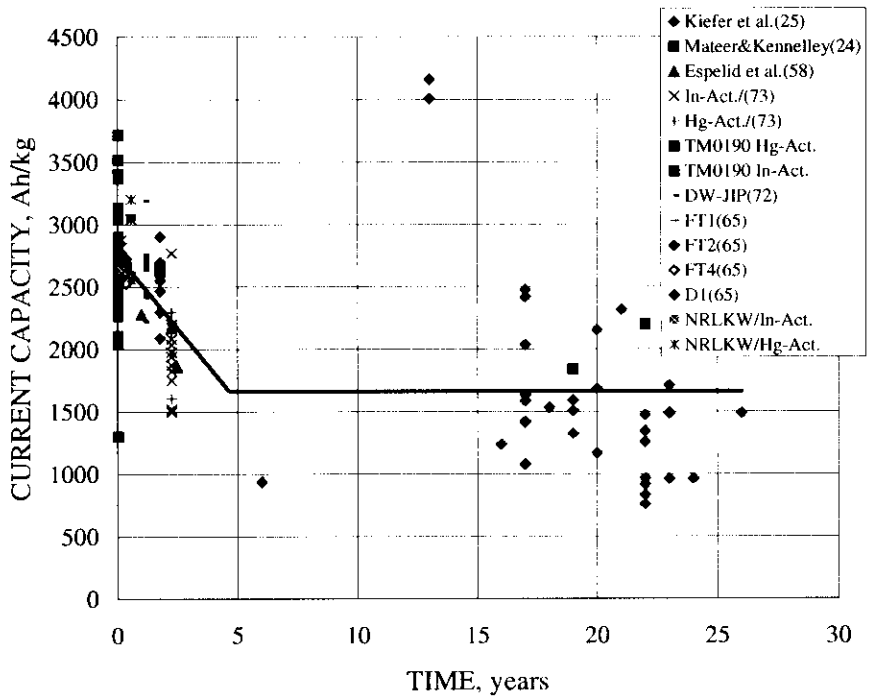

Figure 5-8:Plot of current capacity versus exposure time using selected C data as in Figure 5-7.

The data in Figure 5-8 were also plotted semi-logarithmicly, as shown in Figure 5-9, in an attempt to provide an improved representation. It was concluded from this that an exponential curve fit (solid line) to the data according to the expression

$$C_m = 2{,}598 \cdot e^{-0.032T} \qquad (5\text{-}4$$

($R^2 = 0.61$) was more appropriate than the two step linear one (Figure 5-8).[5] Also shown is the mean-minus-one standard deviation curve (dashed), which superimposes a factor of safety upon the mean relationship (Equation 5-4). The equation for this latter curve can be represented by the expression

$$C_m = \left(2{,}598 - k_c \cdot \sigma_c\right) \cdot e^{-0.032 \cdot T}, \qquad (5\text{-}5$$

[5] The two data points for which $C > 4{,}000$ Ah/kg were disregarded in developing Equation 5-4 and the best fit curve in Figure 5-9.

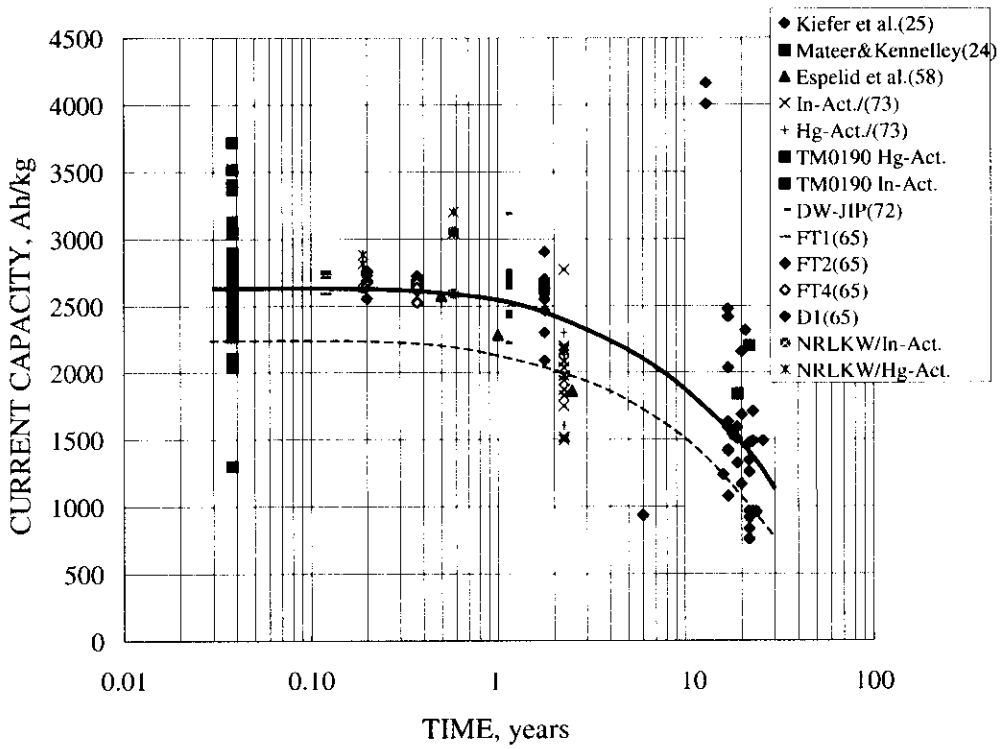

Figure 5-9: Representation of the current capacity versus time data in semi-logarithmic coordinates.

where σ_c is the standard deviation (426 Ah/kg) and k_c is a constant that reflects the degree of conservatism (k_c need not be a whole number).

Any interpretation of the trend in Figures 5-8 and 5-9 is made difficult, however, by the lack of data between about 2.5 and 15 years. The likelihood that C_m decreases with time provides an explanation for why the data of Kiefer et al (25) were so displaced below the C_m-i trend line in Figure 5-7, since these involved exposures of 6-26 years. The accuracy of these capacity values is open to question, however, because weight loss was accessed based upon diver estimated depletion. Greater emphasis should be placed upon improved definition of the long-term value for C_m, as indicated by field experience, in specifying galvanic anode performance data for cp design, either new or retrofit.

Based upon the above, the unified design equation (Equation 1-16) can be modified to incorporate the time dependence of i_m and C_m. Thus, by substituting Equations 1-19 and 5-5 into Equation 1-16,

$$w \cdot R_a = \frac{8.76 \cdot 10^{(a+k_i \cdot \sigma_i)} \cdot T^{b+1} \cdot e^{0.032 \cdot T} \cdot S}{(b+1) \cdot (2598 - k_c \cdot \sigma_c)}, \qquad (5\text{-}6$$

where a and b are 1.51 and –0.41, respectively (the former value differs from that in Table 1-2 because the units for time (T) in Equation 5-6 are in years instead of hours), σ_i and σ_c are the standard deviations for a (0.233 for warm water structures) and, hence, i_m, and C_m (426 $A \cdot h/kg$), respectively, and k_i and k_c represent factors of safety for these latter two parameters (i_m and C_m, respectively). Accordingly, design of a cp system for a new structure can be accomplished whereby the time dependence of i_m and C_m is taken into account. As an example, Figure 5-10 presents a plot of the weight of individual anodes, w, needed to protect a structure in warm water (a = 1.51 and b = -0.41) versus design life, T, as projected by Equation 5-6, with R_a = 0.0426 Ohms (the resistance of a conventional 330 kg anode in 20 $Ohm \cdot cm$ sea water), S = 1.75 $Ohm \cdot m^2$, and for several k values ($k_i = k_c$). These parameters are the same as cited for the design of the cp system for an actual Gulf of Mexico structure by reference 24. The situation of $k_i = k_c$ = 1.47 results in w = 330 kg at T = 20 years and, as such, identifies an effective "factor of safety" for typical Gulf of Mexico cp designs. This, in turn, indicates that if the w versus T data

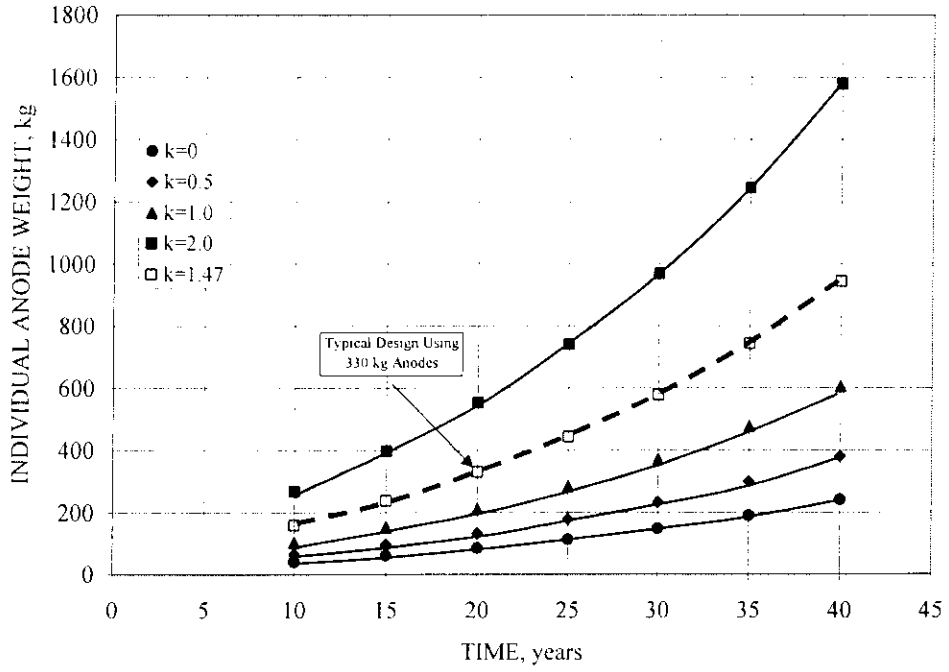

Figure 5-10: Plot of anode weight needed to protect a Gulf of Mexico structure versus design life, as determined from Equation 5-6.

are normally distributed, then the cp system should provide protection for the design life in approximately 92 percent of the cases. In actuality, it is unlikely that k_i and k_c would be equal; and so the k values in Figure 5-10 represent a weighted average of these two component terms.

Remaining Anode Life. The remaining time until anodes on an existing structure waste to a size that corresponds to a particular utilization factor, f_u,[6] is defined as $T_2 - T_1$, where T_1 is the present structure age and T_2 is the structure age of maximum acceptable anode depletion. This remaining life is obtained by combining Equation 1-5 with the appropriate forms of Equations 1-19 and 5-5 and solving for T_2. Thus,

$$w(T_1) - w_o \cdot f_u(T_2) = \frac{8.76 \cdot 10^{(a+k_i \cdot \sigma_i)} \cdot A_c}{N \cdot (b+1) \cdot (2598 - k_c \cdot \sigma_c)} \cdot \left[\left(T_1^{b+1} \cdot e^{0.032 \cdot T_1}\right) - \left(T_2^{b+1} \cdot e^{0.032 \cdot T_2}\right)\right], \quad (5\text{-}7$$

where $w(T_1)$ is the average anode weight that has been lost after time T_1 and w_o is the original individual anode weight. A procedure for remaining anode life determination based upon this equation involves the following steps:

1. Using the protocol in Appendix B, determine i_{maint}.

2. From Equation 1-19 and knowing the structure age, T_1, calculate k_i.

3. Calculate the average anode weight loss, $w(T_1)$, based upon diver estimated depletion or the Appendix B protocol. Determine C_m using Equation 1-5.

4. Using Equation 5-5 and the value for C_m from 3), calculate k_c.

5. By substituting the values for $w(T_1)$, k_i, and k_c, as determined in 1)-4), knowing N, A_c, w_o, and deciding upon an appropriate value for f_u, solve Equation 5-7 for T_2. The remaining anode life is then T_2-T_1.

As an example, consider a 16 year old 10,000 m^2 warm water structure protected by 200 330 kg anodes. Assume that application of the Appendix B protocol reveals i_{maint} as 18 mA/m^2 (Step 1).

---

[6] $f(u)$ is the fraction of the original anode weight that has been consumed at the end of the design life.

Thus, from Equation 1-19, k_i = 1.025 (Step 2). Consider further that the Appendix B protocol indicates an average anode depletion of 45 percent such that $w(T_1)$ is 145.5 kg. Then from Equation 1-5, C_m = 867 Ah/kg (Step 3). Using Equation 5-5, k_2 is 2.703 (Step 4). Lastly, based upon f_u = 0.9, Step 5 then indicates that the time until the amount of anode loss becomes unacceptable or T_2-T_1 is 7.7 years.

Maintenance Current Capacity. The trend lines in Figures 5-8 and 5-9 identify how current capacity varies, on average, with time. As such, these correspond to values of C_m and are indicative of overall anode performance. The value of current capacity at a particular time, on the other hand, C_{maint}, is indicative of present and probably future anode performance. In this regard, the average C_{maint} value reported by Kiefer et al. (25) for the 15 Arabian Gulf structures mentioned above was only 106 Ah/kg with a standard deviation of 79 Ah/kg. Thus, these anodes were performing in a highly inefficient manner in the long-term. If these values are correct and representative, then projections of future cp system performance based upon anode current capacities typically employed in new designs are likely to be highly non-conservative.

It is projected that the abnormally low long-term C_m and C_{maint} values occurred because of, first, the relatively low i_{maint} values that result in the long-term and, second, acidification of the local electrolyte beneath corrosion products on the anode. Both of these factors are likely to promote local action cell activity and to diminish useful charge transfer. In this regard, Table 5-5 presents the results of the pH determinations that were made using the syringe extraction/pH paper technique on anodes from the long-term galvanic anode current capacity determination experiments and Table 5-6 where a micro-pH electrode was inserted into corrosion products, as described above, on both these anodes and those from the flow loop. These data show that this local pH was in the range 2.92 to 7.34 with an average of 4.80. This is generally consistent with the results of Espelid et al. (58). In addition to factors that routinely affect pH measurement reproducibility such as electrode calibration and drift, the data in Tables 5-5 and 5-6 are thought to have been influenced by 1) variations in the degree of corrosion product disruption from one site to the next upon insertion of the electrode such that some mixing of the bulk and occluded electrolytes occurred, 2) differences in the amount and properties (permeability) of the corrosion products from one site to the next such that the degree of occlusion provided to the underlying electrolyte varied, 3) variability associated with positioning of the electrode tip, and 4) differences in corrosion rate from one measurement site to the next. The last of these factors (corrosion rate) is important since it affects the production rate of aluminum ions that are

subsequently available to hydrolyze. In view of uncertainties associated with the pH measurement technique, it may be that the lower pH values are the ones that are representative of conditions at the anode surface.

Table 5-5: Results form pH measurements.

ANODE/CELL NO.	MEASUREMENT 1	MEASUREMENT 2
2	3.5	4
4	4	-
7	4	4
8	4	5.5
9	4	6
10	4	4
11	4	5.5
12	4	4

Table 5-6: Results of pH determinations using the micro-electrode technique.

	ANODE NUMBER	pH	COMMENTS
Long-Term Galvanic	2	4.89 3.90	Reading reached a minimum of 4.83 then increased after accidental removal of probe. Stable upon reinsertion.
	6	2.92	pH stable in are of large corrosion products.
	8	5.65	Small area of corrosion products.
	9	5.10	-
	11	5.70	-
Task II Flow Loop	5	4.69 4.44	Open circuit condition. After attaching anode to cathode (66.3 mA).
	6	7.28	Open circuit. Small area of corrosion products.
	7	6.89 7.03	Closed circuit (53.7 mA). Open circuit. Small area of corrosion products.
	8	3.41 3.77	Closed circuit (71.1 mA). Open circuit. Small area of corrosion products.
	21	7.34	No corrosion products. Open circuit.
	22	3.60 4.04	Closed circuit (5.74 mA). Closed circuit. Upon disconnecting from cathode pH increased to 6.98 over 30 min.
	23	4.63 4.17	Closed circuit (18.7 mA). Open circuit. Small area of corrosion products.

Based upon the above pH data, a series of current capacity determinations was performed for the CT-1 anode material (see Table 5-3) in recirculating natural sea water with pH adjusted to 3.5 ± 0.1. The procedure was in general conformity with NACE International TM0190 except

that three current densities were employed. Table 5-7 presents the results of these tests, and Figure 5-11 shows these is perspective to the data in Figure 5-7 (the current density scale in Figure 5-7 references the anode surface area, whereas the one in Figure 5-11 is for the structure assuming an anode-cathode surface area ratio of 1:50). This indicates that the *C* values measured

Table 5-7: Results of current capacity determinations in acidified sea water.

TEST NUMBER	CURRENT DENSITY, mA/m^2 (anode surface area)	CURRENT CAPACITY, Ah/kg
1	6,200	1,997
2	6,200	2,546
3	6,200	2,466
4	6,200	2,374
5	594	1,414
6	594	1,224
7	594	895
8	594	1,077
9	344	640
10	344	895
11	344	925
12	344	794

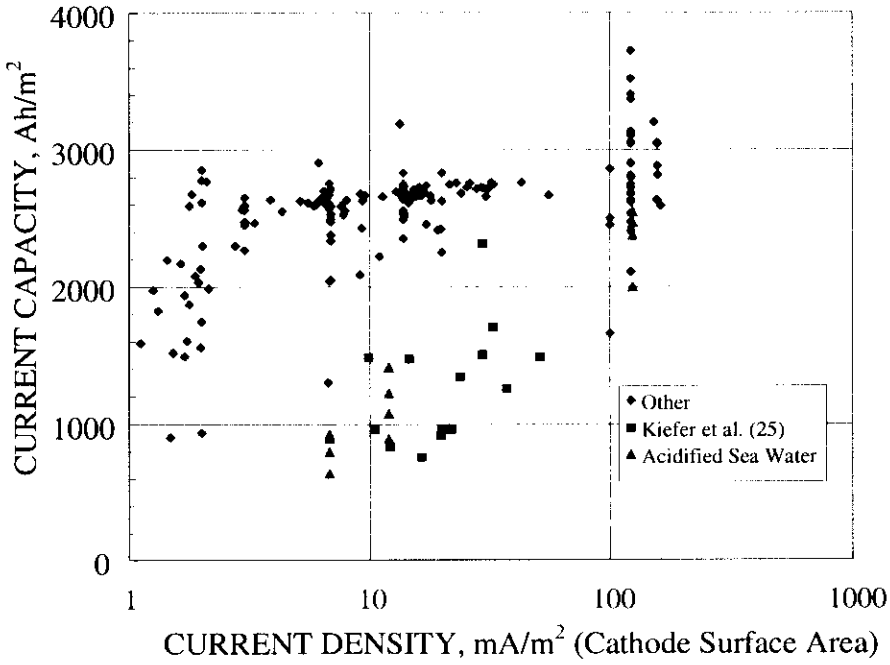

Figure 5-11: Current capacity data in acidified sea water in comparison to results from non-acidified test solutions (Figure 5-7).

in acidified sea water are in good general agreement with those reported by Kiefer et al. (25) which were from structures of ages 6-26 years and suggests that, by using an acid electrolyte, it may be feasible to develop a short term anode test method that projects long-term performance. More research is needed to confirm this and to determine 1) the pH value or range of values and 2) the test duration that should be employed.

VII. CONCLUSIONS

1. Current density demand is a critical parameter with regard to design of retrofit cathodic protection systems for offshore structures. Two techniques, the $\Delta\phi$-*MDE* method (Potential Difference–Modified Dwight Equation) and Swain meter, are appropriate for assessing current density demand of a cathodically polarized offshore structure. A protocol based upon each of these is provided as Appendix B.

2. The need for close interval potential surveys on offshore structures, as currently practiced, is questioned. As an example alternative protocol, if the remote or semi-remote potential in a zone of interest is -0.90 $V_{Ag/AgCl}$ or more negative, then it is unlikely that under-protection exists anywhere in that zone since sea water cannot support a 100 mV voltage drop between different structural members at the current densities present on older structures. Judgement must be exercised in acquiring such ϕ_c data (remote or semi-remote), however, in that consideration should be given to shielded areas such as within conductor arrays and to spatial variations (potential variability with depth, for example).

3. The mean cp current density, i_m, for structures in warm waters such as the Gulf of Mexico and the Arabian Gulf decreases with time according to a power law relationship and for older structures is approximately 25 percent of the value specified in the current recommended practices. This suggests that the cp system for such structures can be designed with considerably less anode mass than is present practice. However, this possibility is offset, at least partially, by the finding that the mean anode current capacity, C_m, decreases with time and in the long-term is less than the present design value. A modified form of the unified design equation that incorporates the time dependence of both i_m and C_m is given by the expression

$$w \cdot R_a = \frac{8.76 \cdot 10^{(a+k_i \cdot \sigma_i)} \cdot T^{b+1} \cdot e^{0.032 \cdot T} \cdot S}{(b+1) \cdot (2598 - k_c \cdot \sigma_c)}, \qquad \text{(C1}$$

where

w is mass of an individual anode (kg),
R_a is anode resistance (Ohms),
a and b are constants (1.51 and –0.41, respectively, for warm water exposures),
T is time (years),
S is the slope parameter ($\text{Ohm} \cdot \text{m}^2$),
σ_i and σ_c are the standard deviations for a (i_m) and C_m, respectively, and
k_i and k_c are factors of safety multiples for a and C_m, respectively.

4. The data that are available in the literature indicate that the mean and maintenance current densities (i_m and i_{maint}, respectively) vary from one structure to the next by about one order of magnitude (values for i_{maint} range from 3.4 to 34.4 mA/m^2 for warm water structures). For laboratory experiments that were part of this project, current density demand varied by a factor of three for apparently identical specimens. Presumably, the quality of the calcareous deposits that formed upon these specimens and structures is affected by some unknown factor(s).

5. From experiments where specimens were sequentially polarized, depolarized or partially depolarized, and then repolarized to simulate a cp retrofit, the steady-state i_{maint} after repolarization, $i_{ss}(repol)$, was about the same as during the initial polarization. Also, a relationship was apparent between $i_{ss}(repol)$ and the steady-state i_{maint} upon partial depolarization, $i_{ss}(depol)$, as

$$i_{ss}(repol) = 1.47 \cdot i_{ss}(depol) + 3.53 . \qquad \text{(C2}$$

Retrofit cp design can be performed using a modified form of this expression,

$$i_{ss}(repol) = 1.47 \cdot i_{ss}(depol) + 3.53 + k\sigma , \qquad \text{(C3}$$

where σ is the standard deviation for $i_{ss}(repol)$ (5.19 mA/m^2) and k is a constant that reflects the degree of conservatism in selecting a design value for $i_{ss}(repol)$.

6. The initial current density required to repolarize a depolarized or partially depolarized specimen, $i_o(repol)$, was less than for the initial polarization. Also, $i_o(repol)$ was related to $i_{ss}(depol)$ by the expression

$$i_o(repol) = 2.31 \cdot i_{ss}(depol) + 32.47 + k \cdot \sigma . \qquad \text{(C3}$$

where σ in this case is the standard deviation for the $i_o(repol)$ data (17.33 mA/m^2).

7. For an aluminum anode of a given composition and microstructure, current capacity is influenced primarily by current density and exposure time. The affect of time apparently is due to acidification of the electrolyte beneath the corrosion products, once these develop. Values for this pH as low as 2.92 were measured. A promising short-term anode test method for projecting long-term performance involves exposure to reduced pH sea water or synthetic sea water. The time dependence of mean current capacity conforms to the relationship

$$C_m = 2{,}598 \cdot e^{-0.032T}, \qquad \text{(C4}$$

An expression that permits a factor of safety to be included in the current capacity – time trend is

$$C = (2{,}598 - k_c \sigma_c) \cdot e^{-0.032T}. \qquad \text{(C5}$$

where k_c and σ_c were defined above.

VIII. ACKNOWLEDGEMENTS

The authors are indebted to Amoco, Chevron, Exxon, Marathon, Minerals Management Service, Mobil, Shell, and Texaco for financial support of this research and to Joe Bondos, Jim Burk, Doug Dopjera, Deyuan Fan, Al Goolsby, Russ Lewis, Buddy Niolon, Raju Pakalapati, John Respass, Jim Skogsberg, Charles Smith, Robert Smith, Steve Smith. Mike Surkein, and Dan Townley who provided technical guidance. Appreciation is also expressed to Eric Wagespack and Pat McGuire who made arrangements for the project team to participate in offshore structure

surveys. Lastly, thanks is given to Keith Lucas of the Naval Research Laboratory in Key West for making that facility available to the project personnel.

IX. BIBLIOGRAPHY

1. "Cathodic Protection Design," *DnV Recommended Practice RP401*, Det Norske Veritas Industri Norge AS, 1993.

2. "Corrosion Control of Steel-Fixed Offshore Platforms Associated with Petroleum Production," *NACE Standard RP 0176-94*, NACE International, Houston, 1994.

3. "Corrosion Control of Steel-Fixed Offshore Platforms Associated with Petroleum Production," *NACE Standard RP 0176*, NACE, Houston, 1976.

4. Evans S., "Use of Initial Current Density in Cathodic Protection Design," *Materials Performance*, Feb. 1988, Vol. 27(2), p. 9.

5. Cochran, J. C., "New Mathematical Models for Designing Offshore Sacrificial Cathodic Protection Systems," paper no. 3858, *Proceedings 1980 Offshore Technology Conference*, May 5-8, 1980, Houston.

6. Cox, G. C., "Anticorrosive and Antifouling Coating and Method of Application," U.S. Patent 2,200,469, 1940.

7. Foster, T., and Moores, V. G., "Cathodic Protection Current Demand of Various Alloys in Sea Water," paper no. 295 presented at CORROSION/86, March 17-2, 1986, Houston.

8. Mollan, R. and Anderson, T. R., "Design of Cathodic Protection Systems," paper no. 286 presented at CORROSION/86, March 17-2, 1986, Houston.

9. Fischer, K. P., Sydberger, T. and Lye, R., "Field Testing of Deep Water Cathodic Protection on the Norwegian Continental Shelf," paper no. 67 presented at CORROSION/87, March 9-13, 1987, San Francisco.

10. Fischer, K. P. and Finnegan, J. E., "Cathodic Protection Behavior of Steel in Sea Water and the Protective Properties of the Calcareous Deposits," paper no. 582 presented at CORROSION/89, April 17-21, 1989, New Orleans.

11. Schrieber, C. F. and Reding, J., "Application Methods for Rapid Polarization of Offshore Structures," paper no. 381 presented at CORROSION/90, April 23-27, 1990, Las Vegas.

12. Wang, W., Hartt, W. H., and Chen, S., *Corrosion*, vol. 52, 1996, p. 419.

13. Wolfson, S. L. and Hartt, W. H., *Corrosion*, vol. 37, 1981, p. 70.

14. Hartt, W. H., Culberson, C. H. and Smith, S. W., *Corrosion*, vol. 40, 1994, p. 609.

15. Lin, S-H and Dexter, S. C., *Corrosion*, vol. 44, 1988, p. 615.

16. Finnegan, J. E. and Fischer, K. P., "Calcareous Deposits: Calcium and Magnesium Ion Concentrations," paper no. 581 presented at CORROSION/89, April 17-21, 1989, New Orleans.

17. Fischer, K. P. and Finnegan, J. E., "Cathodic Protection Behavior of Steel in Sea Water and the Protective Properties of the Calcareous Deposits," paper no. 582 presented at CORROSION/89, April 17-21, 1989, New Orleans.

18. Luo, J. S., Lee, R. U., Chen, T. Y., Hartt, W. H. and Smith, S. W., *Corrosion*, vol. 47, 1991, p. 189.

19. Mantel, K. E., Hartt, W. H. and Chen, T. Y., *Corrosion*, vol. 48, 1992, p. 489.

20. Townley, D. W., "Unified Design Equation for Offshore Cathodic Protection," paper no. 97473 presented at CORROSION/97, March 9-14, 1997, New Orleans.

21. Hartt, W. H., Chen, S., and Townley, D. W., Corrosion, vol. 54, 1998, p. 317.

22. "Design of Galvanic Anode Cathodic Protection Systems for Offshore Structures," NACE International Publication 7L198, NACE International, Houston, TX, 1998.

23. Burk, J. D., "Dualnode Field Performance Evaluation Cathodic Protection for Offshore Structures," paper no. 309 presented at CORROSION/91, March 11-15, 1991. Cincinnati.

24. Mateer, M. W. and Kennelley, K. J., Materials Performance, vol. 33 No. 1, 1994, p. 32.

25. Kiefer, J. H., Thomason, W. H., and Alansari, N. G., Materials Performance, vol. 38 No. 8, 1999, p. 24.

26. Jelinek, J., Herfjord, B. O., Blakset, T. J., Osvoll, H., and Morton, D., Materials Performance, vol. 35 No. 4, 1996, p. 19.

27. Hartt, W. H. and Lemieux, E., "A Principal Determinant in Cathodic Protection Design of Offshore Structures: The Mean Current Density," paper no. 627 presented at CORROSION/99, April 25-30, 1999, San Antonio.

28. Dodson, J. K., DDS Report No. 143, James K. Dodson, Co., Grapevine, TX, 1993.

29. Johnson, D. L., "Diver Installed Anode Replacement Systems for Offshore Structures, paper no. 32 presented at CORROSION/77, March 14-18, 1997, San Francisco.

30. Wyatt, B. S., Brittain, R., and Jones, G. R., "Further Experience in Offshore Structure Retrofit Cathodic Protection Systems," paper no. 148 presented at CORROSION/80, March 3-7, 1980, Chicago.

31. Brandt, J. A., "Optimized Retrofitting of Offshore Cathodic Protection Systems, paper no. 518 presented at CORROSIION/93, New Orleans, March 8-12, 1993.

32. Turnipseed, S. P., "Case Histories of Offshore Platform Cathodic Protection Retrofits," paper no. 547 presented at CORROSION/96, March 24-29, 1996, Denver.

33. Brandt, J. A., "Sacrificial Anode Retrofits: Innovative Solutions for the Challenge of Deepwater and Other Complex Marine Environments," March 9-14, 1997, New Orleans.

34. Cochrane, W. J., Bonner, M., Strommen, R. D., Keim, W, and Morton, D., "A Computerized CP Retrofit Design of the Ninian Northern Platform," paper no. 375 presented at COROSION/90, April 23-27, 1990, Las Vegas.

35. Hartt, W. H. and Chen, S., *Corrosion*, vol. 55, 1999, p. 596.

36. Goolsby, A. D. and McGuire, D. P., "Cathodic Protection Upgrade of the 1,050' Water Depth Cognac Platform," paper no. 472 presented at CORROSION/97, March 9-14, 1997, New Orleans.

37. "Retrofit of Cathodic Protection Systems for Offshore Platforms," Draft 2a of proposed NACE International technical committee report, NACE International Unit Committee T-7L-15, April, 1999.

38. Thomason, W. H., Fischer, K. P., and Rippon, I. J., "In Service Measurement of the Performance of a CP/Coating System on a Gulf of Mexico Jacket", paper no. 516 presented at CORROSION/93, March 8-12, 1993, New Orleans.

39. Mateer, M. W., Often Overlooked Data Available from a Typical Offshore Subsea Survey", paper no 233 presented at CORROSION/91, March 11-15, 1991, Cincinnati.

40. Britton, J. N., Deepwater Corrosion Services, Inc., 7007 Winding Walk, Houston, TX 77095. Personal communication.

41. Sunde, E. D., *Earth Conduction Effects in Transmission Systems*, Dover Publications, Inc., New York, 1968, p. 72.

42. Hartt, W. H., "Fatigue of Welded Structural Steel in Sea Water", paper no. 3982, Proc. Offshore Technology Conference, May, 1991, Houston.

43. Graham, D. P., Cook, F. E. and Preiser, H. S., *Trans. Soc. Naval Arch. and Marine Engrs.*, Vol. 64, 1956, p.241.

44. Peterson, M. H., "A Short History of Marine Cathodic Protection", paper no. 285 presented at CORROSION/86, March 17-21, 1986, Houston.

45. Schrieber, C. F. and Reding, J. T., *Materials Protection*, Vol. 6 No. 5, 1967, p. 33.

46. Sakano, T., Toda, K, and Hanada, M., *Materials Protection*, Vol. 4 No. 12, 1966, p. 45.

47. Reding, J. T. and Newport, J. J., *Materials Protection*, Vol. 5 No. 12, 1966, p. 15.

48. Smith, S. N. and Goolsby, A. D., "A Consumer's Perspective of Aluminum Anode Quality Test Design," paper no. 552 presented at CORROSION/96, March 24-29, 1996, Denver.

49. Bessone, J. S., Suarez Baldo, R. A., and DeMicheli, S. M., *Corrosion*, Vol. 37, 1981, p. 533.

50. Rosasco, A. L., "A Review of the Metallurgical Aspects of Aluminum Anodes for Cathodic Protection," Report No. DTNSRCDC/SME-84-64, October, 1984.

51. Mondoflo, L. F., *Aluminum Alloys: Structure and Properties*," Buttersworth, London and Boston, 1976, pp. 302 and 527.

52. Reboul, M.C. and Delatte, M. C., *Materials Performance*, Vol. 19 No. 5, 1980, p. 35.

53. Reboul, M.C., Gimenez, P. H., and Rameau, J. J., *Corrosion*, Vol. 40, 1984, p. 366.

54. Murray, J. N., Hays, R. A., Lucas, K. E., and Hogan, E. A.," paper no. 545 presented at CORROSION/96, March 24-29, 1996, Denver.

55. Murray, J. N., Hays, R. A., Hack, H. P., and Bieberich, E. B., "Testing of Indium Activated Aluminum Alloys for Consumable Anodes in Cathodic Protection Applications," 9th Internaval Corrosion Conference, Monterey, CA, April, 1992.

56. Hori, Y., Takao, J., and Shomon, H., *Electrochemica Acta*, Vol. 31, 1986, p. 555.

57. Schreiber, C. F., *Cathodic Protection: Theory and Practice*, Chapter 5, Eds. V. Ashworth and C. J. Booker, Ellis Horwood Limited, London. 1986.

58. Espelid, B. Schei, B., and Syderberger, T., "Characterization of Sacrificial Anode Materials Through Laboratory Testing", paper no. 551 presented at CORROSION/96, March 24-29, 1996, Denver.

59. Wolfson, S. L., *Materials Performance*, Vol. 33 No. 2,1994, p.22-28.

60. Smith, S. N., Schrieber, C. F., and Riley, R. L., "Supplementary Studies of the Galvalum III Anode - Exposure Time and Low Temperature", paper no 35 presented at CORROSION/77, March 14-18, 1977, San Francisco.

61. Schrieber, C. F. and Murray, R. W., *Materials Performance*, Vol. 28 No. 7, 1988, p.70.

62. Haney, E. G. and Kurr, G. W., "Seawater Testing of Aluminum Alloy Anodes Containing Zinc, Indium and Cadmium", NACE Northeast Regional Meeting, Hartford, CT, October, 1975.

63. Houghton, C. J. and Ashworth, V., "The Performance of Commercial Zinc and Aluminum Anodes in Hot Sea-Bed Mud", paper no. 81 presented at CORROSION/81, April 6-10, 1981, Toronto.

64. Smith, S. N., Reding, J. T., and Riley, R. L., *Materials Performance*, Vol. 17(3), 1978, p. 30.

65. Goolsby, A. D., Shell Development Company, 3333 Highway 6 South, Houston, TX 77082. Unpublished research.

66. NACE Standard TM0190-98, "Impressed Current Laboratory Testing of Aluminum Alloy Anodes," NACE International, P. O. Box 218340, Houston, TX 77218, June, 1998.

67. Brown, J. F., "Quality Control Testing of Aluminum Anodes, paper no. 346 presented at CORROSION/84, April 2-6, 1984, New Orleans.

68. Murray, J. N. and Hays, R. A., "Testing Indium Activated Aluminum Alloys Using NACE TM0190-90 and Long-Term Exposures," paper no. 534 presented at CORROSION/93, March 8-12, 1993, New Orleans.

69. Murray, J. N. and Hays, R. A., "Correlations of Long-Term Sea Wall and TM0190-90 Short-Term Test Results for Indium Activated Aluminum Alloy Sacrificial Anodes," paper no. 545 presented at CORROSION/96, March 24-29, 1996, Denver.

70. Schrieber, C. F., "Pitfalls Associated with the Laboratory Testing Versus Actual Performance of Aluminum Galvanic Anodes," paper no. 529 presented at CORROSION/93, March 8-12, 1993, New Orleans.

71. Smith, S. N. and Goolsby, A. D., "A Consumer's Perspective of Aluminum Anode Quality Test Design," paper no. 552 presented at CORROSION/96, March 24-29, 1996, Denver.

72. Hartt, W. H., Chen, S., and Wang, W., "Steel Polarization and Cathodic Protection Design Parameters for Deep Water Petroleum Production Structures," Final Joint Industry Project Report submitted to membership by Florida Atlantic University, June 24, 1996.

73. Townley, D. T., Chevron Research and Technology Company, P. O. Box 446, LaHabra, CA 90633. Unpublished research.

Appendix A

Structure Cathodic Protection Survey Protocol Applied to Three Gulf of Mexico Platforms

The protocol is based upon independent anode current output determinations according to 1) Swain meter measurements and 2) $\Delta\phi$-*MDE* calculations. The purpose of the former is to identify accuracy of the latter.

Note: The Swain meter should be tested for accuracy/calibration prior to the survey and at least daily during the survey and at completion.

1. Perform a potential survey of the structure whereby a reference electrode is moved along the surface of individual structural members and anodes, as these are encountered, from one end to the other. From this data, an anode-structure potential difference, $\Delta\phi$, is determined for each anode and the portion of the structure it serves. Swain meter measurements are made on a predetermined number of anodes (standoffs) that have also been potential scanned.

2. A comprehensive video image of the anodes is obtained during the potential scanning. This is to include direct, frontal, and top views in an appropriate perspective such that the anode height, width, and length are viewed relative to 1) one or both standoffs and 2) the tubular structural member (see Figure A1).

   The purpose of the frontal (side) and top imaging is twofold: first, the frontal view provides a means for estimating the distance of the reference electrode from the anode centerline at the time the anode potential measurements are made and, second, both views provide a means for estimating the remaining anode weight. The basis for each of these is described below.

   The distance of the reference electrode from the anode centerline at the time of the potential measurements can be taken as one-half the fouled anode height. Alternately, the anode centerline-to-top surface distance may be estimated by sizing this on the video image relative to the structural member diameter which is known. Each of these is illustrated in Figure A2. A third possibility is that a direct measurement with a scale can be employed.

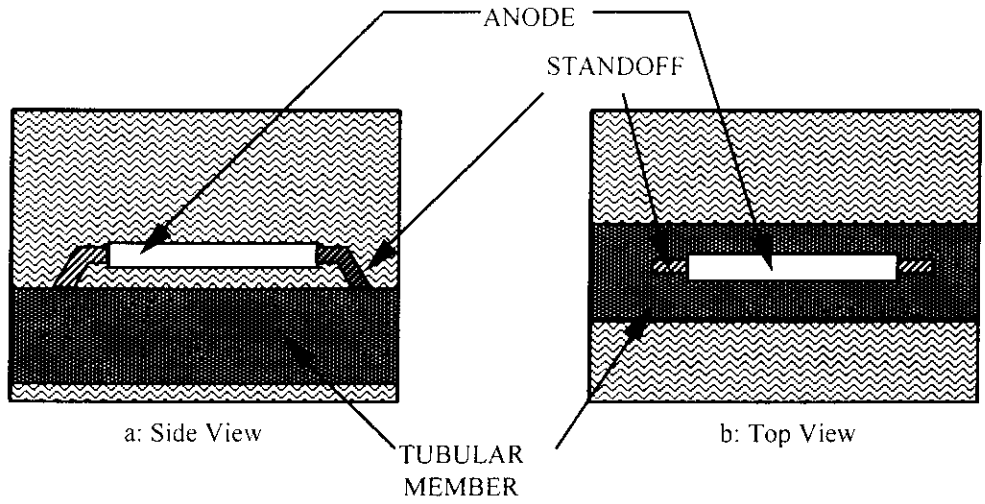

Figure A1: Schematic illustration of simulated video images from which anode dimensional estimates are made.

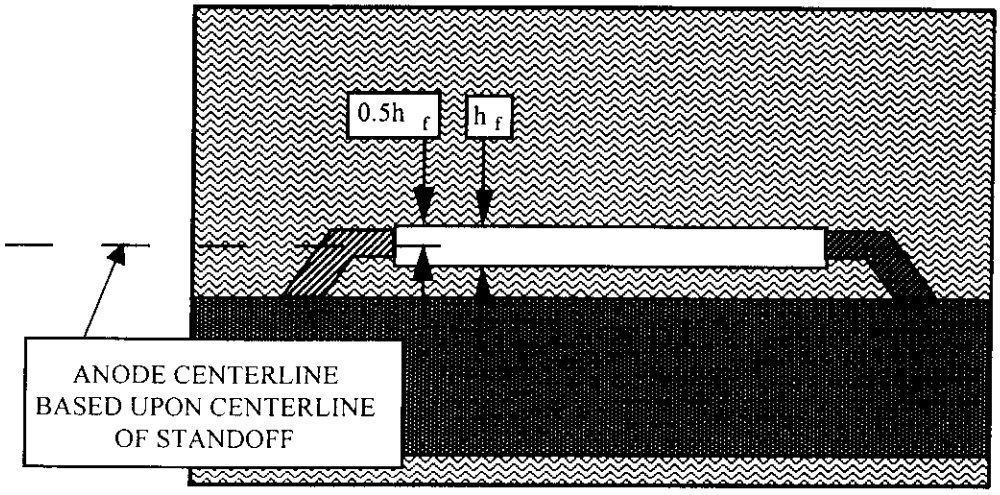

Figure A2: Alternative illustration of simulated video images from which anode dimensional estimates are made.

Anode current output, I, is then calculated from the expression

$$I = \frac{\Delta\phi}{\frac{\rho}{2\pi l}\left(\ln\frac{2l}{0.5h_f} - 1\right)}, \qquad \text{A1)}$$

where $\Delta\phi$ is the anode-cathode potential difference (anode potential measured at $0.5h_f$), ρ is sea water resistivity, and l is anode length.

- By comparing the fouled standoff diameter with the fouled anode height or width (or both) and from knowing the actual standoff diameter (without fouling), which is often 4.5 inches, the unfouled anode dimensions, including radius, can be estimated. This provides then a means for estimating remaining anode weight and, hence, remaining life.

- After the potential survey and Swain meter measurements, several anodes are cleaned and the circumference and length measured. Separate calculations of current output are made using these dimensions in conjunction with Equation A1 and the results compared with those where current output was determined from the video imaging.

Appendix B

Protocol for Field Survey Assessment Of Structure Current Demand

Background

Determination of structure current demand is critical for understanding 1) when a cathodic protection (cp) retrofit should be performed and 2) design of cp retrofits. The protocol provided herein gives guidelines for current demand determinations according to two procedures, each of which has been qualified as appropriate. The first of these is based upon direct measurement of current through each of the two anode standoffs using a Gaussian ammeter (Swain meter), and then summing these to give the net anode current output. The second procedure, termed the *Δϕ-MDE* (potential difference–modified Dwight equation) method, incorporates field measurements and a first principles based calculation procedure.

Gaussian Ammeter

Measurements are made directly by a diver using a hand held clip that is positioned about the anode standoff with the current reading being recorded topside. Three readings should be taken for each standoff, each with the clip in both the forward and reverse orientation (flipped 180°). The absolute value of these readings is then averaged to give the current through the standoff. Measurements should be made for a statistically significant number of anodes with consideration being given to spatial variability. Both the clip and cabling, as presently manufactured, are not particularly rugged; and so consideration must be given to protection of these components. The procedure is not conducive to ROV based measurements because of mechanical damage that invariably occurs in positioning and maintaining the clip about standoffs. The newer, MER (magnetic error reduction) meter model should be employed. The Swain meter should be tested for accuracy/calibration prior to the survey and at least daily during the survey and at completion.

Δϕ-MDE Method

Potential measurements are made along the length of individual anodes at six to eight positions. This is done by placing the reference electrode directly upon the fouled anode surface. Measurements should be acquired for a statistically significant number of anodes with consideration being given to any spatial variability (different zones on the structure). Length and thickness of the anode, including the thickness of any fouling layer, are determined, either by direct measurement or by sizing relative to a known dimension (standoff or tubular member or diver's hand, finger, or tool). This determination should be video recorded, and the measurement can even be made from the video.

A structure potential measurement is taken remote from the anode but in its general vicinity and at approximately the same depth. Water resistivity at this same depth is measured.

The anode-structure potential difference, $\Delta\phi$, is calculated as

$$\Delta\phi = \phi_c(\text{remote}) - \phi_a(\text{min}), \qquad \text{(B1}$$

where

ϕ_c(remote, is the remote structure potential and
ϕ_a
(min, is the most negative potential recorded for the anode in question.

The anode resistance, R_a, is determined using Dwight's modified equation,

$$R_a = \frac{\rho}{2\pi l} \cdot \left[\ln\left(\frac{2l}{r}\right) - 1 \right], \qquad \text{(B2}$$

where

ρ is water resistivity,
l is anode length, and
r is the effective anode radius (including thickness of any fouling layer).

The current output, I_a, of an individual anode is then determined from the expression

$$I_a = \frac{\Delta\phi}{R_a}. \qquad \text{(B3}$$

The average current output for the surveyed anodes on the structure (alternatively, for a zone of the structure), $\bar{I}_a$, is determined, and the net anode current output, I_t, for the structure or zone is calculated from the equation

$$I_t = \bar{I}_a \cdot N, \qquad \text{(B4}$$

where N is the number of anodes, either on the entire structure or in the zone under consideration). Alternatively, the maintenance current density, imaint, can be calculated from the expression

$$i_{ma\,int} = \frac{\bar{I}_a \cdot N}{A_c}, \qquad \text{(B5}$$

where A_c is the structure surface area.